Morphology of domains in and out of equilibrium.

Thibault Blanchard

THÈSE DE DOCTORAT DE
L'UNIVERSITÉ PIERRE ET MARIE CURIE

Spécialité

Physique Théorique

École doctorale Physique en Île de France – ED 564

Morphologie de domaines à l'équilibre et hors d'équilibre

Réalisée au

Laboratoire de Physique Théorique et Hautes Énergies

Présentée par

Thibault BLANCHARD

Pour obtenir le grade de

DOCTEUR de l'UNIVERSITÉ PIERRE ET MARIE CURIE

soutenue le 18 septembre 2014

devant le jury composé de :

M. Marco PICCO	Directeur de thèse
M. Malte HENKEL	Rapporteur
M. Víctor MARTÍN-MAYOR	Rapporteur
M. Bernard DERRIDA	Examinateur
M. Clément SIRE	Examinateur
Mme Leticia F. CUGLIANDOLO	Membre invité

Se non è vero, è ben trovato.

Résumé

Mon travail traite des propriétés géométriques de domaines présents dans un modèle magnétique simple, le modèle d'Ising. Par domaines nous entendons des régions où les spins prennent des valeurs similaires. En plus des propriétés telles que l'aimantation ou la susceptibilité magnétique, il est intéressant d'étudier la structure des domaines qu'il est naturel de décrire dans le cadre de la percolation. Dans cette thèse je me suis intéressé à plusieurs problèmes liés aux domaines de spins à l'équilibre et hors d'équilibre. J'ai ainsi étudié la dynamique des amas après des trempes critiques ou sous-critiques. Dans le cas de trempes cyritiques, le scaling dynamique a été étudié finement et l'influence des propriétés d'équilibre sur la dynamique mise en avant. Pour les trempes sous-critiques, nous avons considéré comme conditions initiales l'équilibre à une température critique ou infinie. Nous avons montré que dans le cas d'une température initiale critique la probabilité que le système finisse son évolution dans un état avec des bandes est exactement celle qu'un amas percole initialement. Concernant une température initiale infinie nous avons mis en évidence un régime transitoire conduisant le système vers le point critique de percolation. À l'équilibre à la température critique, nous avons obtenu une formule exacte pour la probabilité qu'un amas s'enroule autour d'un système avec des conditions aux bords périodiques. Nous avons aussi étudié le comportement critique du modèle d'Ising avec des interactions à longue portée en nous intéressant au passage des comportements longue portée à courte portée.

Abstract

In this work I have considered the geometrical properties of the domains found in the Ising model. Those domains are regions where the spins have the same value. In addition to the properties such as magnetisation and magnetic susceptibility, it is interesting to study the domains' structure and this is done naturally within percolation theory. In this thesis, I considered several situations concerning spin domains be it in equilibrium or out of equilibrium. I studied the dynamics of domains after critical or sub-critical quenches. For critical quenches the dynamical scaling has been carefully checked and the influence of the equilibrium properties on the dynamics has been shown. For sub-critical quenches we have considered both critical and infinite temperature initial conditions. We have shown that for critical initial condition the probability that the system ends up in a stripe state is exactly the probability that a spin cluster percolates initially. For the infinite temperature initial condition, we have discovered a transient regime which brings very quickly the system to a state similar to critical percolation. In equilibrium at the critical temperature we obtained an exact formula for the wrapping probabilities of Ising spin clusters on a system with periodic boudary conditions. We have also studied the critical behaviour of the Ising model with long-range interactions with a special interest to the cross-over between the long-range and short-range regimes.

Remerciements

Je tiens tout d'abord à remercier Marco Picco d'avoir accepter de diriger ma thèse durant ces trois années. Il m'a fait partager son savoir en physique et a su me guider pour que je ne m'égare pas. Il m'a aussi laissé une grande liberté qui m'a permis de pouvoir explorer des sujets différents et pour tout ça je lui en suis très reconnaissant.

Je souhaite également remercier Leticia Cugliandolo avec qui j'ai eu de nombreux contacts pendant nos collaborations. Son dynamisme et son efficacité remarquables ont souvent été décisifs pour la réalisations de nos travaux. Je tiens également à souligner sa disponibilité et ses connaissances étendues qui font qu'il est toujours agréable et instructif de travailler avec elle.

Je remercie les membres du LPTHE pour leur accueil pendant ces trois ans. J'ai une pensée particulière pour les *jeunes* du laboratoire : les anciens (Demian, Julius, Stefano...), les contemporains (Gautier, Pierre, Thomas, Luc...), les affiliés (Jérémy) pour les discussions interminables en salle café, les glandes hebdomadaires (ou plus fréquentes), et la bonne humeur du bureau des doctorants.

Je pense également à ma petite famille et je les remercie de m'avoir supporté pendant ces trois ans, même si ça n'a pas toujours été facile... Céline sans qui tout aurait été plus difficile et pénible, Isaac pour sa curiosité et mon petit Blaise pour son sourire. Pour tout ça et pour mille autres choses merci à vous trois ! Je veux aussi remercier mes parents et mon frère Pierre pour leur soutien durant mes (longues) années d'étude.

Contents

Résumé long

Introduction

Mon travail traite des propriétés géométriques de domaines présents dans un modèle magnétique simple, le modèle d'Ising. Par domaines nous entendons entre autres des régions où les spins prennent des valeurs similaires. En plus des propriétés globales telles que l'aimantation ou la susceptibilité magnétique, il est intéressant d'étudier la structure des domaines. Il est de plus naturel de décrire de tels objets dans le cadre de la percolation. Dans cette thèse je me suis intéressé à plusieurs problèmes liés aux domaines de spins à l'équilibre et hors d'équilibre.

Le modèle d'Ising est un système modèle pour de nombreuses situations que ce soit à l'équilibre ou hors d'équilibre. À l'équilibre et notamment en dimension deux, il s'agit d'un modèle que l'on peut traiter exactement et qui est un paradigme des transitions de phase continues. Hors d'équilibree c'est également un système modèle, par exemple pour la séparation de phases et le vieillissement. Soumis à une trempe d'une température élevée à une température inférieure ou égale à la température critique, le système relaxe lentement vers l'équilibre. Comme il existe deux phases stables, il y a une compétition entre les deux phases et une mosaique de domaines ordonnés grandissant avec le temps apparait. Nous avons étudié plusieurs variantes de cette situation. Les trempes critiques constituent l'objet du premier chapitre et les trempes sous-critiques du second.

Nous avons également considéré deux situations d'équilibre. Dans le troisième chapitre, nous nous intéressons à la probabilité qu'un amas de spins du modèle d'Ising à sa température critique s'enroule autour d'un système avec des conditions aux bords périodiques, c'est-à-dire un tore. Enfin, dans le dernier chapitre, c'est le modèle d'Ising avec des interactions décroissant comme une loi de puissance avec la distance qui est discuté.

Trempes critiques

Nous avons ainsi étudié le modèle d'Ising après une trempe d'une température infinie à la température critique du modèle. En deux dimension deux types d'amas connaissent une transition de phase continue de percolation à la température critique du modèle : les amas de spins et les amas de Fortuin-Kasteleyn. Ainsi pour un système à la température critique les deux types d'amas sont fractals et ont des propriétés d'invariance d'échelle et même d'invariance conforme. Nous avons condidéré les deux types d'amas dans notre étude. Nous avons utilisé le réseau triangulaire pour lequel le seuil de percolation de site vaut $1/2$. Ainsi nous nous sommes placés dans une situation telle que le point initial est le point critique de la percolation pour les amas de spins, ces domaines sont donc initialement dans un état critique et relaxe vers un autre état critique.

Pour décrire un amas de spins on peut mesurer son aire (le nombre de spins le composant), mais également son périmètre (le nombre de spins de signe opposé à son contact), son périmètre en excluant les éventuels trous présent dans l'amas et aussi l'aire incluse dans ce périmètre restreint en bouchant les trous... Pour chacune de ces quantités on peut définir la distribution du nombre d'amas ayant une valeur donnée de cette quantité. Ces distributions dépendent de la quantité considérée mais également du temps mesuré à partir de la trempe. Elle sont construites en analysant un grand nombre d'échantillons indépendants lors de simulations de Monte-Carlo et en construisant les histogrammes provenant de l'analyse de ces configurations. Ces distributions permettent de caractériser le système sur toutes les échelles ce qui permet une analyse plus fine qu'avec des quantités globales.

Un concept important dans l'étude des phénomènes hors d'équilibre est le scaling dynamique. Il s'agit d'une extension du scaling tel qu'il a été développé pour les systèmes à l'équilibre. Dans le cas des systèmes hors d'équilibre, cela donne qu'il existe une longueur unique $\xi(t)$ qui croit avec le temps et que cette longueur est telle que les propriétés du système sont indépendantes du temps quand elles sont exprimés avec cette longueur. C'est donc l'équivalent de la longueur de corrélation à l'équilibre et cela permet une analyse similaire au groupe de renormalisation pour les phénomènes hors d'équilibre. L'objectif de notre travail était d'étudier comment le scaling dynamique s'applique pour ces distributions. Dans le cas des trempes sous-critiques, des expressions exactes ont été obtenues pour diverses distributions et nous espérions également obtenir des expressions dans le cas critique mais nous n'avons pas abouti car la dynamique critique est plus complexe que la dynamique sous-critique. En effet dans le cas sous-critique la dynamique est dominée par la courbure des interfaces et comme les domaines tendent à diminuer la longueur de leur périmètre ils rétrécissent et finissent par disparaitre. Pour la dynamique critique, les interfaces tendent à devenir fractales et les amas peuvent être scindés, fusionnés et non seulement rétrécir indépendamment des autres comme dans le cas sous-critique. Nous avons cependant montré que les distributions sont bien de la forme attendue par les arguments de scaling une fois que le nature fractale des objets considérés est prise en compte. Plus précisément pour un objet de dimension fractale D, les objets de taille inférieure à la taille caractéristique $\xi(t)^D$ sont similaires à ceux présents à l'équilibre à la température

critique tandis que ceux d'une taille supérieure restent similaires à la condition initiale de percolation critique.

Nous avons également des interfaces uniques dont on peut forcer la création avec des conditions aux bords adéquates. Étudier une interface unique est intéressant car à l'équilibre de puissants outils permettant l'étude fine d'interfaces ont été développés, notamment les évolutions stochastiques de Loewner. Ces outils reposent sur le fait qu'ils existent dans beaucoup de situations critiques une symétrie plus forte que la simple invariance d'échelle, à savoir l'invariance conforme. Les interfaces aux points critiques de la percolation et du modèle d'Ising ont notamment été considérées et des résultats rigoureux et très intéressants ont été obtenus. Cela fait de la situation que nous avons choisie où la percolation critique est initialement présente et où le système tend vers l'équilibre à la température critique un cas qui semble propice à l'utilisation de ces idées normalement réservées à l'équilibre. Ainsi nous avons étudié non seulement la dimension fractale de l'interface mais également la statistique des angles pour laquelle des résultats découlant de l'invariance conforme existent à l'équilibre. Nous avons aussi considéré la situation des évolutions stochastiques de Loewner dipolaires pour les trempes critiques et mis en évidence une transition rapide entre les deux régimes conformes.

En conclusion, nous avons étudié les distributions associées à des aspects géomtriques des domaines (taille, périmètre…) et mis en evidence les lois d'échelle dynamiques. L'étude d'interfaces uniques renforce ces lois d'échelle et mets en évidence le rôle des sysmétries plus fortes présentes à l'équilibre. Les différents aspects étudiés montrent clairement que sur des distances bien inférieures à la taille caractéristique des domaines le système est équilibré à la température critique alors que sur les grandes distances il est tout à fait similaire à l'état initial.

Trempes sous-critiques

Nous nous sommes aussi intéressé aux trempes sous-critiques qui même si elles présentent a priori une dynamique plus simple que leurs équivalents critiques font montre d'une grandes richesses de comportement que nous allons décrire. Le fil directeur qui a guidé notre étude des trempes sous-critiques est de comprendre et mettre en évidence le rôle de la condition initiale dans l'évolution qui suit. Il y a naturellement deux conditions initiales possibles : l'équilibre à la température critique et un système à température infinie. La première condition initiale est telle que les spins sont corrélés sur de longues distances et que les amas de spins sont critiques et ce quelque soit le réseau utilisé. La seconde ne présente pas de corrélations entre spins et n'est pas un état critique pour les amas de spins (sauf pour le réseau triangulaire considéré précédemment).

Dans le cas d'une température initiale critique, nous avons constaté numériquement que les états finaux dans lequel le système peut se retrouver après une trempe à température nulle peuvent contenir des amas métastables en forme de bande. Ces amas ont une durée de vie infinie à température nulle mais si la température est non nulle ils disparaissent en un

temps fini. Nous avons mesuré précisément les probabilités d'apparition de ces états finaux avec des bandes de spins pour différentes conditions au bord. Dans chacun des cas étudié, nous avons montré que ces probabilités coincident précisément avec les probabilités qu'il existe un amas du même type percolant le système à l'état initial. Comme l'état initial est un point critique bien étudié, il existe un certain d'expressions pour ces probabilités et nous avons donc pu relié précisément une situation hors d'équilibre à des résultats exacts à l'équilibre. Nous avons même vérifié que pour un système donné c'est bien l'éventuel amas percolant initialement qui va s'épaissir jusqu'à devenir une bande de spins. Nous avons également mesuré la persistence pour cet état initial corrélé et mesuré un exposant différent du cas où la condition initiale est non-corrélée.

Nous nous sommes ensuite intéressé au cas d'une condition intiale à température infinie et donc non corrélée. Dans ce cas, les états finaux obtenus après une trempe à température nulle ont été étudiés dans la littérature et il a été montré par plusieurs auteurs que la probabilité d'apparition d'état finaux avec des bandes coincident numériquement avec la probabilité qu'un amas traverse le système au point critique de percolation. Cela semble similaire au résultat que nous avons obtenu en partant du point critique mais en réalité c'est surprenant car pour la plupart des réseaux les amas de spins sont dans un état sous-critique de percolation initialement pour un système à température infinie. Il semble donc que le système atteigne la percolation critique au cours de son évolution même s'il n'y est pas initialement et que ceci se répercute aux temps longs jusque dans les caractéristiques des états finaux. En observant les configurations de quelques échantillons au cours du temps, on se rend compte que le temps nécessaire pour atteindre la percolation critique est en fait extrêmement court par rapport au temps de thermalisation. Nous avons donc précisément étudié le régime des temps courts pendant lequel s'établit un état critique de percolation pour les domaines.

Des observables naturelles sont les probabilités de percolation et il est notamment intéressant d'étudier leur évolution avec le temps. On se rend ainsi compte que le temps pour atteindre un état critique de percolation croit avec la taille du système et que ce temps dépend du réseau considéré. On constate donc que quelque soit le réseau et sa taille on atteint de façon certaine un état contenant un amas percolant mais il convient de distinguer deux classes de réseaux qui donnent lieu à des comportements très différents. Pour les réseaux dont tous les sites ont un nombre pair de voisins, on observe la dynamique usuelle et même si le système finit fréquemment dans états avec des bandes, il n'y a pas de ralentissement dû à la nature du réseau. Au contraire, pour un réseau contenant une fraction de sites ayant un nombre impair de voisins, on constate que très rapidement la dynamique ralentit fortement et que pour une trempe à température nulle le système se fige dans une configuration contenant une multitude d'amas métastables de toutes tailles. La différence d'avec les réseaux de coordinance paire tient au fait que des sites avec un nombre impair de voisins permettent l'existence d'interfaces stables non rectilignes, ce qui fait qu'une grande variété de structures métastables sont permises et non plus seulement des bandes dont les interfaces sont des droites. Ainsi pour ces réseaux, deux phénomènes coexistent à savoir la mise en place de la percolation et le gel du système. On peut se demander quel

processus est le plus rapide et par exemple si un système peut geler avant d'atteindre la percolation. Il semble que la réponse à cette question soit négative et nous avons même constaté au contraire que le gel du système semble accélérer le développement de structures percolantes.

Les probabilités de percolation nous donne un bon aperçu de la dynamique du système mais en y regardant bien on se rend compte que dans ce régime des temps cours il y en fait une phase d'intermittence pendant laquelle de nombreux amas percolants se font et se défont jusqu'à ce que la struture percolante définitive s'installe et persiste jusqu'à l'état final. On note t_p le temps nécessaire pour atteindre cet état défnitif de percolation qui est celui qui influence le plus le système. En étudiant précisément t_p pour des réseaux de tailles différentes, nous avons montré que t_p varie comme une loi de puissance avec la taille linéaire L du système, c'est-à-dire $t_p \sim L^\alpha$ avec α un exposant dépendant du réseau utilisé. Les valeurs obtenues numériquement pour α sont compatibles avec $\alpha = z/n_c$ où z est l'exposant dynamique et n_c le nombre de coordination du réseau. Il existe donc une échelle de temps supplémentaire par rapport au coarsening standard. En analysant le comportement de fonctions de corrélation entre spins aux temps courts, on se rend compte qu'on obtient un meilleur collapse des courbes en prenant en compte la longueur associée à ce temps et non seulement la longueur caractéristique $\xi(t)$.

Nous avons donc étudié et comparé des trempes sous-critiques pour une condition initiale corrélée ou non. L'apparition de la percolation après les trempes faites depuis une température infinie donne lieu à une nouvelle échelle de temps dont nous donnons quelques conséquences. Pour les deux températures initiales nous étudions et comparons aussi diverses observables tels que la persistence, des fonctions d'auto-corrélation et des distributions de domaines.

Probabilités d'enroulement d'amas de spins d'Ising sur un tore

Nous avons également travaillé sur les probabilités qu'un amas s'enroule autour d'un tore mentionnées précédemment. La motivation pour ce travail vient de l'étude des états finaux avec des bandes en partant d'une situation d'équilibre au point critique. Bien que des résultats aient été obtenus pour les amas de Fortuin-Kasteleyn du modèle de Potts à Q états sur un tore pour une valeur quelconque de Q, aucun résultat concernant les amas de spins n'existait dans la littérature. Les amas de spins, bien qu'ils soient des objets géométriques tout à fait naturel à considérer notamment dans les situations hors d'équilibre ne sont pas directement en lien avec les propriétés magnétiques du modèle. Par exemple leur dimension fractale n'est pas lié à l'exposant magnétique β du modèle d'Ising comme on pourrait s'y attendre, en réalité c'est celle des amas de Fortuin-Kastelyn qui est liée à β. Étudier les amas de spins fournit un autre jeu d'exposants critiques qui est lié à un modèle de Potts avec dilution à son point tricritique. Cette relation a été exploitée et permet d'obtenir un grand nombre de résultats, notamment tous les exposants liés à ces amas. Mais il existe quelques propriétés plus fine telles que les contributions universelles au nombre

d'amas touchant une courbe ou encore les constantes de structures apparaissant dans des fonctions de corrélations de connectivité pour lesquelles l'approche consistant à utiliser directement le résultat pour le modèle de Potts avec dilution correspondant ne donne pas des résultats corrects. Il est donc intéressant de voir ce qu'il en est pour la probabilité qu'un amas de spin s'enroule d'une façon donnée autour d'un tore.

Pour être plus précis sur les grandeurs que nous cherchons à calculer, nous devons décrire les objets de notre étude. Parmis les amas de spins pouvant exister sur un tore nous distinguons les amas qui sont homotopes à un point et que nous appelerons *amas triviaux* des amas s'enroulant d'une façon ou d'une autre autour du tore et que nous appelerons *amas non-triviaux*. Les amas triviaux sont décrits par l'exposant 0 dans nos notations. Les amas non-triviaux peuvent être classés en fonction du nombre de fois qu'ils s'enroulent dans une direction ou une autre sur le tore. Ainsi un amas s'enroulant a fois horizontalement et b fois verticalement sera nommé amas $\{a, b\}$. Seul les amas pour lesquels a et b sont premiers entre eux sont distincts. Ils existent également des amas non-triviaux dont plusieurs sous-parties ont des nombres d'enroulement non-nuls mais différents entre eux. Le cas le plus simple est amas composé d'un sous amas horizontal $\{1, 0\}$ et d'un autre vertical $\{0, 1\}$. Cet amas est en forme de croix et de ce fait nous dénoterons tous les amas de ce type amas-croix et nous utiliserons pour eux l'exposant $+$. Maintenant pour un tore complexe de paramètre τ, nous cherchons à obtenir une expression pour les probabilités $\pi^0(\tau)$, $\pi^{a,b}(\tau)$ et $\pi^+(\tau)$. Les probabilités que nous cherchons à calculer sont en fait simplement le ratio de la fonction de partition restreinte aux configurations contenant le type d'amas considéré sur la fonction de partition total du modèle. La fonction de partition du modèle d'Ising étant connue exactement pour un tore quelconque il nous reste seulement à calculer ces fonctions de partition réduites.

Pour attaquer ce probmème il convient de reformuler la situation initiale. Le modèle de Potts est un modèle avec des variables de spin disposées sur les sites du réseau. Au lieu de considérer la configuration des amas on peut s'intéresser à la configuration de leurs contours qui forment dans le cas du modèle d'Ising des boucles auto-évitantes. Ce modèle de boucles peut être transformé en un modèle de hauteur tel que les boucles séparent des zones de hauteurs différentes. Il est connu que de tels modèles de hauteur sont décrit dans la limite continue par un gaz de Coulomb avec un certain paramètre g. La présence d'amas non-triviaux qui n'ont pas une forme de croix se traduit par des discontinuités dans le champ. Les fonctions de partition pour de tels champs peuvent s'écrire à l'aide de fonctions de partition coulombiques définies par Di Francesco, Saleur et Zuber. Les amas de spins du modèle d'Ising sont décrits par le modèle de Potts à 1 état à son point tricritique. En choisissant la valeur de g correspondant à ce modèle et en sommant correctement sur les discontinuités on peut ainsi obtenir les fonctions de partition réduites désirées. Finalement la formule obtenue s'exprime de façon compacte à l'aide de fonctions theta de Jacobi.

Cette formule est ensuite mise à l'épreuve des données issues de simulations. Pour obtenir ces données numériques nous avons simulé un modèle d'Ising à son point critique et analysé un grand nombre ($\sim 10^6$) de configurations indépendantes pour calculer les probabilités correspondant aux différents groupes d'amas présents. Nous considérons

uniquement des tores tels que $\tau = ir$ avec r le rapport d'aspect prenant des valeurs entre $0,1$ et 1 dans nos simulations. Seuls les amas $\{1,0\}$, $\{0,1\}$, $\{1,1\}$, $\{1,-1\}$ sont suffisamment fréquents pour que les probabilités correspondantes puissent être estimées. L'accord entre la formule obtenue et les données numériques est très bon. Cela indique que dans ce cas l'approche naïve qui consiste à utiliser directement le gaz de Coulomb associé au modèle tricritique pertinent donne un résultat correct.

En conclusion, nous avons obtenu une formule explicite pour les probabilités que des amas de spins s'enroulent autour d'un tore quelconque. Cette formule est obtenue en utilisant le formalisme du gaz de Coulomb et en utilisant la description des amas de spins comme les amas d'un modèle de Potts avec dilution à son point tricritique. Cette formule est testée numériquement et l'accord est très convaincant.

Modèle d'Ising avec interactions à longue portée

Finalement nous avons étudié le comportement critique du modèle d'Ising avec des interaction à longue portée. Ce sujet est indépendant des travaux mentionnés précédemment. Les interactions décroissent comme une loi de puissance $1/r^{d+\sigma}$ avec la distance r et les exposants critiques du modèle varient avec l'exposant $\sigma > 0$ décrivant la portée des interactions.

Ce modèle a été étudié par Fisher, Ma et Nickel grâce au groupe de renormalisation perturbatif peu après l'introduction de la méthode. Ils calculèrent notamment la valeur de la dimension anormale η en fonction de σ. Tout d'abord la dimension critique supérieure d_c, à savoir la dimension au delà de laquelle le modèle est décrit de façon exacte par une approche de champ moyen, vaut $d_c = 2\sigma$. Donc pour $\sigma < d/2$ la dimension anormale prend la valeur donnée par une approche de champ moyen, à savoir $\eta = 2-\sigma$. De plus, en faisant une analyse naïve de l'importance relative du terme correspondant aux interactions à longue portée q^σ par rapport au terme q^2 des interactions à courte portée ils en conclurent que pour $\sigma > 2$ on retrouve le modèle d'Ising avec des interactions à courte portée. Ainsi pour $\sigma > 2$, $\eta = \eta_{SR}$ la valeur standard de la dimension anormale du modèle d'Ising. Dans le régime restant $d/2 < \sigma < 2$, ils remarquèrent que le terme q^σ domine et qu'aucune correction ne vient changer η de sa valeur de champ moyen $2-\sigma$. Donc au final pour $\sigma < 2$ ils trouvèrent que $\eta = 2 - \sigma$ et que $\eta = \eta_{SR}$ pour $\sigma > 2$. Comme $\eta_{SR} \neq 0$ cela signifie que η serait discontinue en $\sigma = 2$. Cela est possible d'un point de vue thermodynamique mais néanmoins surprenant.

Peu de temps après cette analyse a été partiellement remise en cause par Sak notamment concernant cette possible discontinuité de η. Revenant à l'étude des relations de récursions du groupe de renormalisation, Sak réalise qu'en fait le point fixe courte portée est stable en partie pour $\sigma < 2$. Plus précisément il trouve que pour $\sigma > 2 - \eta_{SR}$, la dimension anormale prend sa valeur courte portée. Ainsi la discontinuité $\sigma = 2$ disparait et η est une fonction continue de σ.

Depuis lors de nombreux travaux ont traité de ce modèle arrivant à des conclusions

contradictoires en faveur d'un scénario ou de l'autre. Il y a un peu plus de 10 ans, Luijten et Blöte ont étudié numériquement pour la première fois ce modèle. Leurs simulations excluent une discontinuité de la dimension anormale et ils concluent de leur étude que celle-ci confirme l'analyse de Sak. Plus récemment des simulations plus précises menées par Picco donnent des valeurs de η incompatibles avec le scénario de Sak autour de $\sigma > 2 - \eta_{SR}$. Nous avons donc étudié la stabilité des différents points fixes pour expliquer ces résultats de simulations. Nous avons également étudié ce problème grâce au groupe de renormalisation perturbatif et obtenu dse résultats en bon accord avec les simulations. Plusieurs travaux ont paru depuis dont un par Angelini, Parisi et Ricci-Tersenghi et un autre par Brézin et Parisi. Ces travaux suggèrent que l'origine de ces exposants différents est que la fonction de coorélation présente non pas un comportement simple de loi de puissance mais est en fait composée de deux lois de puissances distinctes. La discussion n'est pas close et il semble que des travaux supplémentaires seront nécessaires pour complètement clarifier le régime intermédiaire entre longues et courtes portées.

Introduction

0.1 Motivations

In this section I describe briefly the motivations and interests that have guided my work during my PhD. I have treated several independent subjects but hopefully this small account will help follow the path of thought we have trodden. Chronologically first, everything started during my master's internship done under the supervision of Marco Picco and Leticia Cugliandolo. The goal of this internship was to extend and complete the research carried out by Leticia and co-workers on the distributions of spin cluster sizes during a subcritical quench. What we had in view was to see if similar formulae could be obtained in the case of critical quenches. Moreover we used a particular setup which makes both the initial and final points of the quench critical points for spin clusters. The hope was to use the wealth of knowledge that exists for those critical points at equilibrium to gain hindsights on the out of equilibrium situation. Even though we have made convincing checks of dynamical scaling concerning distributions of geometrical observables, we were unable to obtain expressions for those distributions due to the greater complexity of critical quenches compared to subcritical ones. This work has been the subject of a publication in the Journal of Statistical mechanics [1], and we argued that the setup used may be appropriate for more analytical works.

After this study of critical quenches, we concentrated on the critical behaviour of the Ising model with long-range interactions and in particular to explain the results of Marco concerning the anomalous dimension in the cross-over region. We studied numerically the stability of the different fixed points and developed a perturbative renormalisation group approach yielding results in good agreement with the numerics. This work was published in EPL [2].

We then came back to quenches and in particular to the study of stripe states appearing after a quench from the critical point. We found that the appearance of stripe states is very well described by crossing or wrapping probabilities of spin clusters at the critical

temperature and wrote about our results in Physical Review E [3]. Doing so we found that no expression for the wrapping probabilities of spin clusters existed in the literature. This triggered the personal work on wrapping probabilities described in the chapter 3 and published in Journal of Physics A as a Fast Track Communication [4].

This study of stripe states led us to re-investigate the appearance of stripe states after a quench from infinite temperature. In this case the appearance of stripe states has been related to critical percolation crossing probabilities. A troubling point is that critical percolation is not obviously present in this setup. Trying to better understand the role of critical percolation, we studied the early time dynamics and the time scale needed to reach the percolation regime. This was the subject of a publication in EPL [5].

In the rest of the introduction we introduce general notions that we will use throughout the manuscript. We will not attempt to make a comprehensive overview of the subjects mentioned but rather to give the elements relevant to our study.

0.2 Percolation

In this section we will define the percolation model and state general results which will be used all along the manuscript. Percolation is interesting because, although it is deceptively simple to define, it is one of the simplest systems exhibiting a continuous phase transition.

0.2.1 Definition

Percolation was introduced by Broadbent and Hammersley in 1957 as a model for random media [6]. One can imagine a porous rock with small channels in which a fluid can flow or not depending on the size of channels. One natural question is whether the fluid can percolate through the rock, that is if it enters it by one side, can it exit it by the opposite side? Percolation models simply this situation but can also be applied to many other random media and situations. We mention two books on percolation among others. The book by Aharony and Stauffer [7] is an introduction to the field by physicists and the mathematical introduction by Grimmett [8] which presents exact results concerning percolation. Many variants of percolation exist but we will focus on two of the most common: bond and site percolation.

In all generality, bond percolation is defined on the edges of a graph, but for simplicity we will consider bond percolation on a d-dimensional lattice such as the hypercubic lattice $\mathbb{Z}^d$. A binary variable is associated with with each edge, so that an edge can be open or closed (remember the origin of the model) and let us note p the probability that an edge is open. Clearly p is also the mean fraction of open edges. Note that each edge is open with probability p independently of the other edges, thus no correlation exists between edges. Percolation is interested in the connected components (clusters) of open edges on the lattice, and particularly in the existence or not of an infinite connected component (on an infinite system). Site percolation is simply defined from bond percolation by considering the vertices (sites) instead of the edges and p is the probability that a site is occupied. In this

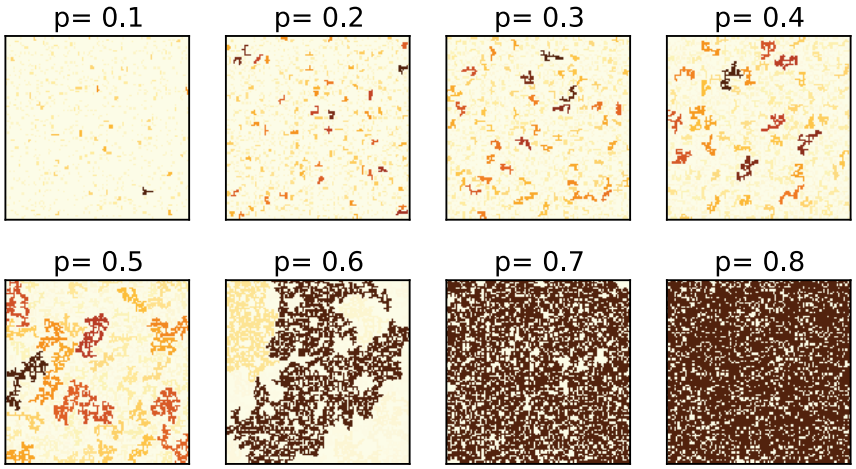

Figure 1 – Sample configurations of site percolation for different occupation probabilities given above the snapshots. The clusters are coloured according to their size, the darker the bigger.

case a cluster is a collection of occupied vertices connected by edges. We will note $\theta(p)$ the probability that an infinite connected component exists. In figure 1, site percolation configurations are represented for various values of p on a square lattice of size 100×100. Each cluster is coloured to its size, that is the number of sites that compose it, the darkest clusters in each configuration being the biggest. If p is very close to zero then only small clusters are present so $\theta(p) = 0$. On the contrary for p close to 1 the lattice is covered with an infinite cluster with only small holes within it, so that $\theta(p) = 1$. It is quite natural that θ is an increasing function of p and a mathematical argument shows that the only possible values are 0 or 1. This suggests that there exists a special probability value p_c such that for $p < p_c$ $\theta(p) = 0$ and $\theta(p) = 1$ for $p > p_c$ which is called the *percolation threshold* of the lattice. p_c depends on the lattice and on its dimension d. For the square lattice, looking only at figure 1, one can expect that $0.5 < p_c < 0.6$ which is correct since $p_c \simeq 0.59$.

The region where no infinite cluster exists is the *subcritical* phase and for $p > p_c$ it is the *supercritical* one and at p_c exactly it is said to be *critical*. The differences between the different phases can be made more explicit by looking at the probability that two points at a distance r belong to the same cluster. In the subcritical phase, the qualitative observation that big clusters are rare is reflected by the exponential decay with r of this probability. In $d = 2$, one can show that $p_c \geq 1/2$ [8], hence the supercritical phase is dual to the subcritical one by looking at the empty sites present with probability $1 - p$. At the critical point $p = p_c$ the aforementioned probability decreases algebraically with the distance r. This is reminiscent of critical points for continuous phase transition and we will make the relation more explicit in the following.

0.2.2 General properties

Let us define P the fraction of sites that belong to an infinite cluster. We have obviously $P = 0$ for $p < p_c$ since no infinite cluster exists. However for $p > p_c$, one can see quite easily from simulations for example that $P > 0$. Thus P can play the role of an order parameter describing the change happening when crossing p_c. For the usual bond and site percolation P is a continuous function of p, making the phase transition happening at p_c a continuous one. It is quite surprising at first that such a simple system can exhibit a continuous phase transition and its associated rich phenomenology, since there is no temperature, hamiltonian, interactions... One has to keep in mind that percolation describes phenomena of purely geometric nature. From there one can apply all the apparatus from statistical physics and it can be useful to make an analogy with a simple ferromagnetic model such as the Ising model. P is analogous to the magnetisation for the Ising model. One can show that for p slightly above p_c that $P \sim (p-p_c)^{-\beta}$ with β the equivalent of the magnetic exponent. All the usual quantities used in statistical physics have an equivalent in percolation. For example in percolation the equivalent of the magnetic susceptibility will be the mean cluster size which also diverges as p approaches p_c.

From the introduction of the model a very important question is whether a cluster percolates the system or not. To be more precise in finite-size lattices with boundaries a cluster is said to percolate whenever it is contact with at least two opposite sides of the system. For systems with no boundaries as it is the case when periodic boundary conditions are used, the equivalent problem is to see if a cluster is winding around the system in which case we will say it is a wrapping cluster. We will often be interested in spanning or wrapping probabilities at the critical point.

0.2.3 Statistical and geometric properties in equilibrium

One essential aspect of percolation is the morphology of clusters. An important object to understand the shape of clusters is the number distribution of cluster size. One can also consider number distribution for other cluster aspects such as the perimeter or hull length, the hull enclosed area... We will give precise definitions of those quantities in time.

Critical distribution

In general, when we consider the probability distribution per lattice site $n(X)$ which follows a power law at the critical point, we denote the related critical exponent τ, i.e.,

$$n(X) \sim X^{-\tau}. \tag{1}$$

The exponent τ is often called the Fisher exponent. Either the clusters or their boundaries are fractal objects at the critical point. Their Hausdorff dimension (referred hereafter as *fractal dimension* even if other fractal dimensions can be defined) is non-trivial and is related to the Fisher exponent. Indeed, the fractal dimension D can be expressed in terms

of τ:

$$D = \frac{d}{\tau - 1}, \tag{2}$$

with d the dimensionality of the lattice [7]. In two dimensions many fractal dimensions are known but this is not the case in higher dimensions.

Subcritical distribution

When $p < p_c$ the distribution is no longer described by a power law and large clusters are exponentially rare. The distribution is then given by:

$$n(X) \sim X^{-\tau} e^{-X/X_*} \tag{3}$$

with X_* cutoff related to the correlation length ξ by $X_* \sim \xi^D$ and τ the Fisher exponent as in (1). This means that for subcritical percolation large clusters are exponentially rare. When the critical point is approached ξ diverges and the exponential factor vanishes so we recover the power law behaviour.

Distribution of largest clusters

We have up to now described the distribution of all the clusters without distinction. One can ask for finer distributions such as the distribution of the biggest cluster for a system with N sites. More generally one may ask for the distribution of the k^{th} largest cluster. We will only discuss in this section the case of the largest clusters. Exact results exist for the distribution of the largest cluster in subcritical percolation [9] and even for the Potts model in general [10]. Let us consider a d-dimensional hypercubic lattice composed of $N = L^d$ sites and let us denote S_i the random variable which equals the size of the largest cluster centred at site i and 0 if no cluster is centred at i. The S_i are identically distributed but are correlated due to excluded volume effects. We note $S_{(N)} = \max_{1 \leq i \leq N} S_i$ the size of the largest cluster. In the case of subcritical percolation, Bazant considered the cumulative distribution function of the largest cluster size $F_N(s) = \text{Prob}(S_{(N)} \leq s)$. As in subcritical percolation the cluster size distribution $n(s)$ decreases exponentially as $n(s) \sim s^{-\tau} e^{-s/s_\xi}$ with s_ξ a crossover size depending on p, Bazant assumes that the correlation of the S_i must be weak so that the S_i are drawn independently from the parent distribution $\text{Prob}(S_i \leq s) \sim 1 - e^{-s/s_\xi}$. The problem is then reduced to the much simpler problem of the extreme statistics of independent identically distributed random variables. Bazant showed that this leads to:

$$\lim_{N \to \infty} F_N(s) = G((s - s_\xi \log N)/s_\xi) \tag{4}$$

with G the Gumbel (or Fisher-Tippet) distribution such that $G(z) = e^{-e^{-z}}$. This form was checked numerically and later proved in [10] where were also treated some other case of correlated percolation.

0.3 Potts model

0.3.1 Definition

The Potts model is defined as a possible generalisation of the Ising model. Instead of being restricted to two values the spin variables can take Q values in the Q state Potts model. We are interested in the ferromagnetic Potts model whose Hamiltonian is written as:

$$\mathcal{H} = -J \sum_{\langle ij \rangle} \delta_{S_i S_j} \ , \tag{5}$$

where the sum is over all nearest neighbours pairs of spins of a d-dimensional system, $J > 0$ and δ the Kronecker delta and S_i the spin at site i taking integer values in $[1, Q]$. The Ising hamiltonian is related to this hamiltonian with the simple transformation $2J_{\text{Potts}} = J_{\text{Ising}}$ and $Q = 2$. This model undergoes a magnetic phase transition at the inverse temperature $\beta_c = 1/T_c$ and this transition is continuous for $Q \leq Q_c(d)$. For $d = 2$, $Q_c(2) = 4$ and $\beta_c = \ln(1 + \sqrt{Q})$ for the square lattice [11].

0.3.2 Random-cluster model

We will now describe a model very closely related to the Potts model and that sheds an interesting light on it. For a general and mathematical introduction of the random-cluster model see the review by Grimmett for example [12], from which we follow the presentation of the model. The random-cluster model (RCM) can be defined on a graph $G = (V, E)$ with V and E the vertices and the edges of the graph. In the RCM, a configuration ω in Ω the space of all configurations corresponds to the states of the edges which can be either open or closed as in bond percolation. An edge $e \in E$ is open if $\omega(e) = 1$ and closed $\omega(e) = 0$. We note $k(\omega)$ the number of connected components of open edges in the configuration ω, which includes the isolated vertices in contact with no open edges. The RCM has two parameters $p \in [0, 1]$ and $Q > 0$ and its partition function equals:

$$\mathcal{Z}_{RCM}(p, Q) = \sum_{\omega \in \Omega} \left[\prod_{e \in E} p^{\omega(e)} (1-p)^{1-\omega(e)} \right] Q^{k(\omega)}. \tag{6}$$

For $Q = 1$, the factor $Q^{k(\omega)}$ equals 1 so the edges are open or closed independently from the others. We thus recover bond percolation but for $Q \neq 1$, the state of an edge depends on the state of the other edges through the term $Q^{k(\omega)}$. This term favours configurations with many (few) clusters for $Q > 1$ ($Q < 1$). The limit $Q \to 0$ describes electrical networks and is linked to works by Kirchhoff in the 19^{th} century. This model was introduced in a serie of articles by the Dutch physicists Cees Fortuin and Pieter Kasteleyn in 1972 [13, 14, 15]. They showed that the partition function of the Potts model can be recast into a RCM partition function as we will explain in more details. This is not obvious at first as the Potts model has its spin variables located on the vertices of the graph or lattice considered and

not on the edges. In the following we will note $K = \beta J$ the coupling appearing in the partition function $\mathcal{Z}(K, Q)$ of the Q Potts at inverse temperature β. The transformation is as follows:

$$\mathcal{Z}(K,Q) = \sum_{\{\sigma\}} e^{K \sum_{\langle i,j\rangle} \delta_{\sigma_i,\sigma_j}} = \sum_{\{\sigma\}} \prod_{\langle i,j\rangle} e^{K\delta_{\sigma_i,\sigma_j}}, \tag{7}$$

then a simple rewriting of the exponential gives:

$$e^{K\delta_{\sigma_i,\sigma_j}} = e^K\ [(1-e^{-K})\delta_{\sigma_i,\sigma_j} + e^{-K}], \tag{8}$$

$$\mathcal{Z}(K,Q) = e^{mK} \sum_{\{\sigma\}} \prod_{\langle i,j\rangle} [p\delta_{\sigma_i,\sigma_j} + (1-p)], \tag{9}$$

with $p = 1 - e^{-K}$. Now we use the identity $a + b = \sum_{n=0}^{1} [a\delta_{n,0} + b\delta_{n,1}]$ on each bond $\langle i, j\rangle$ by introducing an auxiliary variable n_{ij}:

$$\mathcal{Z}(K,Q) = e^{mK} \sum_{\{\sigma\}} \sum_{\{n\}} \prod_{\langle i,j\rangle} [p\delta_{\sigma_i,\sigma_j}\delta_{n_{ij},1} + (1-p)\delta_{n_{ij},0}], \tag{10}$$

$$\begin{aligned}\mathcal{Z}(K,Q) =& e^{mK} \sum_{\{n\}} \left(\prod_{\langle i,j\rangle, n_{ij}=1} p \right) \left(\prod_{\langle i,j\rangle, n_{ij}=0} (1-p) \right) Q^{k(n)} \\ =& e^{mK}\, \mathcal{Z}_{RCM}(p,Q)\end{aligned} \tag{11}$$

where $k(n)$ is the number of bond clusters. Apart from an unimportant overall factor, the Potts partition function is equal to an RCM partition function. One can remark that, in addition to the limit $Q \to 0$ for electrical networks and $Q = 1$ for bond percolation, we can add the Q states Potts model for all integer Q to the family of models described by the RCM. But we also note that under this form Q can be real and not only integer as in the original formulation of the Potts model with its spin variables. The RCM thus interpolates in some sorts between various Potts model, and for example it has been fruitful to study percolation as a limit of the Potts model with $Q \to 1$ [16]. The RCM gives an alternative description of the Potts model in terms of clusters. For example the onset of long-range correlations at the critical temperature corresponds to a percolation transition in the RCM. All the Potts physical observables are equivalent to cluster observables in the RCM, for example the magnetisation is related to the size of the biggest cluster. The clusters generated by the RCM are called the Fortuin-Kasteleyn (FK) clusters and the RCM is often called the Potts model in FK representation in the physics literature.

In addition to the FK clusters, we can also define another type of clusters by the same construction as before with $p = 1$, *i. e.* all bonds connecting spins with equal value are open. We will call the connected components of such a construction same-spin clusters or simply spin clusters. Those clusters are the one occurring naturally in experimental realisations of the Potts model and are most frequently studied in coarsening and more generally

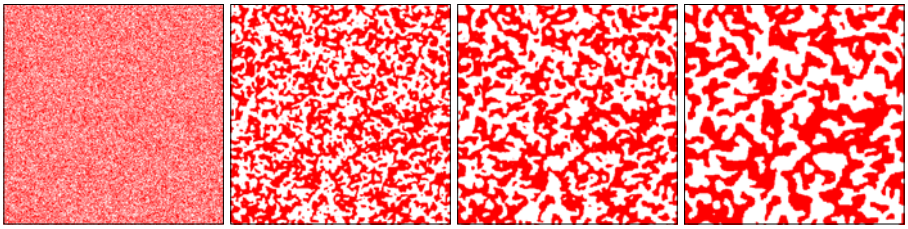

Figure 2 – Spashots of system configuration at different times after a quench from $T_i = \infty$ to $T_f = 0.01T_c$ done at time $t = 0$. The four snapshots correspond from left to right to $t = 0$, $t = 10$, $t = 20$ and $t = 40$ where the time is counted in Monte Carlo steps.

out of equilibrium situations as we will see the next section section and in chapters 1 and 2. The spin clusters also undergo a continuous percolation transition but at a temperature T_s in general different from T_c. It is only in $d = 2$ that $T_s = T_c$, hence both types of clusters are self-invariant at the critical temperature. We will detail more in chapter 3 the physics of spin clusters which is quite subtle.

0.4 Dynamics and coarsening

Up to now we have described percolation and the Potts model in equilibrium situations. However in this manuscript we will often be interested in out of equilibrium situations. In this section we will describe a certain type of out of equilibrium situations, namely phase ordering dynamics which is relevant for our work. As before, we will not attempt to be exhaustive but rather to give a general flavour of the subject and describe in more details the aspects that we will use.

0.4.1 Phase separation

We will often be concerned with a certain type of non-equilibrium situation corresponding to systems quenched from a disordered phase to an ordered one. As a simple case we can consider the ferromagnetic $2d$ Ising model quenched from an initial temperature $T_i > T_c$ to a temperature $T_f \leq T_c$. We show in figure 2 snapshots of a $2d$ Ising model quenched from $T_i = \infty$ to $T_f = 0.01T_c$ at time $t = 0$. The system is out of equilibrium but a mosaic of ordered domains appear which sizes grow with time. The prediction of the domain growth law and of the form of different correlation functions are well known in a variety of situations [17, 18].

0.4.2 The dynamical scaling hypothesis

This type of situations are difficult to study as there exists no such framework as in equilibrium statistical physics. However great advances were done by formulating a simple hypothesis. It was remarked in experimental and numerical studies of coarsening systems

that there exists a unique characteristic length $L(t)$ such that the domain structure is independent of time when all distances are scaled by $L(t)$. This is referred to as the *dynamical scaling hypothesis*. It is an hypothesis because it has only been proved in simple cases such as the one dimensional Ising model with Glauber dynamics and the $O(n)$ with $n \to \infty$, but it is strongly supported by numerous simulations and experiments. The expression of $L(t)$ depends on the characteristics of the system considered and for the Ising model we consider it behaves as $L(t) \sim t^{1/z}$ with z the dynamical critical exponent.

0.4.3 Renormalisation group approach

The idea of dynamical scaling can in fact be extended and used in a powerful way with a renormalisation group approach. For systems at equilibrium, the renormalisation group has brought a systematic approach to critical behaviour by introducing the concept of universality classes [19, 20]. If two (very) different systems are found to be in the same universality class, then there critical behaviour will be governed by the same set of critical exponents. The same kind of classification can be done for the different dynamical behaviours but one has to keep in mind that this relies in general on a scaling hypothesis and no fixed points can be explicitly shown.

In our description of the system considered we have omitted an important aspect: the dynamics type. If the evolution of the Ising model is achieved with a usual single spin flip Monte Carlo algorithm, at each update a spin can be flipped or not using a dynamical rule. It means that the number of up and down spins is not conserved. This type of dynamics is called *non-conserved* order parameter dynamics. If we want to use this system to mimic the phase separation of a binary alloy, the number of atoms of each species has to be conserved. This type of dynamics is called *conserved* order parameter dynamics. The two types of dynamics do not belong to the same universality class and are not governed by the same critical exponent. This shows that the equilibrium and dynamical universality classes are not identical or more precisely that a single equilibrium class can be divided into several dynamical classes depending on the constraints on the dynamics. More generally dynamics can be classified as in the work of Hohenberg and Halperin [21].

0.4.4 Influence of the initial condition

From what we said before, we could imagine that once the type of order parameter, the dimension, the type of dynamics, and the working temperature are fixed the universality class is completely determined. This is however not exact and one has to look more carefully at the initial condition. Taking as before the $2d$ Ising model and quenching it from $T_i \geq T_c$ to $T_f \leq T_c$, how many universality classes are there? Let us first consider quenches with $T_i > T_c$. For all those temperatures in the paramagnetic phase the correlations decay exponentially fast and as we are concerned with the long distance properties all those quenches are similar to the one where $T_i = \infty$. When $T_f < T_c$, the question is whether the thermal fluctuations change the behaviour from the zero-temperature one.

As the infinite temperature point is attractive for the whole paramagnetic phase $T > T_c$, the zero-temperature point is attractive for the ferromagnetic phase $T < T_c$. This can be shown explicitly in some cases where the order parameter is conserved and in those cases a non-zero final temperature simply changes non-universal quantities. The critical point is of course special either as the initial or final temperature. For $T_i = T_c$ the correlations decay algebraically with an exponent related to the anomalous dimension η so they cannot be neglected. When $T_f = T_c$ the properties at equilibrium are different than in the ferromagnetic phase and so we can expect that the dynamic properties are going to be different from $T_f < T_c$. So, similarly to the equilibrium case, we are left with only three different points, the two attractive ones $T = \infty$ and $T = 0$ and the repulsive one $T = T_c$.

0.4.5 Possible types of quenches

As we have seen, there are only three interesting temperature fixed points $T = 0$, $T = T_c$ and $T = \infty$. As the only interesting dynamical cases are $T_f = T_c$ and $T_f = 0$, this makes four possible quenches. We will study the two quenches to T_c in chapter 1 and the two quenches to $T = 0$ in chapter 2. With this we will have exhausted the possible types of temperature quenches. Of course one could imagine other types of quenches starting from a correlated initial condition other than the critical one by crafting one with a certain algebraic decay. It might be interesting to test if the dynamical universality classes depend indeed continuously on the exponent ruling the decay of the initial correlations but we have not considered such cases in this manuscript [22, 23, 24].

0.5 Organisation of the manuscript

This thesis is composed of four chapters which are mostly independent. The two first chapters are concerned with dynamic situations, namely critical and subcritical quenches. They deal with similar subjects but one can be easily read independently of the other. The third chapter deals with wrapping probabilities of Ising spin clusters at equilibrium. The last chapter describes the equilibrium critical properties of the Ising model with long-range interactions. We will indicate during the manuscript if certain pieces have been the subject of a publication.

Bibliography

[1] Thibault Blanchard, Leticia F. Cugliandolo, and Marco Picco. A morphological study of cluster dynamics between critical points. *J. Stat. Mech.: Theo. Exp.*, 2012(05):P05026, May 2012.

[2] T. Blanchard, M. Picco, and M. A. Rajabpour. Influence of long-range interactions on the critical behavior of the Ising model. *EPL*, 101(5):56003, March 2013.

[3] T. Blanchard and M. Picco. Frozen into stripes: Fate of the critical Ising model after a quench. *Phys. Rev. E*, 88(3):032131, September 2013.

[4] T. Blanchard. Wrapping probabilities for ising spin clusters on a torus. *J. Phys. A: Math. Theor.*, 47(34):342002, August 2014.

[5] T. Blanchard, F. Corberi, L. F. Cugliandolo, and M. Picco. How soon after a zero-temperature quench is the fate of the Ising model sealed? *EPL*, 106(6):66001, June 2014.

[6] S. R. Broadbent and J. M. Hammersley. Percolation processes. *Mathematical Proceedings of the Cambridge Philosophical Society*, 53:629–641.

[7] Dietrich Stauffer and Amnon Aharony. *Introduction to percolation theory*. Taylor & Francis, 1994.

[8] Geoffrey Grimmett. *Percolation*. Springer, May 1999.

[9] Martin Z. Bazant. Largest cluster in subcritical percolation. *Phys. Rev. E*, 62(2):1660–1669, 2000.

[10] Remco van Der Hofstad and Frank Redig. Maximal clusters in non-critical percolation and related models. *J Stat Phys*, 122(4):671–703, February 2006.

[11] F. Y. Wu. The Potts model. *Reviews of Modern Physics*, 54(1):235, January 1982.

[12] Geoffrey R. Grimmett. *The Random-Cluster Model*. Springer, December 2006.

[13] C. M. Fortuin and P. W. Kasteleyn. On the random-cluster model : I. introduction and relation to other models. *Physica*, 57(4):536, February 1972.

[14] C. M. Fortuin. On the random-cluster model II. the percolation model. *Physica*, 58(3):393–418, April 1972.

[15] C. M. Fortuin. On the random-cluster model : III. the simple random-cluster model. *Physica*, 59(4):545–570, June 1972.

[16] J. L. Cardy. Critical percolation in finite geometries. *J. Phys. A: Math. Gen.*, 25(4):L201–L206, February 1992.

[17] A.J. Bray. Theory of phase-ordering kinetics. *Advances in Physics*, 43(3):357–459, 1994.

[18] Malte Henkel and Michel Pleimling. *Non-Equilibrium Phase Transitions: Volume 2: Ageing and Dynamical Scaling Far from Equilibrium*. Springer, January 2011.

[19] John L. Cardy. *Scaling and Renormalization in Statistical Physics*. Cambridge University Press, April 1996.

[20] Daniel J. Amit and Victor Martin-Mayor. *Field Theory, the Renormalization Group, And Critical Phenomena: Graphs To Computers*. World Scientific Publishing Company, Incorporated, January 2005.

[21] P. C. Hohenberg and B. I. Halperin. Theory of dynamic critical phenomena. *Rev. Mod. Phys.*, 49(3):435, July 1977.

[22] Alan Picone and Malte Henkel. Response of non-equilibrium systems with long-range initial correlations. *J. Phys. A: Math. Gen.*, 35(27):5575, July 2002.

[23] Alan Picone and Malte Henkel. Local scale-invariance and ageing in noisy systems. *Nuclear Physics B*, 688(3):217–265, June 2004.

[24] Sreedhar B. Dutta. The role of initial conditions in the ageing of the long-range spherical model. *J. Phys. A: Math. Theor.*, 41(39):395002, October 2008.

CHAPTER 1

Critical quenches

Contents

1.1 Introduction

The work presented in this chapter was the subject of the publication [1]. We study the geometric properties of a system initially in equilibrium at a critical point that is suddenly quenched to another critical point and subsequently evolves towards the new equilibrium state. We focus on the bidimensional Ising model and we use numerical methods to characterize the morphological and statistical properties of spin and Fortuin-Kasteleyn clusters during the critical evolution. The analysis of the dynamics of an out of equilibrium interface is also performed. We show that the small scale properties, smaller than the target critical growing length $\xi(t) \simeq t^{1/z}$ with z the dynamic exponent, are characterized by

equilibrium at the working critical point, while the large scale properties, larger than the critical growing length, are those of the initial critical point. These features are similar to what was found for sub-critical quenches. We argue that quenches between critical points could be amenable to a more detailed analytical description.

The relaxation dynamics of a macroscopic system taken to its critical point with some quenching protocol has received much attention. Most of the existing studies focused on the time evolution of global quantities (magnetization, susceptibility, correlation functions, etc.) and characterized their scaling properties with numerical simulations and renormalization group techniques [2, 3, 4, 5]. These studies are not restricted to any spatial nor order parameter dimensionality.

In *two dimensional* critical systems in equilibrium, powerful theoretical tools such as Coulomb gas methods [6], conformal field theory (CFT) [7] and stochastic Loewner evolution (SLE) [8, 9, 10], allowed one to characterize the geometric and statistical properties of a large variety of mesoscopic observables in great detail. These objects give a more complete image of the system's equilibrium configurations than the global observables accessed with scaling arguments and renormalization group techniques. We will discuss an application of Coulomb gas methods to obtain wrapping probabilities in chapter 3. However, as far as we know, nothing is known about these objects during the out of equilibrium evolution of the same (and other) critical samples.

An extensive numerical and analytic investigation of the *coarsening sub-critical dynamics* of two dimensional models from a mesoscopic point of view was carried out in recent years. The models treated were the clean Ising model with non-conserved [11, 12, 13] and conserved [14] order parameter dynamics, the random ferromagnet with non-conserved order parameter dynamics [15] or still the q state Potts model [16, 17]. These studies allowed one to build a rather complete picture of the geometric and statistical properties of the spin clusters in these bidimensional systems. More precisely, their domain and hull-enclosed areas as well as their boundary lengths and the relation between areas and perimeters were analyzed and characterized in detail.

The aim of this chapter is to present a similar study of relevant dynamic geometric objects during the critical non-equilibrium evolution of the $2d$ Ising model evolving from equilibrium at another critical point, in this case an infinite temperature configuration that is equivalent to critical uncorrelated site percolation. We use simple scaling arguments and extensive numerical simulations.

Let us be more specific about the objects of our study. The most natural objects to consider are the spin clusters, i.e. clusters of nearest neighbor spins on the lattice that point in the same direction. These clusters are accessible via direct observation of the system. However, at the critical point, and as we have seen in the introduction, they are not appropriate to describe the critical equilibrium properties of the Ising model since their shape and statistical properties are not only dictated by the physical correlations but also by purely geometrical factors [18, 19]. To remedy this problem one has to consider, in place, smaller clusters, namely the Fortuin-Kasteleyn (FK) ones, that capture exclusively the equilibrium physical correlations in the system. Although not relevant to describe the

equilibrium physical macroscopic properties of the samples the spin clusters are, nonetheless, also critical at the phase transition. Consequently, they are characterized by a different set of exponents from the ones of the FK clusters. For this reason spin clusters are also interesting to analyze and we study both types of clusters here. In fact it is interesting to note that in most out of equilibrium studies, the only clusters studied are the spin clusters while at equilibrium it is mostly the FK clusters.

This chapter is organized as follows. In Sec. 1.2 we list the definitions of the different objects we study and recall the results obtained for subcritical quenches. The concrete analysis is presented next in Sec. 1.3. We first check that the dynamical exponent z governing the critical dynamics of spin clusters is actually the one of the $2d$ Ising model, as obtained with other means, as the dynamic renormalization group method [3]. To the best of our knowledge, this has never been brought to light before. We then study in full extent the number densities of various quantities giving access to the structure of spin clusters on a large interval of sizes. The validity of the dynamical scaling hypothesis is tested upon these number densities. Relations between areas and boundaries are also explored. The same method is applied to the FK clusters. We later turn our attention to the dynamics of a single interface and the comparison with the equilibrium results given by conformal field theory and stochastic Loewner evolution. This is the content of Sec. 1.3. Finally, in Sec. 1.4 we consider a critical quench from the ordered phase.

1.2 Scaling of cluster quantities

1.2.1 A few hints on conformal field theory

The existence of two types of critical clusters, the spin and FK ones belonging to distinct universality classes is valid for all q-state Potts model with $0 \leq q \leq 4$ in two dimensions. In order to understand this point it is useful to consider the Coulomb gas formulation of the Potts model [6]. In this formulation, the $2d$ q-state Potts model can be described by the parameter $\kappa \in [4, 8]$ such that

$$\sqrt{q} = -2\cos\left(\frac{4\pi}{\kappa}\right). \tag{1.1}$$

We choose a convention such that κ also corresponds to the SLE parametrization for the interfaces associated to the q-state Potts model. We will come back to this point in Sec. 1.3.4 where we will study the behaviour of an out of equilibrium interface. The parameter κ is also related to the central charge of the corresponding conformal field theory by the relation [6, 7]:

$$\mathrm{c} = \frac{1}{4}(6-\kappa)\left(6-\frac{16}{\kappa}\right). \tag{1.2}$$

For $\kappa \in [8/3, 4]$ this Coulomb gas representation describes another class of models, the *tricritical Potts model*, i.e. Potts models with dilution. Note that the central charge is

invariant under the transformation $\kappa \to 16/\kappa$ which maps a critical q-state Potts model onto a tricritical Potts model with a different number of states given by eq. (1.1). This means that there exist two critical theories for a given central charge. One is associated to the critical Potts model and the relevant structures are the FK clusters. The other one is the tricritical Potts model and the relevant clusters are the domains or spin clusters. This duality is such that the geometrical clusters of one model are the FK clusters of the other model and vice versa [20, 21].

The tricritical model associated to the $2d$ Ising model ($\kappa = 16/3$) is the dilute $q = 1$ Potts ($\kappa = 3$). Both models possess the same central charge $\mathrm{c} = 1/2$ but the same quantities in the two model are not associated to the same operators of the CFT. In $2d$ the spin clusters of the Ising model are the critical objects of the dilute $q = 1$ Potts model [22]. This explains why the percolation exponents associated to the spin clusters are not related to the Ising model exponents but in fact are those of the tricritical $q = 1$ Potts model, described by $\kappa = 3$.

The critical exponents can then be expressed in term of κ. For instance, the fractal dimensions D_c, D_h and D_{ep} of the cluster area, its hull and its external perimeter (a precise definition of these quantities will be given in subsection 1.2.2) read [23, 20]:

$$D_c = 1 + \frac{3\kappa}{32} + \frac{2}{\kappa}, \tag{1.3}$$

$$D_h = 1 + \frac{\kappa}{8}, \tag{1.4}$$

$$D_{ep} = 1 + \frac{2}{\kappa}. \tag{1.5}$$

Note that the duality $\kappa \to 16/\kappa$ relates the fractal dimension of the external perimeter to the dimension of the hull of the dual model, such as $D_{ep}(\kappa) = D_h(16/\kappa)$ for $\kappa \geq 4$. This relation is called Duplantier duality [20]. For $\kappa < 4$ the external perimeter coincides with the hull since they are no fjords. In this case the relation between D_{ep} and D_h mentioned above does not hold anymore and in fact $D_{ep} = D_h$.

	c	κ	q	D_c	D_h	D_{ep}
percolation	0	6	1	91/48	7/4	4/3
Ising FK clusters	1/2	16/3	2	15/8	5/3	11/8
Ising spin clusters	1/2	3	1	187/96	11/8	11/8

Table 1.1 – Central charge, c, Coulomb gas or SLE parameter, κ, Potts model parameter, q [all these related by eqs. (1.1) and (1.2)], and three fractal dimensions at the percolation threshold, and for FK and spin clusters at the critical point of the $2d$ Ising model. The *c* subscript in the fractal dimension is for the cluster mass, the *h* one for its hull, and *ep* for its external perimeter.

Finally, let us note that the existence of two types of critical clusters at the critical point is specific to the $2d$ Potts model. While the FK clusters can be defined for more general

models, nothing ensures that they are critical at the transition point. For instance, FK clusters are not critical at the critical point in $2d$ parafermionic models [24]. Concerning the spin clusters, it is not even sure that they are critical at the critical point as for example in the $3d$ Ising model for which they undergo a percolation transition at a temperature different from the critical one [25].

1.2.2 Definitions

In this section we define the quantities that we will consider in this chapter. We call a *domain* or *spin cluster* a connected set of sites with spins taking the same value. The *mass* (area in $2d$) of a domain is the number of sites belonging to it. A *broken bond* is a link of the lattice between two neighboring spins with different value (see Fig. 1.1).[1]

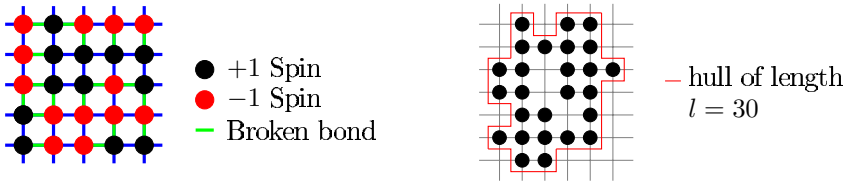

Figure 1.1 – Left: sketch of an Ising spin configuration with the two-valued spins represented by black and red (black and grey) dots on the square lattice sites. Broken bonds are drawn with green (light grey) lines on the edges of the lattice. Right: a domain is singled out and its hull is represented with a thin red line.

The *domain wall* of a spin cluster is its external and internal contour, constructed as follows. One first generates a dual lattice by placing a site at the center of each plaquette of the original lattice. Next, the links on the dual lattice that cross broken bonds on the original lattice are joined together. In this way, one finds a closed loop on the dual lattice that runs along the internal or external boundary of a spin cluster in the way sketched in Fig. 1.1 for the external component. There is not much theoretical knowledge on this object and it is therefore more convenient to study other geometrical quantities which have received a theoretical description in equilibrium.

The *hull* of a cluster is restricted to the external part of the contour, that is to say, one excludes the contribution of the holes of the cluster (see Fig. 1.1). The *hull enclosed area* is the area, i.e. the total number of sites, inside the hull (the holes within the domains are thus filled). In the example in the right of Fig. 1.1 the hull-enclosed area is 29.

The length of the different types of contours defined above and living on the dual lattice is computed by counting the number of broken bonds corresponding to the object of concern that are crossed by the boundary. We can also define the *external perimeter* built by closing the narrow gates of the hull, making in this way a smoother version of the contour by eliminating the deep fjords. The meaning of narrow will be discussed later. As an example, on a square lattice, a cluster composed of a unique spin has a hull of length 4 and

[1] In all the figures we use a square lattice for simplicity. The extension to the triangular lattice considered later should be straightforward.

an area equal to 1 while for a two-spin cluster the hull length is 6 and the area equals 2.

The FK clusters are defined on the edges of the lattice and not on the sites of the lattice as for the spin clusters. Therefore the length of their contour on the dual lattice is not proportional to the number of broken bonds. Indeed some bonds linking two sites of a FK cluster may not be within the cluster if they have not been kept in the construction of the cluster. In order to define the border of an FK cluster we then use a different sub-lattice, with four sites associated to an original one as shown in Fig. 1.2. The distance between two nearest-neighbor sub-sites counts as the unit of length for the contour. As an example, the cluster in Fig. 1.2 has a hull length of 24.

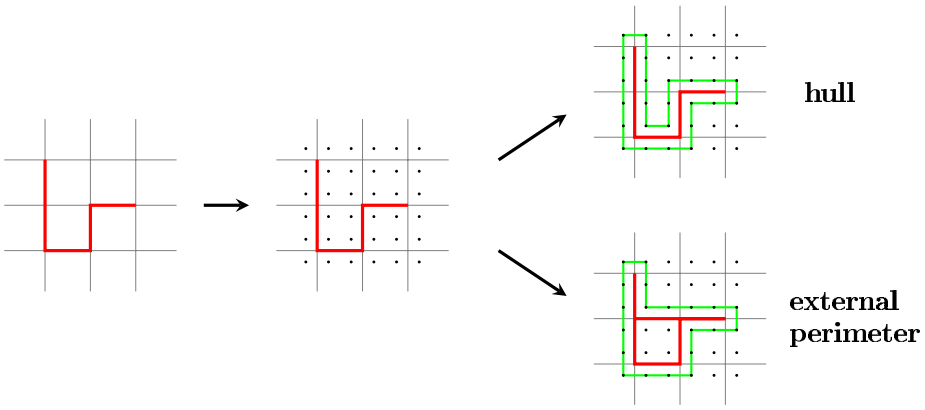

Figure 1.2 – Left: an example of an FK cluster. Center: the sites of the sub-lattice associated to the original square lattice are added as small points. Right: the hull and the external perimeter of the chosen FK cluster are shown with a thin green line.

In Fig. 1.2 we also present the construction of the external perimeter of an FK cluster. To measure its length, the procedure is the following: all the bonds between nearest-neighbor sites (on the original lattice) belonging to the FK cluster are drawn, and then the walker is allowed to wander around this new cluster, that is to say, on the sites of the sub-lattice introduced before. The external perimeter is a smoother version of the hull and it has, consequently, a smaller fractal dimension. The cluster in Fig. 1.2 has an external perimeter of length 20 which is effectively smaller than its hull length.

1.2.3 Dynamical scaling of distributions

This work follows several works [26, 12, 27, 14] concerning the form that probability distributions of geometric observables take after a quench. Those works were carried for different situations but always for subcritical dynamic. The initial goal of the work presented in this chapter was to determine to which extent similar advances could be done for critical dynamics.

We detail here the derivation done in [26]. The authors use a continuum approximation for which it is known that the clusters interfaces have a velocity $v = -(\lambda/2\pi)\kappa$ during a

subcritical quench, where here κ is the local curvature of the interface and λ a constant depending on the system considered. This equation is known as the Allen-Cahn equation. We are interested in the evolution with time of hull-enclosed areas. Let A be a hull-enclosed area, its evolution with time is obtained by integrating the velocity on the hull:

$$\frac{\mathrm{d}A}{\mathrm{d}t} = \oint v \mathrm{d}l = -\frac{\lambda}{2\pi} \oint \kappa \mathrm{d}l. \tag{1.6}$$

To compute the remaining integral they used the Gauss-Bonnet theorem which is a general result connecting the geometry of two-dimensional compact manifolds to their topology. It relates the integral of the curvature on the boundary to the Euler characteristics χ of the manifold $\oint \kappa \mathrm{d}l = 2\pi\chi$. For a disk $\chi = 1$ which finally gives the simple result:

$$\frac{\mathrm{d}A}{\mathrm{d}t} = -\lambda. \tag{1.7}$$

This means that each hull sees its area $A(t)$ decrease at a constant rate independent of A which translates into a certain invariance for the distribution $n_h(A,t)$ of hull-enclosed area in the way that for $t_2 > t_1$, $n_h(A,t_2) = n_h(A + \lambda(t_2 - t_1), t_1)$. This implies that if the distribution is known at one moment it is known at all times. For a system with a triangular lattice, the cluster are initially in a critical percolation state as $p_c = 1/2$. But actually on other lattices we have already mentioned that the clusters become critical percolation like very quickly after the quench, let us say after a time t_p. We will study the apparition of critical percolation in great detail in chapter 2. So in any case the system is at one point a realisation of critical percolation so we need to know the form of hull-enclosed area number distribution in this case. The hull-enclosed areas do not exhibit a fractal structure since they have no holes. Their fractal dimension and their Fisher exponent is therefore 2. Their boundaries behave differently and they are fractal. Furthermore, Cardy and Ziff [28] showed that the number density of hull-enclosed areas behaves as:

$$n_h(A) \sim \frac{C}{A^2} \tag{1.8}$$

for $L^2 \gg A^2 \gg a^2$ with $C = 1/(8\sqrt{3}\pi)$ at the percolation threshold and $C = 1/(16\sqrt{3}\pi)$ for Ising spin clusters. The microscopic cut-off a is the lattice spacing. With this result we can now know the form of the distribution at all times. For infinite temperature, we have $n_h(A,t) = n_h(A + \lambda(t - t_p), t_p) \simeq n_h(A + \lambda t, t_p)$ as t_p is very small so that in practice we consider times such that $t \gg t_p$. For critical initial temperature it gives $n_h(A,t) = n_h(A + \lambda t, 0)$, so to summarise:

$$\begin{aligned} n_h(A,t) &= \frac{2C}{(A+\lambda t)^2} \quad \text{for} \quad T_i \to \infty, \\ n_h(A,t) &= \frac{C}{(A+\lambda t)^2} \quad \text{for} \quad T_i = T_c, \end{aligned} \tag{1.9}$$

where $C = 1/(16\sqrt{3}\pi)$ hence the factor 2 in the numerator of the first equation. In this derivation, we have not used any dynamical scaling hypothesis but we can easily check that the expressions obtained are of the form:

$$n_h(A,t) = (\lambda t)^{-2} f(A/\lambda_h t) \quad \text{with} \quad f(x) = \frac{2C}{(1+x)^2}. \tag{1.10}$$

Indeed since the relevant length during the dynamics is $\xi(t) \sim t^{1/2}$, the typical area is proportional to $\xi(t)^2 \sim t$. The overall factor $\sim t^{-2}$ comes from the fact that hulls disappear during the dynamic. It is quite remarkable that the derivation does not use dynamical scaling and in fact it demonstrates the validity of the dynamical scaling [26].

For a system with periodic boundary conditions, clusters wrapping around the system may be present. In this case their hull is formed of two circles and their Euler characteristic χ is no longer 1 but equals 0. This means that their hull-enclosed area should be constant with time. A consequence of this fact is that they do not shrink and disappear as other clusters and that they are present in the system during all the coarsening regime. We will discuss such clusters in chapter 2.

1.3 Critical dynamics

The stochastic relaxation dynamics after a quench to the critical point has been performed with a time dependent extension of the renormalization group method. Scaling laws for averaged global observable such as correlation functions and others have been obtained in many different systems. The growth of an equilibration length, $\xi(t) \sim t^{1/z}$ with z the dynamic critical exponent, was evidenced. In this section we study the critical dynamics from a mesoscopic point of view and we show that this growing length also plays an important role in the characterization of the statistical properties of fluctuating quantities.

1.3.1 Description of the protocol

In this section we study the evolution of a system after a quench from $T = \infty$ to T_c. We first consider spin clusters on a triangular lattice for which $T_c = 4/\ln 3$. The choice of a triangular lattice is motivated by the fact that the infinite temperature point exactly corresponds to a site percolation critical point on this lattice. Indeed, the site percolation threshold for this lattice is $p_c = 1/2$ [29] so that, if we consider the number density of domains, the system is exactly at the percolation threshold at infinite temperature where the spins take the values 1 or -1 with equal probability. For the quench considered, the system is initially in equilibrium at a critical state and after the quench it evolves towards equilibrium at another critical state, the one at T_c.

At infinite temperature FK clusters are not critical, actually they are trivial, for any lattice so it is immaterial to use the triangular or any other one. For this reason, in our study we used a square lattice. For the square lattice $T_c = 2/\ln(1+\sqrt{2})$ and the infinite

temperature point is *not* a critical one for the spin clusters since here $p_c > 1/2$. (Having said this, the studies in [11, 12, 13] showed that, somehow surprisingly, the sub-critical Monte Carlo dynamics of such a non-critical initial state gets, after a few time steps, very close to the critical percolation point as far as the properties of spin clusters are concerned. For instance, their number densities rapidly develop the critical percolation tails and only later the dynamics evolve towards the target equilibrium state at low temperature. We will discuss this phenomenon in chapter 2.)

The simulations were carried out on a lattice of linear size L with periodic boundary conditions in both directions. For the initial condition at infinite temperature, the spins were chosen randomly with equal probability of being up or down. Once the system was prepared in the desired initial condition, single spin updates were performed at the temperature of the quench. A Monte Carlo time step (MCs) corresponds to L^2 single spin updates. The updates were accepted or rejected via the standard Monte Carlo Metropolis scheme. We gathered around $6\ 10^5$ independent samples. Unless stated otherwise, the lattice used has a linear size $L = 1000$ for the analysis of spin clusters and $L = 320$ for the study of FK clusters. For each sample we computed the desired quantities every 2^n MCs with $n \in [1, 12]$.

For the spin clusters, the algorithm distinguishes first between the internal and external part (hull) of the perimeter and then calculates the length of the hulls, i.e. the number of broken external bonds. To do so the lattice is scanned and when a broken bond that has not been counted yet is found, the algorithm follows the boundary in a precise direction and keeps track (with a cumulative angle) of the path followed. Then, depending on the sign of the angle the boundary drawn is an external or an internal one. Some clusters (wrapping ones) have a boundary with a vanishing angle. Those boundaries run across the system from one side to another so they are not homotopic to a point on the torus. We checked that these clusters are sufficiently rare so that we can discard them without affecting the statistics. For the FK clusters the process is the same on the sub-lattice evoked above. The algorithm walks on the sub-lattice around the FK clusters and once a contour is formed, the angle is measured to discriminate between internal and external contours and their lengths are computed.

The number densities obtained via this Monte Carlo method present a great dispersion, especially for large clusters which are much rarer than the small ones. This dispersion has been greatly suppressed by choosing appropriate bin sizes to construct the histograms, and to extract from them the distributions.

1.3.2 Spin clusters

We first briefly present the simulations performed to check whether the dynamical exponent governing the dynamics of the spin clusters conforms to the one extracted from the analysis of the correlation functions that is well documented in the literature [30, 31, 4]. Then we present the results for the spins clusters on a triangular lattice after the quench.

The dynamic exponent

As explained in Sec. 1.2.1, the critical geometric clusters of the $2d$IM are well understood as they are the FK clusters of the tricritical $q = 1$ Potts model. However, it is not obvious whether this correspondence should hold in an out of equilibrium situation, typically a quench towards the critical point. In particular, one may wonder whether the dynamical exponent z for spin clusters is the Ising one. To check this reasonable assumption, we calculated specific quantities that allow us to extract spin clusters exponents. For example, in equilibrium, the size of the largest spin cluster scales as $L^{-(\beta/\nu)_{tri}}$ where $(\beta/\nu)_{tri} = 5/96$ and β_{tri} is the magnetic exponent of the tricritical $q = 1$ Potts model, ν_{tri} is the exponent associated to the divergence of the correlation length and L is the linear size of the sample. We denote this quantity M_g. We now consider a quench from $T = 0$ to T_c for different system linear sizes L, and we compute $M_g(t)$. We consider this quench since the scaling form is simple in this case and the dynamical exponent should not depend upon the initial condition as long as we quench at the critical temperature. The inset of Fig. 1.3 shows the relaxation of this quantity for several sizes. We then apply the following scaling $M_g(t) \to M_g(t)L^{(\beta/\nu)_{tri}}$ and $t \to t/L^z$. The collapse of the different curves giving access to z is presented in Fig. 1.3. The value obtained is compatible with the most accurately estimated value $z = 2.1667\ (5)$ [31]. This gives strong evidence that the dynamics of the spin clusters are indeed governed by the Ising dynamical exponent z. In consequence we will use the same z for all the quantities computed in this work.

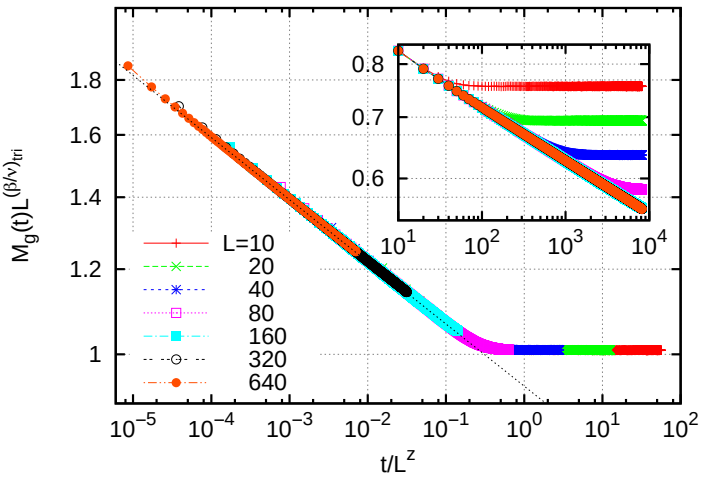

Figure 1.3 – Geometrical cluster magnetization $M_g(t)$. The main part shows the collapse onto a master curve with the rescaling $t \to t/L^z$ and $M_g(t) \to M_g(t)L^{(\beta/\nu)_{tri}}$. In the inset we show the raw data $M_g(t)$ versus time for different system linear sizes L.

Hull-enclosed area number density

In Fig. 1.4 we present the distribution of the hull-enclosed areas, $n_h(A,t)$, at different times after the quench. In the first panel, Fig. 1.4(a), we display the distributions, n_h, versus the hull-enclosed area A. As expected from the results of Cardy and Ziff [28], the slopes of the initial and asymptotical (equilibrium at T_c) distributions equal -2 in a double logarithmic plot but the prefactors are slightly different. For this reason, the changes occurring in the distributions are very small. Equilibrium data (generated with a special purpose algorithm at T_c) are shown with (green at $T \to \infty$ and red at T_c) dashed lines. The bumps at large sizes correspond to the spanning clusters with a linear size of the order of L, the linear size of the system, are finite size effects. Note that the position of the bump and the very last part of the $n_h(A,t)$ close to it, are almost time-independent (within our numerical accuracy and for the times accessed in the simulation).

For hull-enclosed areas dynamic scaling suggests

$$n_h(A,t) \simeq A^{-\tau}\, g\left(\frac{A}{t^{\alpha}}\right) \tag{1.11}$$

for $A_0 \ll A \ll L^2$ with $A_0 = a^2$ a microscopic area scale and L^2 the macroscopic one. To make the notation lighter we did not add any sub-script to τ and α. The exponents are given by

$$\tau = 1 + d/D, \qquad\qquad \alpha = D/z. \tag{1.12}$$

Since these areas are regular, i.e. they have no holes, $D = d = 2$ and

$$\tau = 2, \qquad\qquad \alpha = 2/z. \tag{1.13}$$

Consistency with the asymptotic limit requires $g(y \to 0) = C$ and $g(y \to \infty) = 2C$.

In order to test the dynamical scaling hypothesis, we impose the value $\tau = 2$ and rescale the areas by a factor t^{α} with α a free parameter whose value is determined by the collapse of the numerical data on a master curve. The best collapse is obtained for $\alpha = 0.92\ (5)$ and is seen in Fig. 1.4(b) with the theoretical percolation and Ising critical distributions being just horizontal after the given ordinate rescaling. The numerical equilibrium critical distributions (red dashed line for T_c and green dashed line for $T \to \infty$) have been placed at convenience (horizontally) to ease the comparison with the other distributions. The horizontal dotted lines correspond to the exact prefactors $C = 1/(16\sqrt{3}\pi)$ and $2C$ for the critical Ising and percolation distributions, respectively. The value of α is in agreement with the expected value $\alpha = 2/z \simeq 0.92306$ with $z \simeq 2.1667\ (5)$ [31] since the typical hull-enclosed areas scale as the square of the dynamical length scale $\xi(t) \sim t^{1/z}$. It is quite remarkable that, while no time-dependent rescaling has been applied to the distribution, the curves collapse so accurately in the vertical direction. One may remark that the scaling is not so good for times that are smaller than 64 MCs, which is not surprising since the dynamical scaling hypothesis only holds after a non-universal time-scale.

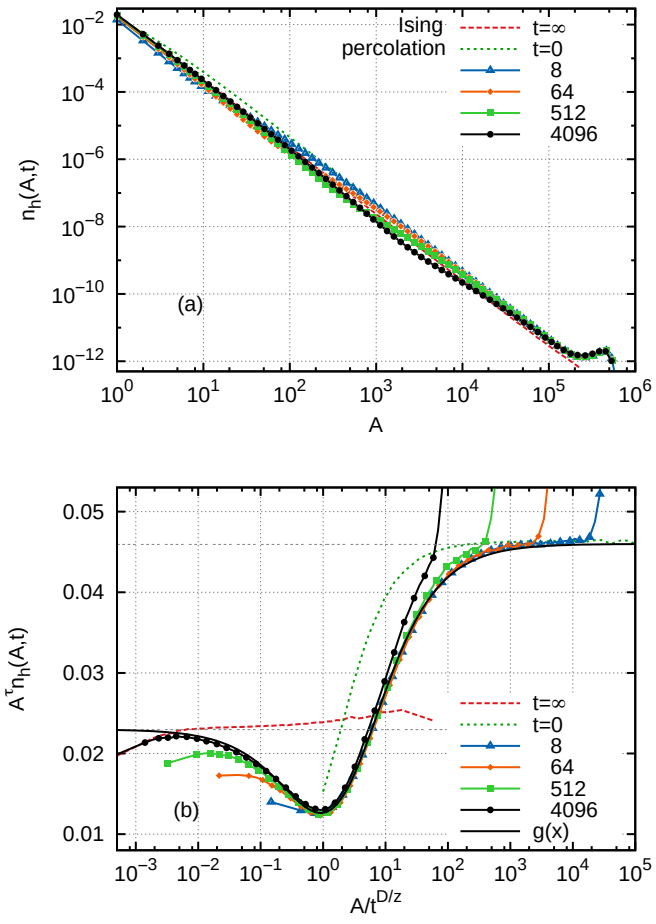

Figure 1.4 – Spin clusters hull-enclosed area number densities in the $2d$IM on a triangular lattice are presented. (a) With dashed (red and green) lines equilibrium data at $T \to \infty$ and T_c. With solid lines the raw dynamic data for the times given in the key (in MCs) including the spanning clusters using a double logarithmic scale. (b) The areas in the x-axis are rescaled by the factor t^α, with $\alpha = 0.92$ consistently with the expectation $\alpha = D/z = 2/z$. The distributions in the y-axis (in linear scale) are multiplied by $A^\tau = A^2$. The grey dotted horizontal lines at 0.046 and 0.023 are the theoretical predictions for the $T \to \infty$ critical site percolation point and the T_c one, respectively, and $g(x)$ is the fitting function defined in eq. (1.11), and discussed in the text.

In curvature-driven coarsening we know from [12, 14], that $n_h(A,t) = 2C/(A + \lambda_h t)^2$ if we use an infinite temperature initial condition, i.e. $n_h(A,0) = 2C/A^2$, with λ_h a non-universal parameter as we have already discussed. It implies

$$A^\tau n_h(A,t) = f(A/\lambda_h t) \quad \text{with} \quad f(x) = \frac{2C}{(1+1/x)^2}. \tag{1.14}$$

$f(x)$ looks like the right part of $A^\tau n_h(A,t)$ for $A > t^{2/z}$ in our case. Since we consider a

situation with two critical points and not only one as in the sub-critical case we are tempted to think that the minimum of $g(x)$ around $x \simeq 1$ and more generally its non-monotonic behaviour can be reproduced with a sum of two functions similar to $f(x)$, one decreasing from C to 0 and one increasing from 0 to $2C$. This suggests for $g(x)$ defined in eq. (1.11) the form:

$$g(x) = C\left(\frac{1}{(1+ax^b)^c} + \frac{2}{(1+(ax^b)^{-1})^c}\right). \tag{1.15}$$

We left the powers b and c as free parameters as there is a priori no reason for them to be simple integers as in the sub-critical coarsening situation. Numerical inspection of the data shows a good fit for the values $a \simeq 0.65$, $b \simeq 0.79$ and $c \simeq 2.3$. Roughly speaking, a fixes the position of the minimum, b its width and c its depth. Note that c is chosen to allow the fitting curve $g(x)$ to go through the minimum of the numerical data but we do not attribute a special meaning to this value. Indeed the expansion of $g(x)$ close to the asymptotic values C and $2C$ is proportional to x^b and x^{-b}, respectively, both independent of c.

Hull-enclosed areas and hull lengths

As in [12, 14, 17] we study the relation between the hull-enclosed areas and the hull lengths by tracing an averaged scattered plot of A against p in Fig. 1.5. In panel (a) we show the raw data for different times after the critical quench. In panel (b) we scale the data by the relevant typical growing scales. In the case of the hull-enclosed areas this is the linear growing length, $\xi(t)$, to the power of their fractal dimension that is simply $D = d = 2$ for these regular objects. In the case of the hull lengths, instead, the relevant linear scale is still the growing length, $\xi(t)$, now to the power of the hulls fractal dimension in the critical Ising point, which is $D_h^I = 11/8$, as given in Table 1.1. The master curve shows a clear cross-over between two power law behaviors with the powers $D/D_h^I = 16/11 \simeq 1.45$ controlling the small scales and $D/D_h^P = 8/7 \simeq 1.14$ controlling the large scales. Summarizing,

$$\left(\frac{A}{t^{D/z}}\right) \simeq \left(\frac{p}{t^{D_h^I/z}}\right)^{\zeta} \qquad \text{with} \qquad \zeta = \begin{cases} D/D_h^I & \text{for} \quad p/t^{D_h^I/z} \ll 1, \\ D/D_h^P & \text{for} \quad p/t^{D_h^I/z} \gg 1. \end{cases} \tag{1.16}$$

Hull length number density

Next we proceed with the hull length distribution displayed in Fig. 1.6. In the first graph, Fig. 1.6(a), we show the distributions $n_h(p,t)$ vs. p for various times after the quench where p stands for the hull length. For this quantity, the equilibrium behavior for the critical Ising model is $n_h(p) \sim p^{-27/11}$ and it is different from percolation criticality where $n_h(p) \sim p^{-15/7}$. These equilibrium curves are drawn with dashed lines in the figure. We see in Fig. 1.6(a) that the dynamic curves interpolate between these two critical laws. For example, we can observe that for $t = 4096$ MCs there is a qualitative change for $p \sim 2000$. However, since the difference between $27/11$ and $15/7$ is small it is still difficult to get a precise picture of what is happening with this data representation.

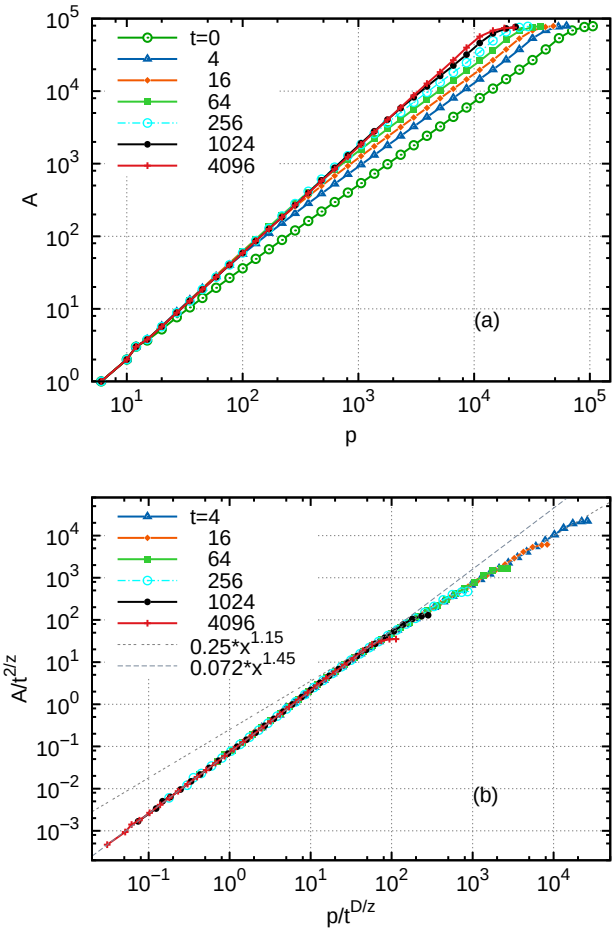

Figure 1.5 – The hull-enclosed area against the length of the hull at different times after the critical quench for $L = 400$. (a) Raw data. (b) Scaled plot. The master curve crosses over from x^{d/D_h^I} to x^{d/D_h^P} with $d/D_h^I \simeq 1.45$ and $d/D_h^P \simeq 1.15$.

Note that, contrary to what happens with the area number densities, the time-dependence is seen in the full extent of the curves and not only for (relatively) small scales. Even the bump is displaced towards shorter lengths in the course of time.

A better description is given in Fig. 1.6(b) where we drew the same distribution multiplied by p^τ with $\tau = 27/11$, the exponent of the tail in the equilibrium distribution at T_c, so that the Ising equilibrium critical distribution is horizontal. As before, the lengths are rescaled by a factor t^α to take into account the growing length scale. Searching the value of α that gives the best horizontal collapse we find $\alpha = 0.63\ (3)$. This fits well with the value expected from dynamical scaling argument such that p is rescaled by $\xi(t)^{D_h}$ with

$D_h = D_h^I = 11/8 = 1.375$ the fractal dimension of Ising clusters' hulls. $D_h/z \simeq 0.6348$ is in good agreement with the measured value and this clearly supports the idea that the growing clusters have a fractal boundary. It is interesting to notice that this does not happen in sub-critical coarsening where the domain growth is curvature-driven and the boundaries of clusters that are smaller than the cross-over scale are smooth and do not have a fractal structure (see [12] e.g. for the study of such a case in the $2d$IM). The asymptotic value, for $p/t^{D_h/z} \ll 1$, coincides with the expected equilibrium value, as obtained from the equilibrium simulations and shown with the (red) dashed horizontal line.

The behavior in the large scale or short time limits, $p \gg t^{D_h^I/z}$, is also interesting. Since there is a one-to-one relation between areas and perimeters, we can use $n_h(A,t)dA \simeq n_h(p,t)dp$ where A and p are related by eq. (1.16) (note that we use the same symbol n_h to represent two different functions). Using $n_h(A,t) \simeq A^{-\tau}$ with $\tau = 1 + d/D$ for large values of A and the value of the exponent ζ given in eq. (1.16) for large scales we find

$$n_h(p,t)p^{\tau_h^I} \simeq \left(\frac{p}{t^{D_h^I/z}}\right)^{\gamma} \qquad \text{with} \qquad \gamma = d\,\frac{D_h^P - D_h^I}{D_h^P D_h^I} = \tau_h^I - \tau_h^P \tag{1.17}$$

independently of D. We used the super-script I to stress that the τ-value in the factor in the left-hand-side corresponding to critical Ising equilibrium was used in the scaling of data in Fig. 1.6(b). The bump at the end of the data is just the contribution of the spanning clusters. The growing part of the master curve is very well described by the power law given above. Indeed, close to it we placed the data obtained in equilibrium at $T \to \infty$ (dashed green line) that in the representation used in the plot is given by x^γ, with the value of γ given in eq. (1.17). The two curves are parallel in the selected range of variation (within numerical accuracy) confirming our prediction.

Domain area number density

We have checked that the area-hull relation for the domains conforms to the scaling in eq. (1.16) with the relevant ζ given by the fractal dimension of the domains.

Finally, we present the spin clusters (or domain) area distributions at several instants after the quench in Fig. 1.7. Again the two equilibrium distributions appear as (green and red) dashed lines. Even for the relatively short time $t = 8$ MCs the change in the distribution is rather drastic, and we can observe that the system has been depleted from small clusters with area up to 80 because of the onset of the interactions. This is related to the fact that the fractal dimension of the Ising clusters at equilibrium is greater than the dimension of the percolation clusters. Qualitatively we can explain this fact by saying that the Ising clusters are less porous because of the interactions. We perform again the rescaling of the areas by t^α and we multiply the distributions by A^τ, with $\tau = 379/187 \simeq 2.027$ being the critical Ising exponent for the distribution of domain areas (see the Table). Here the best collapse (Fig. 1.7(b)) is obtained for the value $\alpha = 0.90\ (3)$. The fractal dimension of the geometrical clusters at the critical point is $D_c = 187/96 \simeq 1.948$. Then the value of α is in good agreement with the value expected from scaling arguments $D_c/z \simeq 0.899$.

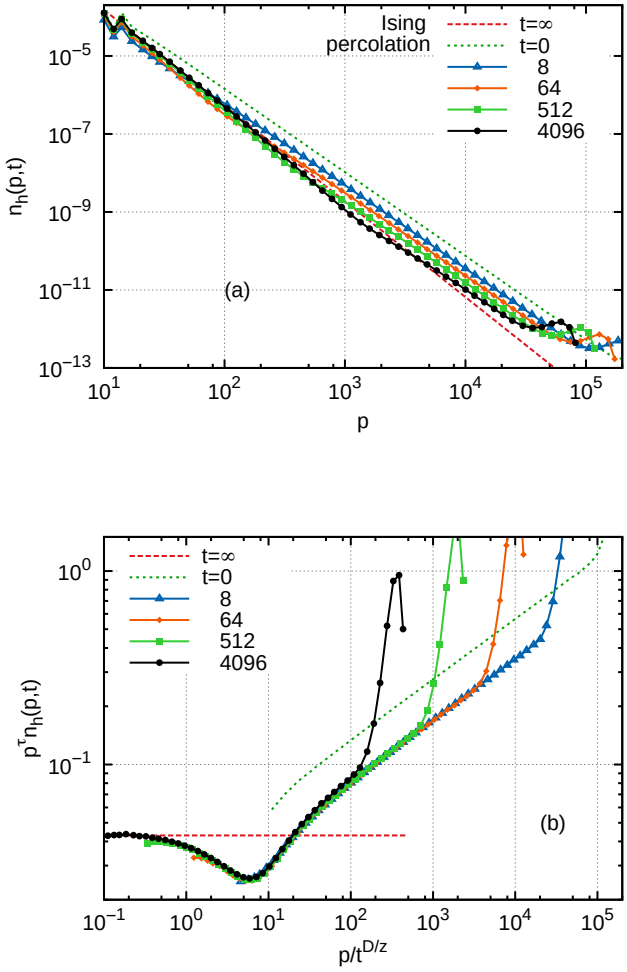

Figure 1.6 – Time-dependent distribution of the hull length p of the spin clusters, in a double logarithmic scale for the times given in the key in MCs. (a) Raw data dynamic data together with the ones for equilibrium at the departure and arrival values, $T \to \infty$ and T_c, that are shown with dashed (red and green) lines. (b) Same as in (a) but the distributions are multiplied by p^τ with $\tau = 27/11$ the exponent of the equilibrium number density at T_c and the lengths are divided by t^α with $\alpha = D_h/z \simeq 0.63$ with D_h the fractal dimension of the equilibrium hulls at T_c.

Note that if we had neglected the fractal character and used $D_c = 2$, we would have obtained $2/z \simeq 0.923$ which is also in the interval of confidence of our numerical estimate but we think the value D_c/z with $D = 187/96$ is the correct one. The scaling just discussed gives evidence for the importance of the fractal structure of the spin clusters at the critical point. The values obtained suggest a fractal front, whose fractality is the critical Ising one, propagating on increasingly larger scales and bringing the system towards a new

equilibrium, although very slowly, with a law governed by the dynamic exponent z.

1.3.3 Fortuin-Kasteleyn clusters

In this subsection we present the results of simulations in which we analyze the FK clusters. These clusters are critical at $T = T_c$ but they are not critical at $T \to \infty$ since at infinite temperature $p = 1 - e^{-2\beta} = 0$ and they are all composed of only one site. We constructed the dynamic FK clusters adapting the usual procedure explained in subsection 1.2.2 to the time-dependent domains. At different instants after the quench from $\beta = 0$ to β_c we used the probability $p = 1 - e^{-2\beta_c}$ to erase bonds from the spin domains existing at the chosen times. We next studied various distribution functions associated to the FK clusters. We recall that in this study we used a square lattice for simplicity and that the initial point (infinite temperature) is *not* critical for the spin clusters either.

We have checked that the number density of hull-enclosed and domain FK areas as well as the area-perimeter relations satisfy the expected scaling relations already discussed for spin clusters in Sec. 1.3.2, so we prefer to show the data for other observables.

Hull length

In Fig. 1.9(a) we show the hull length distributions at $T \to \infty$ and at T_c as well as the distributions of the same quantities at several times after the quench. We can easily see that the initial distribution is not a critical one since it is not a straight line in this log-log graph. As time elapses, the distribution approaches a power law behavior since it heads towards criticality. Again, to get a better description, the curves are collapsed on Fig. 1.9(b) by using the now usual rescaling $p^{\delta} n_h(p,t) = f(p/t^{\alpha})$. The best collapse onto a master curve is obtained for $\delta = 2.12$ and $\alpha = 0.87$. These values are compatible with $\tau = 2.2$ and $D_h/z \simeq 0.77$, the values at the Ising critical point, cf. Table 1.1, though here the agreement is not as good as for the hulls of the spin clusters. We notice that for times longer than 2000 MCs the curves do not collapse anymore for large sizes. This is expected since it roughly corresponds to the moment when the dynamical length scale reaches the order of the linear size of the system $\xi(t) \sim L$. After this time we are no longer in the regime of unconstrained domain growth as the clusters are sensitive to the finite size of the system.

External perimeter

The same scaling is finally applied to the external perimeter distributions of the FK clusters, the idea being to check whether the consequences of Duplantier's duality hold out of equilibrium. The curves are not shown since they are very similar to the ones in Fig. 1.9. The curves collapse for $\delta = 2.56$ and $\alpha = 0.63$. To compare this values with the related equilibrium exponent at T_c we must remember that, according to the duality relation evoked before [$D_{ep}(\kappa) = D_h(16/\kappa)$ for $\kappa \geq 4$], the external perimeters of the FK clusters

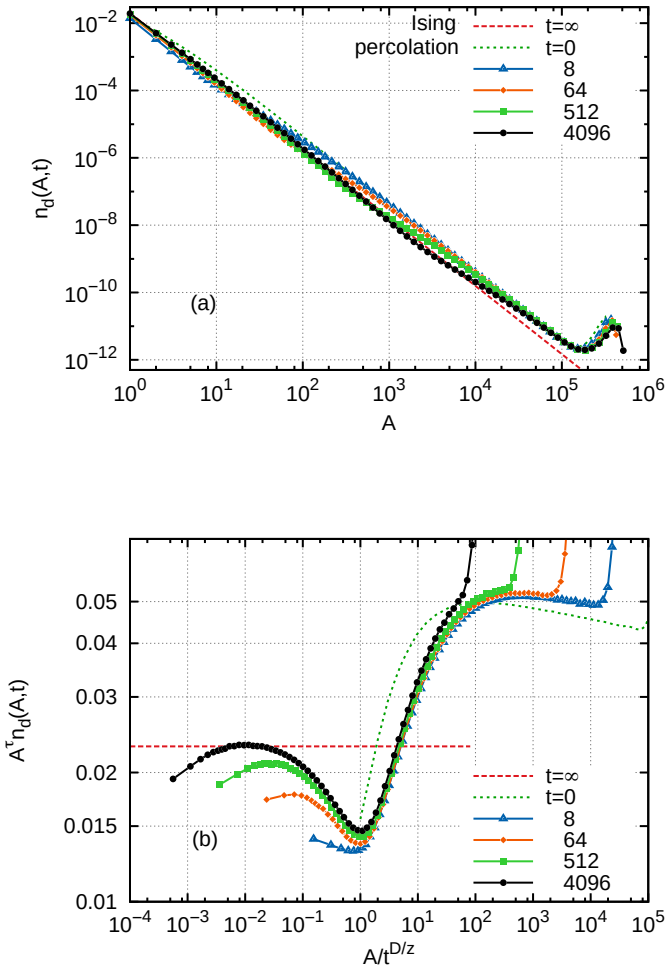

Figure 1.7 – Time-dependent domain area distribution. (a) Raw data at the times given in the key in MCs. (b) Same as in (a) with the distributions multiplied by $A^\tau = A^{2.025}$ and the area rescaled by t^α with $\alpha = D/z \simeq 0.90$.

at T_c should scale at equilibrium like the hulls of the spin clusters, that is possess also at T_c a fractal dimension $D_{ep}(\kappa = 16/3) = D_h(\kappa = 3) = 11/8$. This gives $\tau \simeq 2.45$ which is compatible with δ and $\alpha = D_{ep}/z \simeq 0.63$. Therefore the relation between the statistical and geometric properties of the external perimeters of FK clusters and the hulls of spin clusters proven in equilibrium, seems to remain valid out of equilibrium for the growing FK clusters.

1.3.4 Interfaces

In the previous sections, we have seen fractal dimensions appear while considering the dynamic scaling of several probability distributions. A different strategy, that has proven to be very useful in the analysis of the equilibrium critical points and in particular in the context of the study of SLE [8, 9, 10], is to study the fractal properties of an artificially generated interface. This is the line of research we follow here by generating the interface as follows. We take a $2d$IM on a triangular lattice and we quench the system from equilibrium at $T \to \infty$ to T_c at $t = 0$. With appropriate boundary conditions we force the existence of a unique curve, defined on the edges of the dual honeycomb lattice, separating spin clusters of opposite sign and going, say, from top to bottom. One such curve is shown in Fig. 1.8, their properties are analyzed in this section.

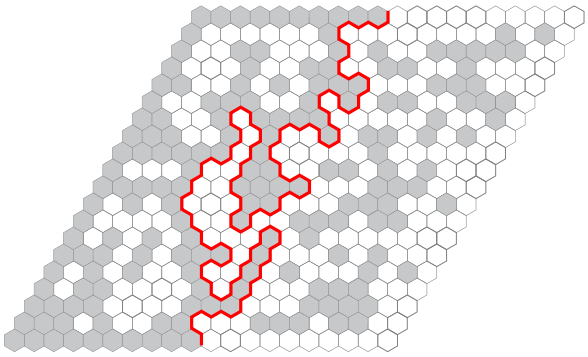

Figure 1.8 – An interface in a $2d$IM on a triangular lattice created by imposing spin up boundary condition on the left (grey hexagons) and spin down on the right (white hexagons). The curve is defined on the edges of the dual lattice, the honeycomb lattice represented in the figure.

Fractal dimension

We are interested in the fractal dimension of the interface. To compute this quantity we measured the length of the curve $l(L,t)$ with L the linear size of the system as a function of the time t. If the curve is fractal at time t, then the fractal dimension $d_f(t)$ is defined by $l(L,t) \propto L^{d_f(t)}$. An effective $d_f(t)$ is obtained from the slope of $l(L,t)$ between two sizes L and L':

$$d_f(L,L',t) = \frac{\ln l(L,t) - \ln l(L',t)}{\ln L - \ln L'}. \tag{1.18}$$

This yields a fractal dimension depending on time but also on the two lengths L and L' because of finite-size corrections. In Fig. 1.10 we draw this fractal dimension vs. time t rescaled by L^z for several values of L and L' with z the dynamical exponent employed in Sec. 1.3.2 and Sec. 1.3.3.

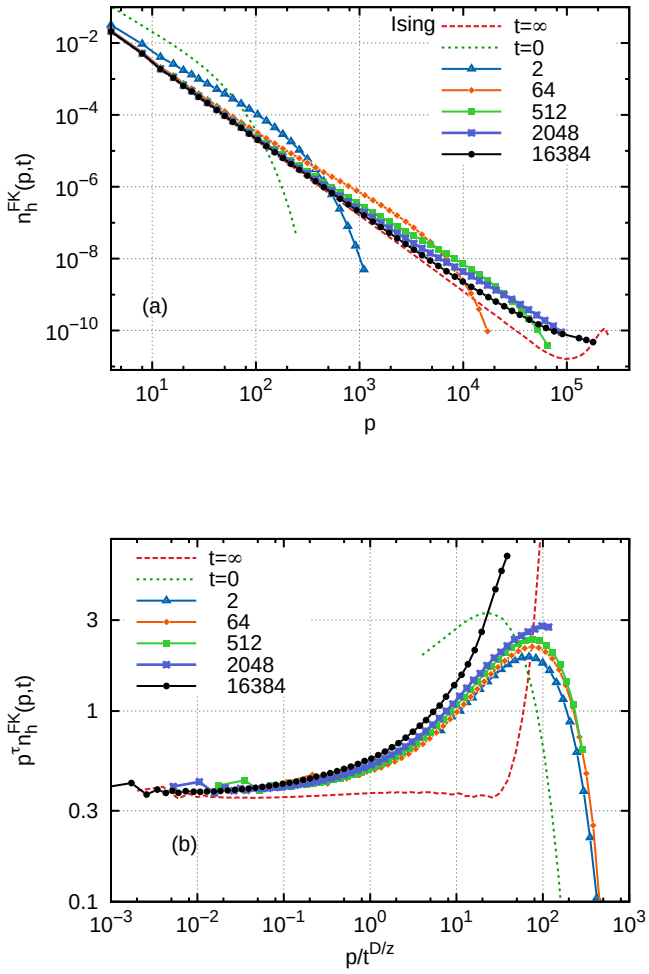

Figure 1.9 – Number density of FK hull length p at several times after the quench given in the key for a system of linear size $L = 320$. (a) Raw data. (b) Same data presented in the rescaled form $p^\tau n_h^{FK}(p,t)$ vs. p/t^α with $\tau = 2.12$ and $\alpha = 0.87$ that gives the best data collapse.

We observe that for short times, i.e. $t \ll L^z$, the fractal dimension is compatible with $7/4 = 1.75$ the fractal dimension of the hulls at the percolation threshold, while for long times it is closer to $11/8 = 1.375$ the fractal dimension of the Ising clusters' hull at the critical point. The compatibility is strong since even the finite-size corrections for the short (long) scales correspond to the related equilibrium values. The points completely on the left correspond to the initial values being rejected to $-\infty$ in the log scale. The dynamical scaling is also very accurate here since the curves perfectly collapse apart from finite-size corrections.

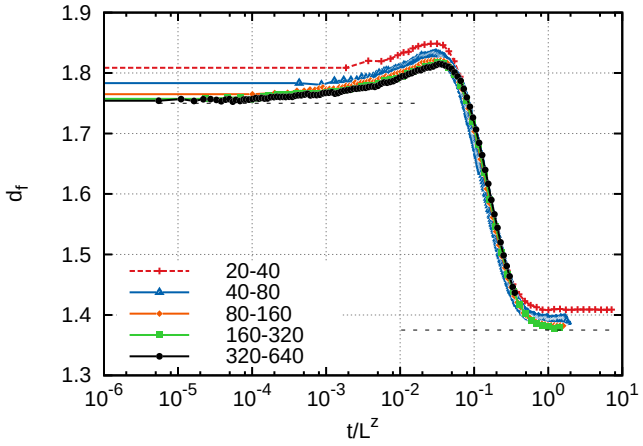

Figure 1.10 – Fractal dimension of an interface vs. t/L^z, as deduced from eq. (1.18) for several couples of system sizes L and $L' = 2L$ given in the key.

The main disadvantage of calculating a fractal dimension this way is having to handle the two lengths in the interpretation of the fractal dimension. This is uneasy. We use a different and more performant approach in the next subsection.

The winding angles

The percolation and Ising model hulls, at equilibrium and in the continuum limit, are conformally invariant curves described by a stochastic Loewner evolution SLE_κ with $\kappa = 6$ for percolation [32] while $\kappa = 3$ for Ising hulls [33, 34]. The parameter κ can be determined numerically by computing the variance of the winding angle for two points chosen at random on a conformally invariant curve at a distance l along the curve which equals

$$\langle \theta^2 \rangle = \mathrm{ct} + \frac{4(D-1)}{D} \ln l, \tag{1.19}$$

where D is the fractal dimension of the curve [35, 36, 37] and ct is a constant. Finally, using eqs. (1.4) and (1.19), we obtain the following form for the variance of the winding angle:

$$\langle \theta^2 \rangle = \mathrm{ct} + \frac{4\kappa}{8+\kappa} \ln l. \tag{1.20}$$

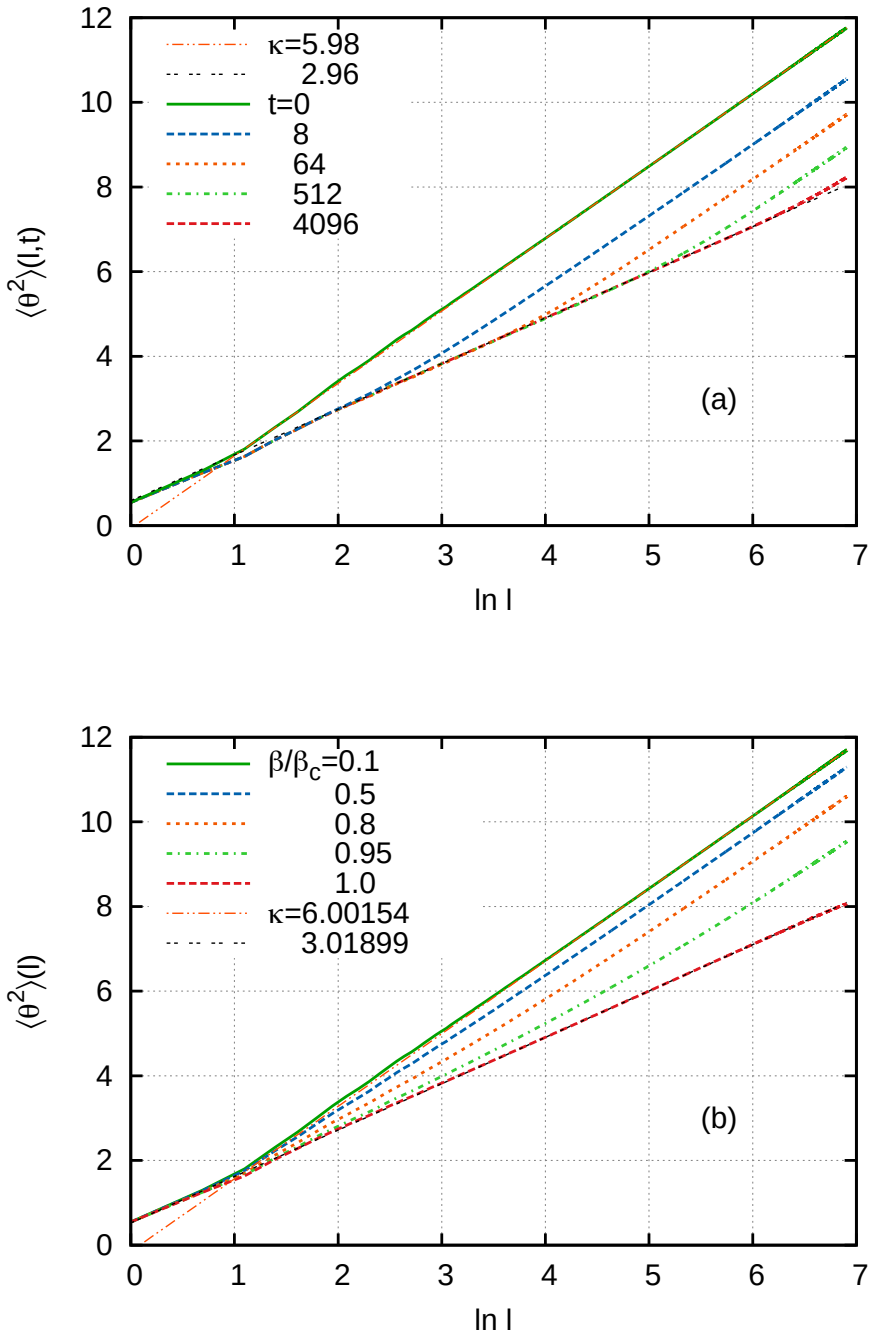

Figure 1.11 – Variance of winding angle of interfaces out of equilibrium (a) and in equilibrium (b) for a system of linear size $L = 1280$. (a) $\langle\theta^2\rangle$ vs. $\ln l$ for different times after the quench from $T = \infty$ to $T = T_c$. (b) $\langle\theta^2\rangle$ vs. $\ln l$ at equilibrium for different inverse temperatures $\beta = 1/T$ in unit of β_c given in the key.

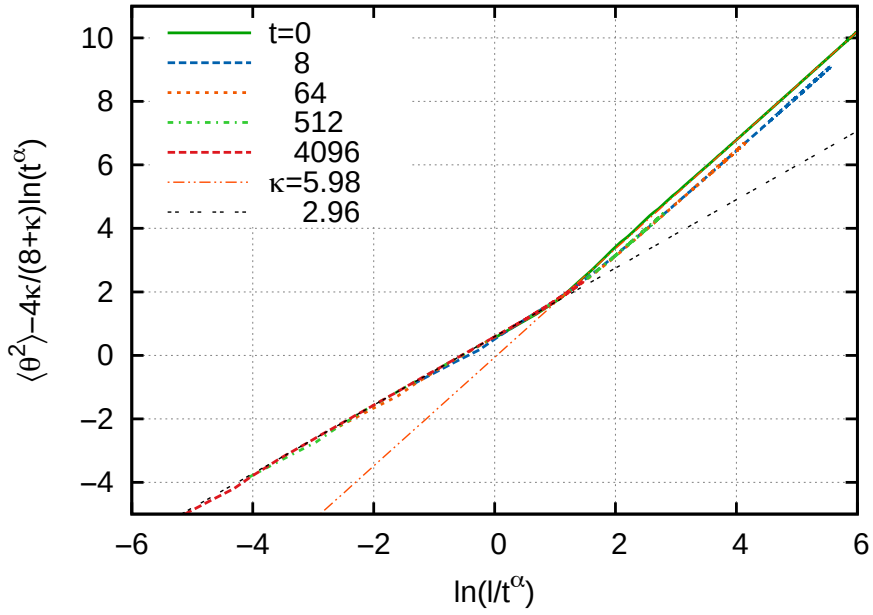

Figure 1.12 – Same curves as in Fig. 1.11(a) with the rescaling $l \to l/t^\alpha$ and $\langle\theta^2\rangle(l,t) \to \langle\theta^2\rangle(l,t) - 4\kappa/(8+\kappa)\ln t^\alpha$ with $\alpha = 0.65$. The dashed lines are our best fits to the small and large scale behavior and yield the κ values given in the key.

The winding angle variance, $\langle\theta^2\rangle(l,t)$, is measured as a function of the distance l for different times after the quench. The results for a system of linear size $L = 1280$ are given in Fig. 1.11(a). For the time $t = 0$ corresponding to percolation, a fit of the form (1.20) yields $\kappa = 5.98$ in excellent agreement with the exact result $\kappa = 6$. For the largest time simulated $t = 4096$ MCs, a fit of the form (1.20) yields $\kappa = 2.96$. For this fit we kept the data with $\ln l < 6.5$ since for larger distances, the variance starts deviating from a straight line. This value is in excellent agreement with the exact result for Ising model spins clusters in equilibrium, $\kappa = 3$. The best fits for $t = 0$ MCs
and $t = 4096$ MCs are represented as dashed lines in Fig. 1.11(a). We now wish to collapse these curves to make the dependence of the growing length scale upon time explicit. The length l along the curve is divided by t^α and the winding angle variance corresponding to a length t^α is subtracted. Thus, in Fig. 1.12, we plot $\langle\theta^2\rangle(l,t) - 4\kappa/(8+\kappa)\ln t^\alpha$ vs. $\ln(l/t^\alpha)$. The curves collapse very well for $\alpha = 0.65$ which is in good agreement with $D_h/z \simeq 0.63$ with $D_h = 11/8$ the fractal dimension of Ising clusters' hulls. This means that the same rescaling as the one used for the distributions works for the winding angle variance as well. In the latter case, however, the transition between the two equilibrium regimes is more rapid. Indeed, for distances smaller than the characteristic length $\xi(t)^{D_h} \sim t^{D_h/z}$ the interface is, at least for the observable $\langle\theta^2\rangle$, as if the system were in equilibrium at T_c and

for larger distances as if the system were still in the independent percolation regime. In the previous section, we have observed a similar crossover in the behavior of the probability distributions, with small and large scales being the ones of the initial regime of percolation and the ones of the state towards which the system is converging, respectively, but the crossover was far less abrupt.

For comparison, we present the plot of $\langle\theta^2\rangle$ against $\ln l$ in *equilibrium* for various temperatures in Fig. 1.11(b). It is known that the high temperature phase of the Ising model at zero field on the triangular lattice is peculiar in the sense that it is critical and in the universality class of uncorrelated percolation [38, 39]. This is not true for other planar lattices. As we have already seen, the contours of percolation clusters on the triangular lattice are described by SLE_6. This explains why for sufficiently large sizes (larger than the correlation length induced by the interactions between spins) we recover a dependence of $\langle\theta^2\rangle$ with $\ln l$ that is compatible with $\kappa = 6$, i.e. the behavior of the interface is governed by the attractive infinite temperature point.

Both Figs. 1.11(a) and 1.11(b) are compatible with $\kappa = 6$ at large scale. However, for shorter distances the behavior of the quenched and equilibrium curves are very different. In the case of the quench, for sufficiently small size and up to $l \sim t^{D_h/z}$ the curves are compatible with $\kappa = 3$ (Ising spin clusters) but for the curves at equilibrium the critical Ising behavior is not observed at all.

Thus during the coarsening process the interface has a radically different behaviour from the one obtained by considering data for equilibrium at indermediate temperatures. In the first case, we flow from $T = \infty$ to T_c, with an increasing scaling length $\xi(t) \sim t^{1/z}$. In the second we flow from T_c to $T = \infty$ with a correlation length $\xi \sim |T - T_c|^{-\nu}$ with $\nu = 1$. In this second case we can only observe the critical large scale behaviour dominated by the percolation point while in the first case we distinguish two behaviors with a crossover controlled by the characteristic length $\xi(t) \sim t^{1/z}$.

Dipolar SLE

We have been a bit further in the characterisation of the spin clusters boundaries. Among the different SLE setups we have considered the one called dipolar SLE introduced by Bauer *et al.* [40]. In our case it consists in forcing the spins of the lower horizontal side of a rectangular system to be $+1$ in the right part and -1 in the left one. This forces the creation of an interface but contrarily to the setup already mentioned the second end of the interface can wander freely and end up in any given position on the upper horizontal side. If the position of the middle of the upper horizontal side is chosen as the origin of the position x, Bauer *et al.* showed the probability distribution for the upper end to finish in the reduced position $x' = x/L$ is given by:

$$P(x') = \frac{1}{I}\left[\cosh\left(\frac{x'}{2}\right)\right]^{-4/\kappa} \tag{1.21}$$

where I is the normalisation constant, L the system horizontal size and κ the SLE parameter. The vertical system size is taken as 1.

We have measured the boundary excursion probability for an interface following a critical quench from the infinite temperature. At the initial time on the triangular lattice the probability distribution is exactly Eq. (1.21) with $\kappa = 6$ for critical percolation. We observe that at all times after the quench the probability distribution assumes with a good accuracy a similar form but with κ varying with time. By fitting the probability distribution, one can extract a value $\kappa(t)$. We do not show a plot of this quantity as it is very similar to the evolution of the fractal dimension of the interface with time as in Fig. (1.10). We can do exactly the same rescaling of time by L^z and the curves for different system sizes perfectly collapse except for some small finite size corrections. This good agreement of the out of equilibrium boundary excursion probability with the equilibrium one strengthens the statement made before that excluding length-scales comparable with $\xi(t)$ the properties of the out of equilibrium interface are given very precisely by the corresponding critical points. The correspondence is not only limited to scale invariance properties but also to the more stringent properties related to conformal symmetry.

1.4 Quench from the ordered phase

An other interesting case is a critical quench starting from the ordered phase. For simplicity we will only consider completely magnetised systems, that is systems initially at zero-temperature. Only one cluster occupies all the sites of the lattice and we expect that the thermal fluctuations at T_c will create clusters growing with time. We will only consider the hull-enclosed area number distribution but we expect that the features displayed in this case are also present in the other distributions. In the main plot of figure 1.13 this distribution is plotted versus the area for different times after the quench. Qualitatively, we can see that the distribution for a given time looks like a power with a cut-off increasing with time. To study the evolution of the distribution we multiply it by A^2 the equilibrium power law and plot it with the ordinate in logarithmic scale (not shown). We remark that the remaining decrease is compatible with an exponential decay with a time dependant rate. This indicates that the distribution is of the form $n_h(A,t) \sim e^{-A/A_c(t)}/A^2$ with $A_c(t)$ a time dependent area that sets the rate of the exponential decrease. This form is similar to the distribution of cluster areas in subcritical percolation where in this case the cutoff is simply the correlation length depending on the occupation probability p to the power of the fractal dimension of the clusters $\xi(p)^D$. By rescaling the areas by a factor t^α and multiplying the distributions $t^{2\alpha}$ in the inset of figure 1.13, we obtain a convincing collapse for $\alpha = 1.02(3)$. This means that the distributions follow the relation $t^{2\alpha} n_h(A,t) = f(A/t^\alpha)$ as expected from the subcritical form we propose. However the value of α is markedly different from what we would expect if $A_c(t) \sim \xi(t)^2$ that gives $\alpha = 2/z \simeq 0.92$. This discrepancy might come from the fact that this cut-off increases slightly faster than the dynamical length which is surprising or more simply that the numerics are not precise

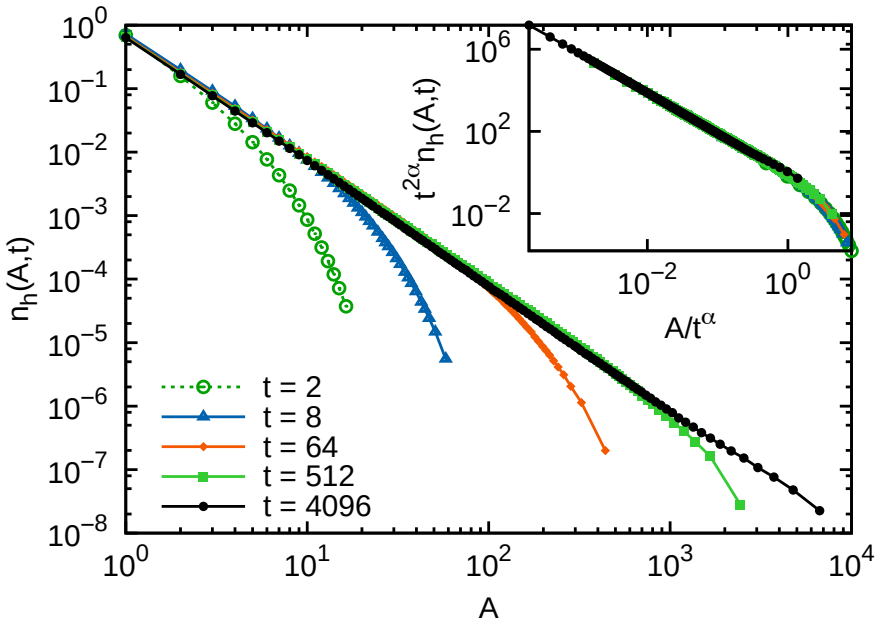

Figure 1.13 – Several hull-enclosed area number distributions vs. area A after a critical quench from $T = 0$ for a system of linear size $L = 320$. In the inset is plotted $t^{2\alpha} n_h(A,t)$ vs. A/T^{α} with $\alpha = 1.05$ for the same times.

enough to conclude as it is often difficult to extract precise estimates from the collapse of distributions.

Interestingly in the second chapter we will see plots very similar to the one in figure 1.13 of distributions going from a subcritical to critical form but this evolution will not be due to coarsening.

1.5 Conclusion

In this paper we analyzed the dynamics of a system instantaneously quenched from one critical point to another one. We used the prototype statistical model, the $2d$ Ising model, quenched from $T \to \infty$, i.e. critical site percolation on the triangular lattice, to the Ising critical point.

As observed in [11]-[17] for sub-critical quenches, the typical growing length, $\xi(t) \simeq t^{1/z}$ in this case, separates two length scales. In the smaller one, all mesoscopic observables (areas, perimeters, etc.) satisfy the statistical and geometric properties of the working temperature equilibrium state. Instead, in the largest scale, these same observables are the ones of the initial state. In sub-critical quenches, this result could be shown analytically for the hull-enclosed area distribution [11, 14] and it was confirmed numerically for different

quantities and in different systems.

The attraction of quenches between critical points is that, in the departing and arrival equilibrium conditions, very powerful analytic methods (Coulomb gas, conformal field theory, SLE) allowed one to compute a myriad of geometric properties including fractal dimensions and related critical exponents. Could these methods be extended to deduce, analytically, the results presented in this manuscript for a particular case, the $2d$ Ising model, that we conjecture apply to all critical quenches, at least in bidimensional systems? This is definitely an interesting question which calls for other works.

Bibliography

[1] Thibault Blanchard, Leticia F. Cugliandolo, and Marco Picco. A morphological study of cluster dynamics between critical points. *J. Stat. Mech.: Theo. Exp.*, 2012(05):P05026, May 2012.

[2] P. C. Hohenberg and B. I. Halperin. Theory of dynamic critical phenomena. *Rev. Mod. Phys.*, 49(3):435, July 1977.

[3] H. K. Janssen. *From Phase Transitions to Chaos—Topics in Modern Statistical Physics*, page 68. World Scientific, Singapore, 1992.

[4] Pasquale Calabrese and Andrea Gambassi. Ageing properties of critical systems. *J. Phys. A: Math. Gen.*, 38(18):R133, May 2005.

[5] U. C. Täuber. *Critical dynamics - A field theory approach to equilibrium and non-equilibrium scaling behavior*. in preparation.

[6] B. Nienhuis. *Coulomb gas formulation of two dimensional phase transitions*, volume 11 of *Phase Transitions and Critical Phenomena*, chapter 1, page 1. Academic Press London, 1987.

[7] J. Cardy. *Conformal Invariance*, volume 11 of *Phase Transitions and Critical Phenomena*, chapter 2, page 55. Academic Press London, 1987.

[8] J. Cardy. *Ann. Phys.*, 318:81, 2005.

[9] Ilya A Gruzberg. Stochastic geometry of critical curves, Schramm–Loewner evolutions and conformal field theory. *J. Phys. A: Math. Gen.*, 39(41):12601, October 2006.

[10] M. Bernard and D. Bernard. *Phys. Rep.*, 432:115, 2006.

[11] Jeferson J. Arenzon, Alan J. Bray, Leticia F. Cugliandolo, and Alberto Sicilia. Exact Results for Curvature-Driven Coarsening in Two Dimensions. *Phys. Rev. Lett.*, 98(14):8, 2007.

[12] Alberto Sicilia, Jeferson J. Arenzon, Alan J. Bray, and Leticia F. Cugliandolo. Domain growth morphology in curvature-driven two-dimensional coarsening. *Phys. Rev. E*, 76(6):061116, 2007.

[13] K. Barros, P. L. Krapivsky, and Redner S. *Phys. Rev. E*, 80:040101, 2009.

[14] A. Sicilia, Y. Sarrazin, J. J. Arenzon, A. J. Bray, and L. F. Cugliandolo. *Phys. Rev. E*, 80:031121, 2009.

[15] Alberto Sicilia, Jeferson J. Arenzon, Alan J. Bray, and Leticia F. Cugliandolo. *EPL*, 82:10001, 2008.

[16] M. P. O. Loureiro, Jeferson J. Arenzon, Leticia F. Cugliandolo, and Alberto Sicilia. Curvature-driven coarsening in the two-dimensional Potts model. *Phys. Rev. E*, 81(2):021129, February 2010.

[17] M. P. O. Loureiro, Jeferson J. Arenzon, and Leticia F. Cugliandolo. Geometrical properties of the Potts model during the coarsening regime. *Phys. Rev. E*, 85(2):021135, February 2012.

[18] M F Sykes and D S Gaunt. A note on the mean size of clusters in the Ising model. *J. Phys. A: Math. Gen.*, 9(12):2131, December 1976.

[19] A Coniglio and W Klein. Clusters and Ising critical droplets: a renormalisation group approach. *J. Phys. A: Math. Gen.*, 13(8):2775, August 1980.

[20] Bertrand Duplantier. Conformally invariant fractals and potential theory. *Phys. Rev. Lett.*, 84(7):1363, February 2000.

[21] Wolfhard Janke and Adriaan M.J. Schakel. Geometrical vs. Fortuin-Kasteleyn clusters in the two-dimensional q-state Potts model. *Nucl. Phys. B*, 700(1-3):385, November 2004.

[22] A. L. Stella and C. Vanderzande. Scaling and fractal dimension of Ising clusters at the d=2 critical point. *Phys. Rev. Lett.*, 62(10):1067, March 1989.

[23] B. Duplantier and H. Saleur. Exact fractal dimension of 2D Ising clusters. *Phys. Rev. Lett.*, 63(22):2536, November 1989.

[24] M Picco, R Santachiara, and A Sicilia. Geometrical properties of parafermionic spin models. *J. Stat. Mech.*, 2009(04):P04013, April 2009.

[25] H. Müller-Krumbhaar. Percolation in a lattice system with particle interaction. *Phys. Lett. A*, 50(1):27, November 1974.

[26] Jeferson J. Arenzon, Alan J. Bray, Leticia F. Cugliandolo, and Alberto Sicilia. Exact results for curvature-driven coarsening in two dimensions. *Phy. Rev. Lett.*, 98(14):145701, April 2007.

[27] Alberto Sicilia, Jeferson J. Arenzon, Ingo Dierking, Alan J. Bray, Leticia F. Cugliandolo, Josu Martínez-Perdiguero, Ibon Alonso, and Inmaculada C. Pintre. Experimental test of curvature-driven dynamics in the phase ordering of a two dimensional liquid crystal. *Phys. Rev. Lett.*, 101(19):197801, November 2008.

[28] John Cardy and Robert Ziff. Exact results for the universal area distribution of clusters in percolation, Ising, and Potts models. *J. Stat. Phys.*, 110:1, 2003.

[29] M. F. Sykes and J. W. Essam. Some exact critical percolation probabilities for bond and site problems in two dimensions. *Phys. Rev. Lett.*, 10(1):3, January 1963.

[30] R. Bausch, H. K. Janssen, and H. Wagner. Renormalized field theory of critical dynamics. *Z. Phys. B*, 24(1):113, March 1976.

[31] M. P. Nightingale and H. W. J. Blöte. Monte Carlo computation of correlation times of independent relaxation modes at criticality. *Phys. Rev. B*, 62(2):1089, July 2000.

[32] S. Smirnov. Critical percolation in the plane: conformal invariance, Cardy's formula, scaling limits. *C.R.A.S. - Series I - Mathematics*, 333(3):239, August 2001.

[33] Stanislav Smirnov. Towards conformal invariance of 2D lattice models. *Proc. Int. Congr. Math.*, 2:1421, 2006.

[34] Dmitry Chelkak and Stanislav Smirnov. Universality in the 2D Ising model and conformal invariance of fermionic observables. *arXiv:0910.2045*, October 2009.

[35] Bertrand Duplantier and Hubert Saleur. Winding-Angle distributions of Two-Dimensional Self-Avoiding walks from conformal invariance. *Phys. Rev. Lett.*, 60(23):2343, June 1988.

[36] Bertrand Duplantier and Ilia A. Binder. Harmonic measure and winding of conformally invariant curves. *Phys. Rev. Lett.*, 89(26):264101, December 2002.

[37] Benjamin Wieland and David B. Wilson. Winding angle variance of Fortuin-Kasteleyn contours. *Phys. Rev. E*, 68(5):056101, November 2003.

[38] W. Klein, H. Eugene Stanley, Peter J. Reynolds, and A. Coniglio. Renormalization-Group approach to the percolation properties of the triangular Ising model. *Phys. Rev. Lett.*, 41(17):1145, October 1978.

[39] Andras Balint, Federico Camia, and Ronald Meester. The high temperature Ising model on the triangular lattice is a critical bernoulli percolation model. *J. Stat. Phys.*, 139(1):122, February 2010.

[40] M Bauer, D Bernard, and J Houdayer. Dipolar stochastic Loewner evolutions. *J. Stat. Mech.: Theo. Exp.*, 2005(03):P03001, March 2005.

CHAPTER 2

Sub-critical quenches

Contents

2.1 Introduction

In the first chapter we have discussed the dynamical scaling of quantities related to clusters. We were concerned with the coarsening regime during which the dynamical scaling is valid. This regime starts after a microscopic time scale till the dynamic correlation length $\xi(t)$ reaches the system linear size. In this chapter we will on the contrary study what happens very early or very late after a quench and see how it is sometimes surprisingly related. We will consider in all this chapter the situation of a bi-dimensional Ising model quenched from an initial temperature T to zero temperature. One of the question that one can ask is the nature of the final states reached by a system after a zero temperature quench.

The ground states are of course the first answer but, since the zero temperature dynamics only allows the energy to decrease, the system may also end up in a local minimum of the energy landscape, *i.e.* a metastable state. This depends of course on the initial condition and then a legitimate question is the influence of this initial condition on the appearance of metastable states as final states of a zero temperature dynamic. Furthermore if the system falls in metastable states, at which moment of the evolution can we be certain that it will happen? In this chapter we will answer such questions concerning the 2d Ising model.

We will first consider the situation where the initial temperature is the critical one and study the appearance of stripe states as final states of a zero temperature dynamic. We will then consider the same situation where the initial temperature is infinite and also study final stripe states and their relation to an initial transient regime leading to critical percolation. We will see that the infinite temperature initial condition exhibits a more complex behaviour than the critical initial one.

2.2 Critical intial condition

In this section we will concentrate on the critical initial condition. As we have already seen in the introduction and used extensively in the first chapter, at T_c the spin clusters are in a critical state and their properties can be described in various ways that are based on scale and conformal invariance. We will explore the consequences and relevance of those properties for out-of-equilibrium processes.

2.2.1 Stripe states

The results presented in this subsection have been published in the Phys. Rev. E [1]. Somewhat surprisingly, even with such a simple set up as the two dimensional nearest neighbour ferromagnetic Ising model quenched to zero temperature, a variety of final states can be reached with non trivial probabilities. It was first noticed by Lipowski [2] that an anomalous scaling for the equilibration time of the kinetic Ising model arises from the existence of stripe states. In an interesting series of papers, Krapivsky, Redner and collaborators noticed as well the presence of stripes states after a quench from infinite temperature, and analysed both the dynamics and the final states. They measured numerically the probability of getting stuck in stripe states and found that it was around $1/3$ but were at first unable to explain it [3, 4]. In the same situation but with different goals, Sicilia *et al.* studied the geometry of spin clusters, and noticed that after a few Monte-Carlo steps at $T < T_c$, an infinite temperature system on a square lattice is very similar to the critical percolation point for the spin clusters [5, 6]. So, even though the initial occupation probability of $1/2$ for a type of spins is inferior to the critical site percolation probability for the square lattice $p_c \simeq 0.59$, the system is rapidly very similar to a critical percolation system. This correspondence enabled Krapivsky and collaborators to give an explanation for the probabilities of appearance of stripe states in terms of critical percolation probabilities, be it for free or periodic boundary conditions [7, 8].

The study of crossing probabilities has a long history and a landmark in this topic is due to Cardy and his eponymous formula [9]. This formula gives the probability of left-right crossing of an incipient spanning cluster at the critical percolation threshold on a rectangle. This probability depends only upon the aspect ratio r of the rectangle and can be expressed in terms of hypergeometric functions. Since then a number of percolation probabilities have been studied either for percolation [10, 11, 12] or other models [13, 14, 15, 16, 17]. One aspect that is particularly interesting is that although Cardy and others found those formulas using conformal field theory (CFT), *i. e.* in a non rigorous way mathematically speaking, rigorous tools have been developed which can be used to tackle those systems. Schramm introduced the stochastic Loewner evolution (SLE) [18] which describes numerous physically occurring curves (see [19] with Lawler and Werner *e.g.*) and showed that SLE proves Cardy's formula if the continuum limit of percolation is conformally invariant. In a slightly different line of research Smirnov proved the existence of a conformal scaling imit of the percolation critical point for site percolation on the triangular lattice and thus gave the missing piece to the proof of Cardy's formula [20].

The correspondence discovered by Krapivsky *et al.* is thus very interesting since it relates a non-equilibrium situation to exact results. It is remarkably accurate and based on the observation of Sicilia *et al.* and general considerations on coarsening dynamics and it was supported by numerical results on a lattice with different aspect ratios. We will give more details on those results and clarify the role of percolation later in this chapter in subsection 2.3.3. The underlying question to those studies is to what extent the initial condition influences the final one? In this regard, it is interesting to study the same situation with a different initial condition to extract the universal behaviors from the rest. For the Ising model, the results discussed above have to hold for any starting temperature above the critical temperature since for an initial condition at $T > T_c$ the long distance properties are governed by the infinite temperature fixed point. Since the subcritical region is trivial from the spin clusters point of view, the critical temperature point only remains and is absolutely non trivial concerning spin clusters as we have already discussed.

In the following we study as before the ferromagnetic Ising model whose hamiltonian is written as:

$$\mathcal{H} = -\sum_{\langle ij \rangle} J S_i S_j \ , \tag{2.1}$$

where the sum is over all nearest neighbors pairs of spins of a two dimensional system and $J > 0$. The system considered is rectangular and three boundary conditions will be considered : free, periodic and fixed. The lattices used will be discussed in each case.

Method

In the simulation that we will consider here, we started from a system equilibrated at the critical temperature. The equilibration is obtained with the Wolff cluster algorithm [22]. We generate a large number of independent configurations, at least one million for each size considered. For each configuration, we determine the probability that there exists at

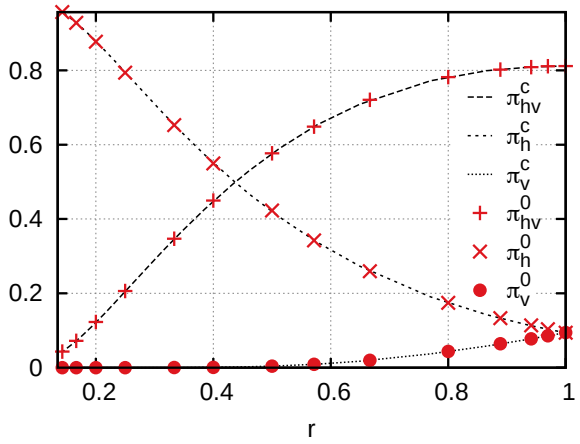

Figure 2.1 – Crossing probabilities for free boundary conditions versus r. The lines corresponding to π^c_h, π^c_v and π^c_{hv} are from the results given in [21] for the critical Ising model. The points correspond to our data for π^0_h, π^0_v and π^0_{hv} obtained after a quench at zero temperature.

least one cluster of spins crossing the horizontal or vertical direction. We denote these probabilities π^c_h or π^c_v. The probability that a spin cluster is crossing in both directions will be denoted π^c_{hv}. Next, we perform a quench at $T = 0$. We then let the system evolve with a Glauber dynamics with a suitable algorithm described below until it reaches a stable state. We record similar (stripe) probabilities that we denote by π^0_h, π^0_v for the horizontal or vertical stripes and π^0_{hv} for the stripes in both directions, *i. e.* a ground state. Note that the clusters contributing to the π_h (π_v) only span horizontally (vertically).

One difficulty is that it can take a tremendous amount of (Monte-Carlo) time to reach the final state where no spins can be updated without increasing the energy of the system because the system tends to wander in long-lived iso-energetic states. A simple kinetic Monte Carlo algorithm [23] with Glauber dynamics bypasses this issue quite easily.

Free Boundary conditions

We will first describe our results for a system with free boundary conditions. The probabilities π^c_h, π^c_v and π^c_{hv} were already considered in equilibrium at T_c by Lapalme and Saint-Aubin [21]. These authors measured these quantities on the triangular lattice. They also tried to find a way to predict the behaviour of these crossings in a way analogous to the Cardy formula for percolation. They obtained a differential equation on a four point correlation function related to π^c_h but were unable to solve it so they resorted to a numerical solution in good agreement with their measurements.

We considered systems of size $L \times L/r$ with $L = 256$ while varying r. We only study the case $r \leq 1$, the case with $r > 1$ being obtained by a trivial duality relation exchanging the vertical and horizontal directions. Our results are shown in Fig. 2.1. In this figure we

compare the situation at T_c and the final states of the evolution at $T = 0$. To do so we present the probabilities of getting a crossing π_h^0, π_v^0 and π_{hv}^0 for various values of ratio r obtained at $T = 0$ as crosses and in the critical case, π_h^c, π_v^c and π_{hv}^c shown as lines. The agreement between the π^c and the π^0 is excellent, this is one of the main results of the present work. The values of the π^c are those obtained by Lapalme and Saint-Aubin in [21]. Note that these authors considered the case of a triangular lattice while our measurements have been done on a square lattice. As a check, we also repeated the measurement of the π^c on the square lattice and of the π^0 on the triangular lattice and our results are in perfect agreement with the ones of Lapalme and Saint-Aubin obtained on the triangular lattice. This supports the universality of these quantities.

In conclusion, the crossing probabilities are the same for the equilibrium at T_c and in the blocked states obtained after a quench at $T = 0$ starting from the critical point. This first result confirms the idea that the final state is dictated by the topology of spin clusters in the initial one.

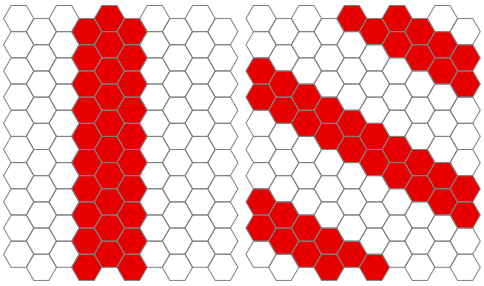

Figure 2.2 – Two possible types of stripes of the alternate triangular lattice with periodic boundary conditions. The vertical stripes on the left can exist for arbitrary aspect ratios r contrarily to the stripes on the right which only exists for $r = 2n/\sqrt{3}$ with $n \in \mathbb{N}^*$. Actually the stripe on the right wraps in both directions around the torus.

Periodic Boundary conditions

To make this fact more explicit we move on to the case of periodic boundary condition (PBC). Here the situation is a bit more complicated since clusters can wind in various ways around the torus. We will discuss wrapping probabilities in great details in chapter 3 and we will just give now the facts that we need for our study. Wrapping clusters can be classified according to the number of times they wind in the horizontal and vertical direction. We note $\pi^{a,b}$ the probability that a cluster wraps a times in the horizontal direction and b times in the vertical direction. The clusters wrapping in both direction but with a cross shape are counted separately and the associated probability is denoted π^+. We will use this notations in chapter 3 but here we will note those probabilities differently for the sake of coherence with the other types of boundary conditions. Hence we will note $\pi_h = \pi^{1,0}$, $\pi_v = \pi^{0,1}$ and $\pi_{hv} = \pi^+$. We consider the triangular lattice. With this choice of lattice and boundary condition only vertical stripes are stable at $T = 0$ for arbitrary aspects

ratios (see Fig. 2.2). This means that $\pi_h^0 = 0$ and $\pi_{hv}^0 = 1 - \pi_v^0$ thus we only need to consider π_v^0. As is shown in Fig. 2.2, diagonal stripes are stable in addition to the vertical ones for the aspect ratios $r = 2n/\sqrt{3}$ with $n \in \mathbb{N}^*$, but their rarity (π_{diag} is at most 6.10^{-8}) forbids their study numerically as has been done in [8]. The factor $\sqrt{3}/2$ in the definition of the aspect ratio takes into account the actual horizontal system size. We have seen that different percolation probabilities of same spin cluster for free boundary conditions has been studied numerically and analytically in [21]. We found no such study for the PBC. This motivated us to extend the work of Arguin [24] which deals with the probability that a given configuration contains a Fortuin-Kasteleyn cluster winding a times horizontally and b times vertically around the torus. Arguin used the mapping between the Fortuin-Kasteleyn clusters and a Coulomb gas with parameter $g \in [2, 4]$. A correspondence is usually expected between Ising spin clusters and clusters of the $Q = 1$ Potts model with dilution at its tricritical point [25] corresponding again to a Coulomb gas. Using this correspondence we have been able to obtain an explicit formula for such a probability for Ising spin clusters [26]. The details of the derivation and numerical checks will be provided in Chapter 3. In the case where the spin cluster winds only vertically around the torus, the formula reduces to:

$$\pi_v^c(r) = \frac{1}{2r|\eta(ir)|} \frac{\theta_3\left(\frac{i}{12r}\right) - \theta_3\left(\frac{3i}{4r}\right) - 2\theta_2\left(\frac{3i}{4r}\right)}{|\theta_2(ir)| + |\theta_3(ir)| + |\theta_4(ir)|} \tag{2.2}$$

where η is the Dedekind η function and the θ_i are the Jacobi θ functions. In Fig. 2.3, the

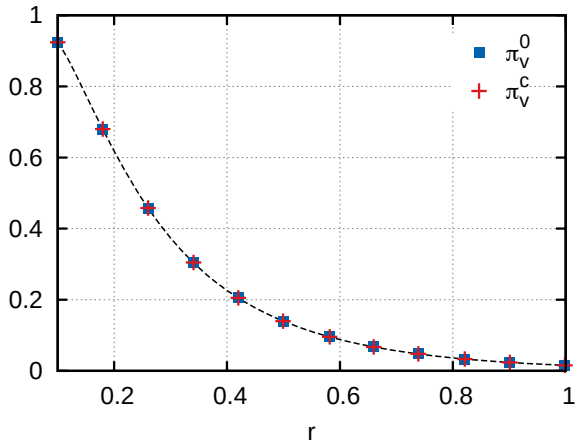

Figure 2.3 – (Vertical percolation probability π_v^c at T_c (red crosses) and vertical stripe probability π_v^0 at $T = 0$ (blue squares) for various aspect ratio $r = L_y/(\sqrt{3}L_x/2)$ with $L_y = 128$. The dashed line corresponds to the expression in Eq. (2.2).

results for the triangular lattice with PBC are presented. The agreement between π_v^c, π_v^0 (dots) obtained from the simulations and the theoretical prediction from Eq. (2.2) for π_v^c (dashed line) is very good. This second case confirms the link between probabilities of

blocked stripe states and initial crossing probabilities of spin clusters.

Fixed Boundary conditions

Finally, we will look at a last case in which we impose fixed boundary conditions with $S = -1$ on the left and right sides of a rectangle and with $S = +1$ on the top and bottom sides. This case is interesting because it has been extensively studied analytically at T_c by several authors using CFT and multiple stochastic Loewner evolutions [14, 15, 16], so there exists a number of theoretical predictions to compare our simulations to; moreover it is really easy to simulate and analyze as we will see below.

These boundary conditions will force the existence of two interfaces. The two possible configuration types are represented in Fig. 2.4. In the first case, the first interface goes

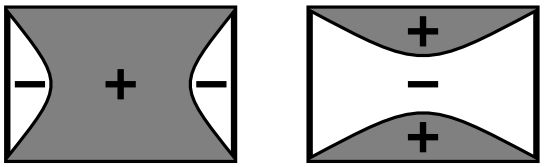

Figure 2.4 – Schematic representation of the two configuration types with fixed boundary conditions. Is is easy to see that beginning with the left (respectively right) configuration we will end up in a state where all spins equal $+1$ (-1) except the fixed ones.

from the left top corner to the left bottom corner and the second interface connects the right top corner to the bottom right corner. In the second case the interface goes from the left top corner to the right top corner and the second interface connects the bottom left corner to the bottom right corner. The probabilities for these two situations at T_c can be written in several equivalent forms, we use Kozdron's version written only in terms of the hypergeometric function F [16]. The probability for the left situation in Fig. 2.4 is given by:

$$P(x) = \frac{F(\frac{4}{3}, 3, \frac{8}{3}; 1-x)}{F(\frac{4}{3}, 3, \frac{8}{3}; x) + F(\frac{4}{3}, 3, \frac{8}{3}; 1-x)} \tag{2.3}$$

where $x \in (0, 1)$ is related to the aspect ratio r by:

$$r = \frac{K(x)}{K(1-x)} \tag{2.4}$$

with $K(x)$ the complete elliptic integral of the first kind. For the case of infinite initial temperature, the probabilities for the two situations of Fig. 2.4 are given by Cardy formula [9]. Indeed, in the case of percolation, the fixed boundary condition considered in [14, 15, 16] coincides with the situation considered by Cardy.

As previously we quench the system from T_c to $T = 0$ but also from $T = \infty$ to $T = 0$ as we found no mention of this case in the literature. With this boundary condition the

analysis of the final state is really easy, the sign of magnetization suffices to indicate the state of the system as bulk spins are all of the same sign in the end. We show the results of our simulations for $L = 1280$ for the initial temperatures T_c and $T = \infty$ in Fig. 2.5. The agreement with the theoretical prediction (dashed lines) is again excellent in both cases.

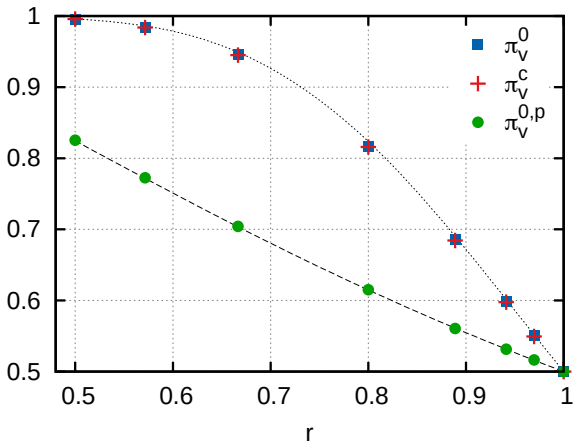

Figure 2.5 – Crossing probabilities versus r. The dashed lines correspond to the formula proved in [14, 15, 16] for the critical Ising model and in [9] for percolation. The symbols correspond to our data for π_v^0 (blue filled square) (respectively $\pi_v^{0,p}$ (green dots)) obtained after a quench at zero temperature from T_c (respectively $T = \infty$). Note that the values measured for π_v^c (red crosses) are indistinguishable from the probability π_v^0 since they are numerically very close.

We have thus shown the connection between crossing probabilities and the probabilities of existence of stripe states after a $T = 0$ Glauber dynamics in the case of the critical Ising model for various boundary conditions. We have obtained clear results showing that the final state of the evolution is strongly correlated to the initial condition. This result is interesting since it allows to relate an out-of-equilibrium situation to exact results at equilibrium.

2.2.2 How much is determined by the initial condition?

We have seen that the stripe probabilities are directly equal to crossing probabilities of spin clusters at the critical temperature. We can go further and ask whether, for one sample, it is really the clusters crossing the system initially that persist until the end to become stripes. If yes the conclusion would be much stronger than before because what we have established up to now is that the initial condition imposes the precise proportion of stripe states in the end but only statistically speaking. If each crossing cluster becomes a stripe then the final state of a sample is directly determined as soon as the initial configuration is chosen. To address such a question one has to study the right quantities.

We are interested in the evolution of the percolative state after the quench. For a system with FBC, we note $n_h(t)$ [$n_v(t)$] the number of horizontal (vertical) crossing clusters at

time t. Just a word of caution, the clusters crossing the systems vertically and horizontally contribute to $n_h(t)$ and $n_v(t)$, so this differs from previously where those clusters were contributing to π_{hv} but not to π_h and π_v. These two numbers encode all the information concerning the percolative state of the system at time t. For example the crossing probabilities studied previously can be expressed, albeit in a rather cumbersome way, with these numbers of clusters as $\pi_h(t) = \langle (1 - \delta_{n_h(t),0})\delta_{n_v(t),0} \rangle$ with $\langle \cdots \rangle$ the average over initial configurations and thermal histories, and δ_{ab} the Kronecker delta. Here we want to go further and compare the percolative states between two times t_1 and t_2. This leads us quite naturally to define the two times autocorrelation function $\mathcal{A}_c(t_1, t_2)$:

$$\mathcal{A}_c(t_1, t_2) = \langle \delta_{n_v(t_1)n_v(t_2)}\delta_{n_h(t_1)n_h(t_2)} \rangle \ . \tag{2.5}$$

Quite simply the product of Kronecker deltas equals 1 if there is the same number of vertical and horizontal crossing clusters at t_1 and t_2 and it equals 0 otherwise. We note that $\mathcal{A}_c(0, t)$ is the correlation function measuring if the current state of the system is the same as it was initially.

Percolative correlation with the initial state

To answer the question about the influence of the initial condition we can look at the restricted correlation function $\mathcal{A}_c(0, t)$. It is of course a decreasing function of time but one can wonder if it reaches a finite value for $t \to \infty$. If it is the case then some information is conserved from the initial condition even in the thermodynamic limit. So we compute the quantity $\mathcal{A}_c(0, \infty)$ which should be understood as $\lim_{t\to\infty} \mathcal{A}_c(0, t)$. Of course in MC simulations the infinite time limit is unreachable in general but here it is actually exact since the system freezes at some finite time and stays in this state forever after. In figure 2.6 we represent $\mathcal{A}_c(0, \infty)$ vs. the linear system size L for $32 \leq L \leq 1024$. We can see that $\mathcal{A}_c(0, \infty)$ not only has a finite value for all the L used but that it actually increases with L and it makes little doubt that it converges to 1 as $L \to \infty$. We highlight the convergence towards 1 in the inset by representing $1 - \mathcal{A}_c(0, \infty)$ vs. L in double logarithmic scale. We remark that the approach to one is compatible with a power-law decay. This means that the statement made in subsection 2.2.1 that the final states probabilities are given by the initial crossing probabilities is strengthened as the results discussed above show that each single system stays in the same percolative state during all the evolution. The most stringent test of this statement could be achieved by defining and computing a quantity which equals 1 only if a system stays strictly in the same state after each single update and zero otherwise. But computing such a quantity requires a test of the percolative state of the system after each update which requires a time roughly proportional to the number of spins in the system. Another approach is to use an algorithm which labels each clusters and relabels the clusters if necessary after an update. This way the computational cost of the operation would not be prohibitive. We have not used such an algorithm but we consider nevertheless that the conclusions drawn from the study of $\mathcal{A}_c(0, \infty)$ are convincing enough.

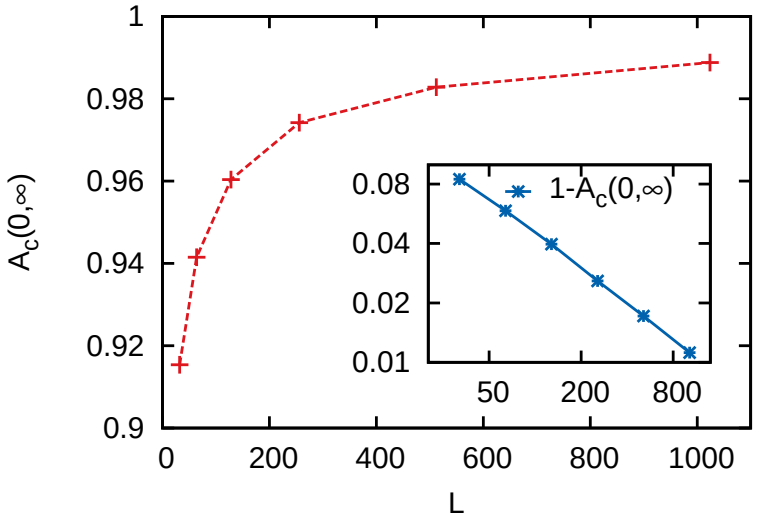

Figure 2.6 – Autocorrelation function $\mathcal{A}_c(0,\infty)$ vs. linear system size L and in the inset $1-\mathcal{A}_c(0,\infty)$ is plot vs. L in double logarithmic scale.

Overlap with the initial state

The overlap with the initial state $q(t)$ at time t is simply defined as:

$$q(t,L) = \frac{1}{N}\sum_i \langle s_i(0)s_i(t)\rangle \tag{2.6}$$

for a system of linear size L and $N = L^d$. The values of $q(\infty, L)$ were measured for different system sizes and plotted vs. L in double logarithmic scale (not shown). The behaviour is compatible with a power law behaviour and a fit yields that $q(\infty, L) \sim L^{-0.125(1)}$. This value coincides with the magnetic exponent $\beta/\nu = 1/8$ of the Ising model, and this is not by chance as we are going to see. We are giving below two explanations for this exponent one qualitative and another more quantitative. As defined in equation (2.6) we can see that $q(\infty, L)$ is the product spin by spin of the initial and final configurations. Considering for the moment only the samples which end up in a ground state where all spins take the same value ± 1, in this case $\sum_i s_i(0)s_i(\infty) = \pm\sum_i s_i(0)$, which means that the overlap for this sample equals plus or minus its initial magnetization depending of the final ground state. Furthermore as we have argued earlier the initial spanning clusters dictates the ending of the evolution. For samples which final states are completely magnetized there must have been initially one cluster spanning both directions. Since this cluster is also certainly the biggest thus imposing the sign of the magnetization, the final magnetization should be of the same sign as the initial one. This can be verified directly and for a system with FBC a little bit over 93% of samples have an initial and final magnetization of the same sign almost independently of the system size. This means that a majority of the sums $\sum_i s_i(0)s_i(\infty)$ are positive thus the overlap behaves as the mean absolute value of the magnetization. As

the latter behaves as $L^{-\beta/\nu} \sim L^{-1/8}$ this explains the behaviour observed for $q(\infty, L)$. It seems that the stripe states do not alter this behaviour since the exponent measured is in really good agreement with β/ν.

We called this quantity overlap to be coherent with other quantities we studied but actually in this case it coincides the usual autocorrelation function $\langle s_i(0)s_i(t)\rangle$. The autocorrelation function is known to decay with time as $L(t)^{-\lambda}$ which defines the exponent λ where $L(t)$ is the dynamic length scale which grows as $t^{1/2}$ for a dynamics with non-conserved order parameter. λ is a non-trivial exponent which equals approximately 1.25 for bi-dimensional systems quenched from a supercritical temperature, *i.e.* a short-range correlated initial condition. An RG treatment of the coarsening from a correlated initial condition has been described in an article by Bray *et al.* [27]. Taking the form of the initial correlation as $\langle s_i(0)s_j(0)\rangle \sim r_{ij}^{-d-\sigma}$ with d the dimension of the system, they concluded that the speed of the decrease of the autocorrelation function vary with the exponent σ describing the initial decay of long-range correlations. There is a value of the exponent σ_c such that for $\sigma > \sigma_c$ the initial correlations decay fast enough for the autocorrelation to take the same form as for short-range correlated initial condition, *i.e.* that the exponent λ has its short-range (SR) value $\lambda = \lambda_{\text{SR}}$. For $\sigma < \sigma_c$ the exponent σ appears in the time dependence of the autocorrelation function and Bray *et al.* showed that $\lambda_{\text{LR}} = (d+\sigma)/2$ so that it behaves as $t^{-(d+\sigma)/4}$. Furthermore they showed that the transition between those two regimes happens at $\sigma_c = 2\lambda_{\text{SR}} - d$ so λ is a continuous function of σ. This situation is very similar to the Ising model with long-range interactions at equilibrium which we will talk about in great details in chapter 4. For the Ising model equilibrated at its critical temperature which is of interest for us here the correlations decay as $1/r_{ij}^{d-2+\eta}$ with the anomalous dimension $\eta = 1/4$ in $d = 2$. This means that $\sigma = \eta - 2 = -7/4$ which is less than $\sigma_c = 2\lambda_{\text{SR}} - d \simeq 0.5$ so in our case the initial correlation are relevant and the autocorrelation function decays as $t^{-\eta/4} \sim t^{-1/16}$. This is completely consistent with the long-time behaviour of the overlap with the initial condition studied before as we found that it depends on the system size as $L^{-0.125(1)}$ and we conjectured in the previous paragraph that it should be $L^{-\beta/\nu}$ with $\beta/\nu = 1/8$. One can show from scaling relations that $\eta = 2\beta/\nu$ which means that $q(\infty, L) \sim L^{-\eta/2} \sim L^{-2\lambda_{\text{SR}}}$ in perfect agreement with the RG result. It is interesting that our simple argument yields the exact result from a completely different way.

Overlap between two copies

Another approach to the influence of the initial condition is to say that if the initial condition really persists later in the evolution then two systems with an identical initial spin configuration evolving under different thermal histories should be somehow correlated. The overlap is a quantity which can make this correlation more obvious. Here we will use a variant of the overlap already discussed which is actually closer to the historical use of this notion [28, 29, 30, 31]. The overlap between two copies of the system is defined as follows: at $t = t_w$ one makes two copies of the configuration, say $s_i(t_w) = \sigma_i(t_w)$, and lets

them evolve with different noises. The overlap between the clones at time t is then

$$q_{t_w}(t, L) = \frac{1}{N} \sum_i \langle s_i(t)\sigma_i(t) \rangle \ , \tag{2.7}$$

where the angular brackets indicate an average over different realizations of this procedure. The two-time scaling properties of this quantity, in the limit $L \to \infty$, were used to distinguish domain-growth processes from glassy ones [29, 30]. It was recently shown that $q_{t_w=0}(t, L)$ and $q_{t_w=0}(\infty, L)$ decrease algebraically with t and L, respectively [31]. The fact that $q_{t_w=0}(t, L)$ decreases with t is clear. We will for now only consider the case with no waiting time $t_w = 0$, but we will see later that the introduction of a non-zero waiting time can be very informative.

In figure 2.7 $q_0(t, L)$ is plotted as a function of time t for different system sizes L. It first decreases on a very short time and reaches a minimum at around $t \simeq 1$MCs and

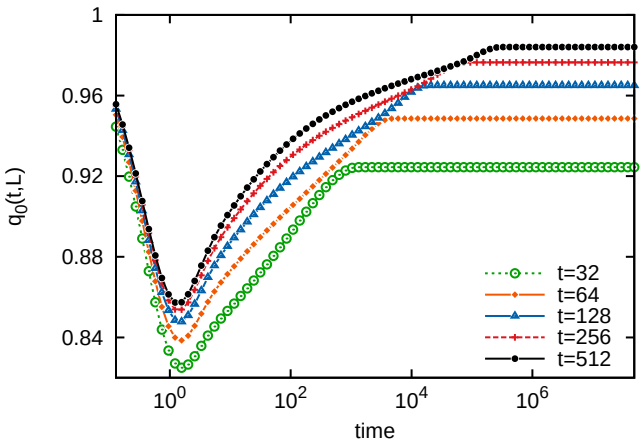

Figure 2.7 – Overlap $q_0(t, L)$ vs. time t the different linear system sizes given in the key. The abscissa is in log-scale.

then increases until it reaches a constant value corresponding to the moment when all systems have reached their final state. A fit of the form $c + aL^{-b}$ confirms that, as for the autocorrelation function $\mathcal{A}(0, \infty)$, $q_0(\infty, L)$ converges towards 1 in the large system limit. Indeed, in figure 2.8, $1 - q_0(\infty, L)$ is plotted vs. system size L in a double log-scale. It is well described by a power law behaviour. Excluding the three smallest sizes yields the best fit quality and gives an exponent equal to $0.57(1)$. As we will see in subsection 2.3.3, one can also study an exponent describing the behaviour of the overlap but this time with an infinite temperature initial condition. In this case the results is $0.50(1)$ which means that the two values are incompatible. This shows that when changing the initial condition from super-critical to critical but keeping the working temperature $T = 0$, the behaviour of the overlap is governed by a different exponent. We do not have an explanation for this fact as before for the overlap with the initial condition so further studies (numerical and

analytical) would be very interesting to clarify this feature as we have found no mention of it in the literature. For example one can wonder if this exponent can be expressed in terms of other known exponents.

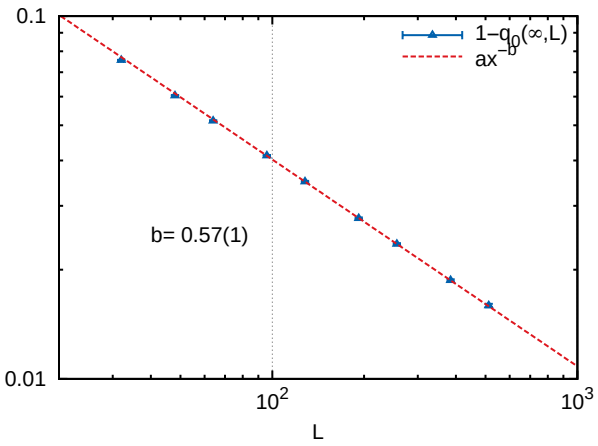

Figure 2.8 – $1 - q_0(t, L)$ vs. linear system size L in double logarithmic scale.

Persistence

Another interesting quantity to measure how much of the initial condition remains is the persistence $\mathcal{P}$. Persistence is a very general notion related to first passage times, see [32] for a recent review on the subject. For a random walker on a line it is the probability that its position remains positive up to time t starting from a given position. For spin systems $\mathcal{P}(t)$ simply equals the fraction of spins that have never flipped at time t since a zero-temperature quench or equivalently the probability that a single spin has not flipped up to time t. It is different from a two time quantity such as the autocorrelation function defined previously. Indeed it contains informations from every update, about all the history of the system. In a lot of cases, the persistence decreases algebraically for long time as $\mathcal{P}(t) \sim t^{-\theta}$ with θ a non trivial dynamical exponent.

The persistence has been studied mostly starting from an infinite temperature, *i.e.* uncorrelated, initial condition. We will talk about this case in more details in the next section but we will recall here the main results that we need now. We concentrate on local persistence even if other types of persistence can be defined and studied. It was first studied numerically for the one dimensional Ising model [33], but one can in general consider a Q state Potts model in d dimensions after a zero temperature quench from $T = \infty$ evolving with a Glauber dynamic [34, 35]. The persistence decreases in a power-law fashion $\mathcal{P}(t) \sim t^{-\theta}$ with θ a universal exponent depending only on Q and d. The exact value of θ was obtained explicitly in $d = 1$ for all values of Q by mapping the domain walls to particles which diffuse, annihilate and coalesce [36, 37]. No such exact result exist in higher

dimensions. Nevertheless a perturbation scheme was developed in [38, 39] and an approximate value of $\theta \simeq 0.19$ was obtained for the bi-dimensional Ising model. This value is in agreement with the slightly superior numerical estimate [35] and the experimental value of [40]. We will estimate precisely θ in this case in subsection 2.3.4.

We will now concentrate on the zero-temperature quench from a critical initial condition. As for the overlap, we can either follow the behaviour of the persistence with time or check the size dependence of the final value for $t \to \infty$. We plot the value $\mathcal{P}(\infty, L)$ vs. system linear size L (not shown) for systems with PBC and study its behaviour. A function of the form aL^{-b} yields a fit of good quality giving $b = 2\theta_c = 0.07(1)$. Excluding the three smallest system sizes greatly improves the fit's quality. Studying the time dependence is tricky as the long time regime where the real persistence dominates is only attained for big systems ($L \geq 1000$). Nevertheless one can measure $\theta_c = 0.06(2)$ which is close but not completely in agreement with the value measured from the long time limits. It is likely that the value obtained from the fit of $\mathcal{P}(\infty, L)$ is more accurate than the one extracted from the time dependence since the slope of the persistence with time approaches only slowly the universal value. We will explore the difficulties to measure precisely the persistence exponent in subsection 2.3.4 concerned with infinite temperature initial condition.

One can derive a bound on the persistence exponent from geometrical arguments. As we have seen only spanning or wrapping clusters survive the coarsening process as all the others clusters shrink and eventually disappear. This means that the only spins contributing to $\mathcal{P}(\infty, L)$ have to belong to the initial spanning clusters. In the simplest case where one clusters spans both direction for a system with FBC, the initial spanning cluster is certainly the largest cluster whose mass scales as $\sim L^D$ with D its fractal dimension. Thus the persistence $\mathcal{P}(\infty, L)$ must decay at least as fast or faster than the fraction of spins in the initial spanning cluster L^{D-d}. As we have seen $\mathcal{P}(\infty, L) \sim L^{-2\theta_c}$, implying that:

$$2\theta_c \geq d - D. \tag{2.8}$$

Remembering that $D = d - (\beta/\nu)_{tri}$ where $(\beta/\nu)_{tri} = 5/96$ are the exponents associated to the magnetization of the tricritical model or giving the size of the biggest spin cluster, one can rewrite Eq. (2.8) as $2\theta_c \geq (\beta/\nu)_{tri}$. The exponent measured follows this inequality as $2\theta_c = 0.07$ and $(\beta/\nu)_{tri} = 5/96 \simeq 0.052$. We must note that while we have assumed that all the persistent states in the final state belonged to the initial spanning cluster, we think that this assumption is very likely. However during the evolution, the persistent sites can of course belong to any clusters, so that we cannot apply a similar argument at any time.

One may rewrite this inequality in another way considering the spatial distribution of persistent sites. Several authors have shown that the persistent sites of a system quenched from infinite temperature have a non trivial spatial distribution [41, 42, 43, 44, 45]. Indeed persistent sites form fractal clusters of dimension $D_p = d - z\theta$ with $z = 2$, as can be easily seen from the infinite time value of the persistence $\mathcal{P}(\infty, L)$ which scales as $L^{-2\theta}$ so the number of persistent sites behaves as $L^{d-2\theta}$. While we have not checked that the persistent sites have a fractal structure in the case of a critical initial condition, they quite likely do

in analogy to the previous case. We will therefore assume that the persistent clusters have a fractal dimension $D_p = d - z\theta_c$, which is compatible with the value of the persistence in the final state. The inequality (2.8) can then be rewritten as $D_p \leq D$, which is natural since the persistent sites in the final state are a subset of the initial largest cluster so their fractal dimension must be less than the biggest cluster's one.

The value measured for $\theta_c \simeq 0.035(5)$ is clearly different from the value measured and computed analytically for the persistence exponent $\theta \simeq 0.19$ for an infinite temperature initial condition. The difference between the two situations is that no long-range correlations exists at infinite temperature contrarily to the critical case. It is the assumption made for the analytical derivation of θ, *i.e.* that the initial correlation are short-ranged so that they play no role in the universal behaviour of the dynamic. Moreover, it is quite natural that $\theta_c \leq \theta$ as one expects that less spins will flip when the initial condition is more preserved as it is the case for the critical initial condition compared to the infinite temperature one as we will see more precisely in the next section. It is however far from rigorous and it would be very interesting to carry an analysis similar to [38] for this situation and maybe give a theoretical explanation to θ_c. As before for the overlap with the initial state we should consider an initial spin configuration s^0 which would no longer be uncorrelated as $\langle s^0(x)s^0(y)\rangle = \delta(x-y)$ but with long-range correlations typical of critical points $\langle s^0(x)s^0(y)\rangle \sim 1/|x-y|^{d+\sigma}$ with $\sigma = \eta - 2$. It is however unclear to us where this correlations would enter the method of [38, 39]. We nonetheless expect that there should be a special value σ_c of the exponent of the initial correlations such that for correlations decaying faster than this we recover the short-range case. This would be quite interesting to test numerically.

2.3 Infinite temperature initial condition

We will now consider systems quenched from infinite to zero temperature. We have interests similar as the ones in the previous section, we want to study final states and see how much is kept from the initial condition. We will show that the evolution is more complex than before and that an additional transient regime exists.

2.3.1 Stripe states

As we have shortly discussed in subsection 2.2.1, several works have studied the appearance of stripe states during subcritical coarsening. It has implication for the thermalisation time [2] because diagonal stripe states for which the thermalisation time is much higher appear in a finite fraction of samples. Indeed, in this case, the stripe boundaries have to diffuse until they collapse in order to reach a ground state and this interface diffusion regime lasts much longer than the usual coarsening thermalisation time [3, 4]. In 2009 Barros *et al.* finally gave a very interesting explanation of the probabilities for which the stripes are found in final states [7]. They showed numerically that those stripe probabilities agree very precisely with critical percolation crossing probabilities for various boundary

conditions. In 2012 Olejarz *et al.* strengthened this correspondence by showing that it also holds for stripes winding in both directions around a system with PBC [8]. In this case one has to add short-range interactions going beyond the nearest neighbours to stabilise the stripes. These works draw a nice and convincing picture that critical percolation is indeed an essential ingredient to understand precisely the final states.

The explanation proposed in [7] for the success of percolation crossing formula for the appearance of stripe states is based on two observations. On one hand, very soon after the quench the typical domain size is much larger than the lattice spacing, so the discrete nature of the underlying lattice is forgotten and the system is now a realisation of continuum percolation for which $p_c = 1/2$. At infinite temperature the concentration for both spin values is $1/2$ and it stays close to it in the short-time regime, so the system quickly corresponds exactly to the critical point of continuum percolation. On the other hand in the coarsening regime the evolution of cluster interfaces only tends to reduce local curvature and clusters just shrink until they disappear. With this kind of evolution no change of topology (in the sense of percolating clusters) is to be expected once the dynamic length-scale $\xi(t) \sim t^{1/2}$ is much larger than the lattice spacing. Considered together this provide a convincing scenario for the presence of critical percolation probabilities in the final states.

We can note that even though fairly probable the first of those two observations lacked a more rigorous study. One had to assume that the dynamics brings the system to a state in which its spin clusters possess critical percolation properties. But several questions remain unanswered among which an important one is how and when the system reaches critical percolation? This question is completely absent of the traditional theory of coarsening [46] which is otherwise very successful to explain and characterize a wealth of other phenomena. The study of this question is the subject of the rest of this section along with some related issues.

2.3.2 Onset of critical percolation

Overview

It is a priori difficult to have an intuition of when the system becomes similar to critical percolation. In the works of Sicilia *et al.* the authors noticed that after a few Monte-Carlo steps at $T < T_c$, an infinite temperature system on a square lattice is very similar to the critical percolation point for the spin clusters [5, 6]. So it seems that it is on a very short time scale that the critical percolation appears. It is very interesting to look at snapshots of some samples during their evolution to understand what happens. In figure 2.9 we show such snapshots for a system on a square lattice of linear size $L = 128$. $+1$ spins (-1 spins) are shown as white (red) dots. Since we are interested in clusters spanning the system, we colour $+1$ spins (-1 spins) spanning clusters in clear blue (black).

The times chosen to draw the snapshots correspond to all the times when the percolative state of the system changes. As expected at the initial time no spanning cluster is present as their probability to appear decreases exponentially fast with the system size in subcritical percolation. While looking at these snapshots, several facts are quite surprising: the first

time when a spanning cluster appears is very small (less than 1MCs in figure 2.9), the systems changes of percolative state a great number of times and the last change occurs quite early ($t = 7.46$MCs for this sample) compared to the thermalisation time proportional

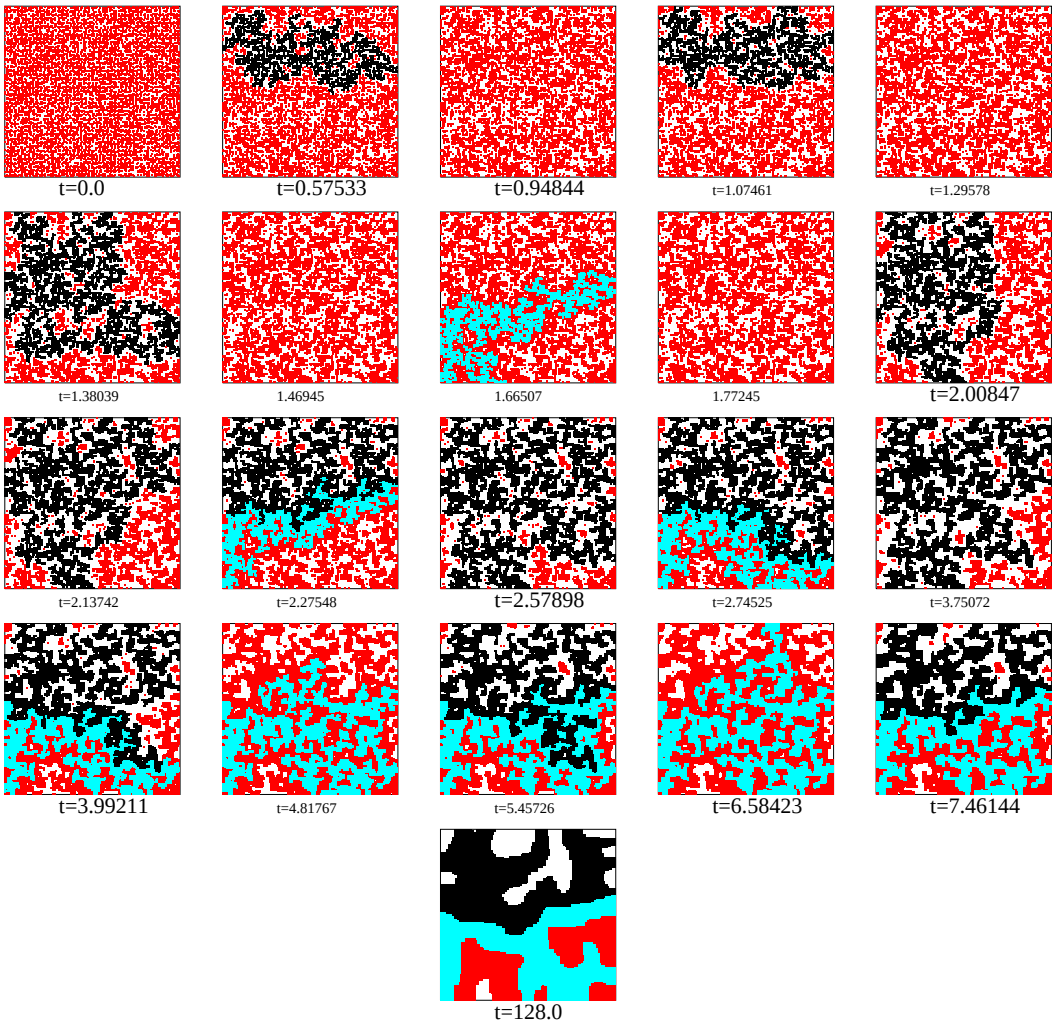

Figure 2.9 – Snapshots of a $2d$IM on a square lattice with $L = 128$ and FBC. A quench from $T_i \to \infty$ to $T = 0$ was performed at $t = 0$. Spins $S_i = -1$ ($S_i = +1$) are shown in red (white). A percolating cluster of spins $S_i = -1$ ($S_i = +1$) is shown in black (clear blue).

to L^2. So in general the evolution of a system follows the different phases: at $t = 0$ the spins take random values and no spanning cluster is present. At a time $t_f \ll L^2$ a first spanning cluster appears. Then follows a period $t_f < t < t_p$ with $t_p \ll L^2$ in which spanning clusters appear and disappear typically 10 to 20 times in our simulations. At t_p the number and type of spanning clusters are equal to the number and kind of stripes in the final state. The regime $t_f < t < t_p$ is interesting and we will clarify it in subsection 2.3.2.

The fact that $t_p \ll L^2$ is intriguing as it indicates that the fate of the Ising model is sealed very soon in the evolution, we will study this phenomenon in subsection 2.3.3.

Crossing probabilities

Square lattice To study spanning clusters, natural quantities to consider are crossing probabilities as we have done in subsection 2.2.1 for the quench from critical to zero temperature, but here we will follow their evolution with time. In figure 2.10 the probability $\pi = \pi_h + \pi_v + \pi_{hv}$ that a cluster spans the system in one or two directions vs. time is shown for different system linear sizes L. Even though for one sample the evolution of the percolative state is stochastic and full of events as we have seen in the previous subsection the average probability has a very smooth behaviour. As mentioned above, the total crossing probability $\pi(0)$ at $t = 0$ equals zero since the configuration is subcritical on the square lattice. This probability rapidly increases until it reaches 1 after a few MCs. It is clear that the time at which the system contains a spanning with probability 1 increases with the system size. It is also interesting to understand the time dependence of the probability when it approaches 1. In figure 2.11 the probability $1 - \pi(t)$ that no cluster spans the system at time t is plotted in double logarithmic scale. After a short time the approach to percolation seems to be compatible with a power law behaviour of the type $\pi(t) = 1 - at^{-b}$ with b an exponent which appears to be size dependant. To estimate the time needed to reach percolation we rescale the time by a size dependent factor L^α in the inset of figure 2.11. A collapse for the tail is obtained for $\alpha = 0.29(4)$. This collapse is convincing but it does not work for the intermediate regime preceding the power law regime. While looking more closely at the

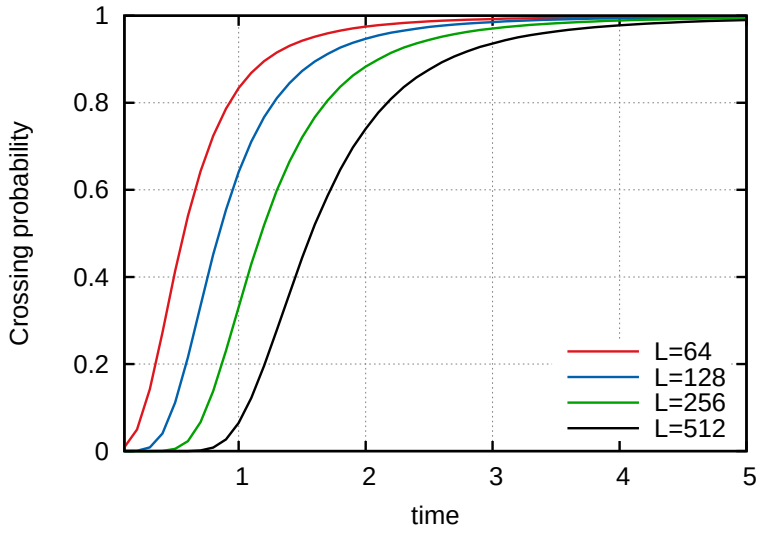

Figure 2.10 – Crossing probability vs. time t for several system linear sizes L given in the key on a square lattice with FBC.

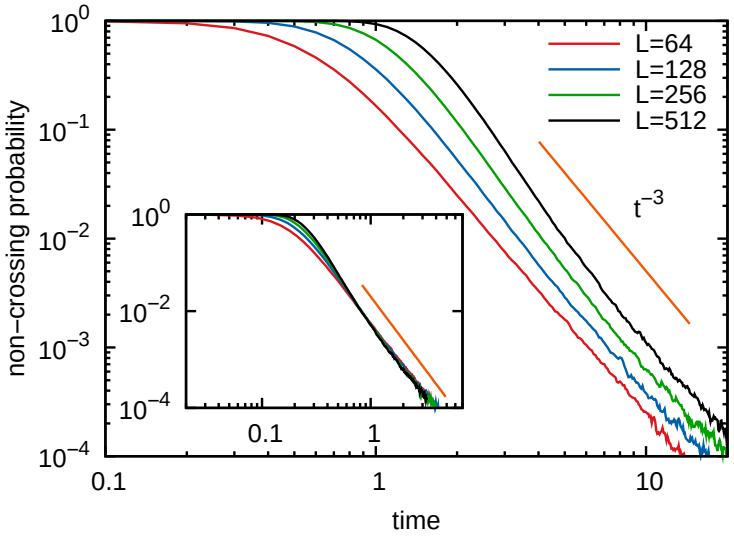

Figure 2.11 – Non-crossing probability $1-\pi(t)$ vs. time t for several system linear sizes L given in the key on a square lattice with FBC in double logarithmic scale. The straight line is a guide to the eye. In the inset the same quantity is plotted but the time has been rescaled by a factor L^{α} with $\alpha = 0.29(4)$.

different types of spanning clusters, we can see that in an intermediate regime a significant fraction (more that 10%) of the samples are in a state with only one cluster spanning in one direction. Those configurations are counter-intuitive since one would expect that the interface of a $+$ stripe should also be the boundary of a $-$ stripe and therefore that clusters spanning in only one direction come in pairs. This is however not always the case since on the square lattice, a stripe boundary containing a step in addition to another cluster of the same sign having a corner on the opposite direction can cut the cluster neighbour of the stripe into two. From the point of view of domain walls drawn on the dual lattice, this corresponds to a point where two domain walls pass by the same point. This situation does not last very long since a corner is unstable at $T = 0$ and therefore disappears to form a straight interface. The temporary existence of those configuration may explain that the collapse does not work for all t and in particular just before the power law regime.

Kagome lattice We have studied the same quantities and situation on the kagome lattice. It is a regular lattice where all sites possess four neighbours with a site percolation threshold $p_c^K \simeq 0.65$. So we expect the situation to be similar to the one on the square lattice since the initial condition is subcritical. The crossing probability $\pi(t)$ is shown in figure 2.12 for different system sizes. L_x (L_y) is the number of sites in the horizontal (vertical) direction. The values chosen correspond to an aspect ratio $r = (\sqrt{3}92/2)/80 \simeq 0.9959$ close to 1 so that the horizontal crossing probability equals the vertical one. As expected the curves are very similar to previous case, going quickly from a non percolating initial condition to a

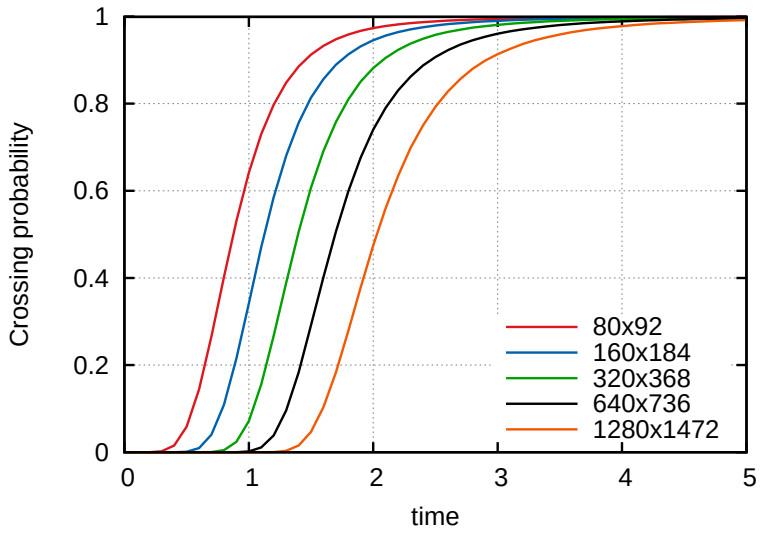

Figure 2.12 – Crossing probability $\pi(t)$ vs. time t for several system sizes $L_x \times L_y$ given in the key on a kagome lattice with FBC.

percolating one. As before the approach to 1 is compatible with a power law behaviour with an exponent close to 3.5 and we can also rescale the time dependence by a size dependent factor L^α with $\alpha \simeq 0.25$. This indicates that the exponent related to the time needed to reach a percolating configuration is lattice dependent so not universal.

There is on the kagome lattice a feature that is absent from the other lattices studied up to now. When a stripe state occurs there are spins between the stripes that possess two neighbours of each sign and can therefore flip indefinitely with no energy change, see figure 2.13. It is quite remarkable that the system can end up in an ensemble of iso-energetic final states in such a simple set-up. In $3d$ it is very common as it is for example the predominant scenario on the cubic lattice with entangled spanning clusters and sites which can blink indefinitely [47, 48]. In this case the ground states are almost never reached. With the presence of those blinkers we had to refine the condition that a final is a state where no spin updates are possible, by adding that states possessing sites with an equal numbers of neighbours of opposite sign with no possibility of change are also considered final. Numerically it is fairly easy to detect them as the blinkers come in numbers multiple of the linear horizontal system size.

Odd coordinated lattices In this paragraph we are interested in the same set-up on odd coordinated lattices, that is lattices which sites have an odd number of neighbours. It has been known for a long time that in this case the dynamics is very different than on even coordinated lattice due to the existence of metastable spin droplets [49]. For a zero temperature dynamics those metastable droplets live indefinitely, hence the system quickly get frozen

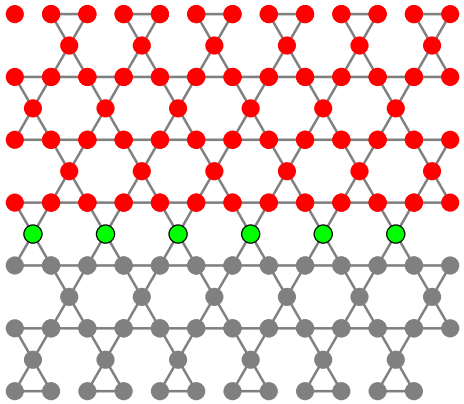

Figure 2.13 – Configuration presenting blinkers (in green) on a kagome lattice with FBC.

in a configuration with many metastable droplets with no possible updates. More generally this happens on any lattice where a fraction of sites have an odd number of neighbours. Seven out of the eleven archimedean lattices are odd coordinated, the hexagonal lattice with coordination 3 being the most common. More generally among lattices with several types of vertices, those having only even coordination numbers are uncommon. It is therefore interesting to study odd coordinated lattices and in particular we would like to know what happens on these lattices concerning the approach to critical percolation studied above for even-coordinated lattices.

We will concentrate on the hexagonal lattice. As mentioned the coarsening dynamics was studied on this lattice in [49] by Takano and Miyashita which focused on the thermalisation time at small but finite temperature. These authors observed that the magnetisation does not behave as on the square lattice, presenting a plateau during the evolution. They also remarked that the thermalisation time increases as the temperature decreases. The dynamics can be separated in three phases: for $t < t_1$ the magnetisation evolves and the number of sites with 2 or 3 neighbours of opposite signs decreases quickly; for $t_1 < t < t_2$ the magnetisation has a fixed value and for $t > t_2$ the magnetisation finally evolves towards its equilibrium value. They measured that the dependence of t_1 on the temperature and system size L was small contrarily to t_2 which varies greatly with those two parameters. The first phase corresponds to the onset of metastable clusters formed by gluing together a certain number of same-spin hexagons. The smallest metastable cluster consist of six spins with the same sign taking the form of an hexagon. It is easy to see that the destruction of such a cluster with single spin flips requires an energy increase for the first spin flip and then the flips of the other spins are favoured energetically. For bigger metastable clusters, the process has to be repeated for each elementary hexagon forming it. This energy increase makes this process very slow at low temperature due to the time needed to overcome the activation barrier. At zero-temperature such an energy increase is impossible thus the evolution comes to an halt at the time t_1 mentioned previously. We

know that the plateau is simply the time needed for the activated process. The time needed to jump a barrier ΔE at inverse temperature β scales as $e^{\beta\Delta E}$ so in our case $e^{2\beta J}$. Takano and Miyashita checked numerically that the magnetisation behaves as $f(t/(e^{2\beta J}L^2))$ for the late stage of the evolution. Thus when the activation time-scale is taken into account, one recovers a scaling t/L^2 as for other lattices.

A similar activated process was studied by Spirin*et al.* in [3] on the square lattice when horizontal or vertical stripes form during an evolution at low temperature. As we have seen those stripes last forever at zero-temperature but at finite temperature they are only metastable and disappear at some point and then the system can reach equilibrium. The destruction of a stripe begins by forming a dent, *i.e.* flipping a spin at its boundary, which, if it expands and reaches the system boundary, removes a line of L spins off the stripe. This process has to be repeated until the whole stripe has been unknitted. This is very similar to the destruction of the metastable clusters on the hexagonal lattice but there are nonetheless differences. On the hexagonal lattice, once the first spin has successfully flipped and is followed by a second spin, the other spins of the hexagons which do not belong to another hexagon quickly flip and the open hexagon is destroyed. Indeed this process of destroying the open hexagon makes the energy decrease after the initial activation, so the destruction is inevitable once it has begun. On the square lattice on the contrary, the two kinks formed on the stripe boundary after an energy increasing spin flip move at no energy cost in one direction or the other. They behave as random walkers which have to travel to the system boundary before colliding into the other kink. Using first-time passage arguments the authors of [3] showed and checked that the time needed to destroy a stripe scales as $L^3e^{4\beta J} \gg L^2$. This time is much longer than the usual thermalisation time L^2 so the situation, though similar, is not the same as for the hexagonal lattice. On the hexagonal the thermalisation time still depends as L^2 on the system size and only the prefactor depends on the temperature.

Let us now consider the early times of the evolution on the hexagonal lattice at $T = 0$, corresponding to $t < t_1$. An interesting question is whether the onset of critical percolation occurs before the system freezes. One way to look at this problem is as before to compute the crossing probabilities. The crossing probabilities (not shown) reveal that one can observe the very fast approach to critical percolation even for fairly big systems ($L < 1024$) as on even-coordinated lattice. For those sizes this means that the system reaches percolation before freezing. We show another way to study this problem in figure 2.14 where the distribution of the areas of spin clusters $n_d(A, t)$ is plotted for various times after the quench. As for other lattices with $p_c > 0.5$ the initial distribution $n_d(A, 0)$ decays exponentially but already at $t = 4\mathrm{MCs}$ the percolation-like power law tail is established. The peaks for small sizes corresponds to the discrete values of possible area values for metastable clusters which sequence begins as $6, 10, 13, 14 \ldots$ But for areas $A > 50$ no such effect is noticeable and the distribution is exactly as expected for critical percolation. This confirms that the onset of percolation is faster than the freezing at least for systems smaller than $L = 1024$.

To have a deeper understanding of the relative speed of the approach to percolation

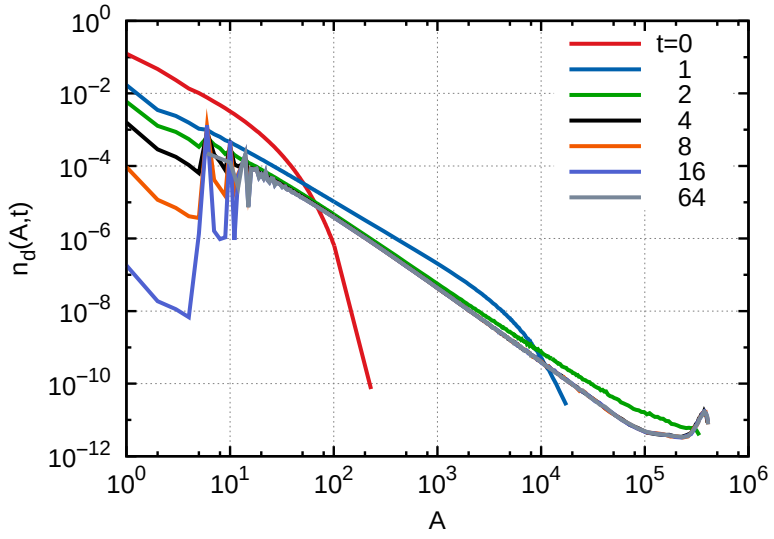

Figure 2.14 – Spin clusters area distribution $n_d(A,t)$ vs. area A for several times t given in the key on a hexagonal lattice of linear size $L = 1024$ with FBC in double logarithmic scale.

compared to the freezing process, let us focus on the latter. In [49] the authors only remarked that the time needed to reach the plateau of magnetisation depends weakly on the system size and on temperature. We define the *freezing time* of a system as the time when no updates are possible, which means that flipping any spins of the system increases its energy as the system is in a local minimum of energy. This time is easy to compute with a CTMC algorithm for the evolution as the implementation of this algorithm requires to keep a list of all the sites which can be updated. In figure 2.15, the mean freezing time $t_*(L)$ is plotted as a function of the system linear size L. The evolution of the freezing time is compatible with a logarithmic growth $t_*(L) \sim a \log L + b$. This result is interesting because if the time needed to reach percolation grows algebraically with the system size as for the other cases seen before then systems big enough will freeze before percolation has the time to be established. It is not clear to us how this size dependence arises. The freezing process goes as follows: any spin with at least two neighbours of opposite sign can be updated but as soon as a spin belongs to an hexagon of spins of same value it is frozen. This must be qualified as in fact any structure composed of loops linked together are stable as any spin composing it have exactly two neighbours aligned with it. But coarsening tends to make the clusters compact over distances of a few lattice spacing very quickly so it is certainly accurate to consider that all frozen spins belong to elementary hexagons. In analogy with the dynamical length scale one can define a time dependent freezing length $\xi_*(t)$. From the dependence of the freezing time with the system size we can say that this freezing length grows exponentially fast with time $\xi_*(t) \sim e^{at}$ with a a positive constant. This is obtained from the behaviour of the freezing time but it would a very interesting to see if this length

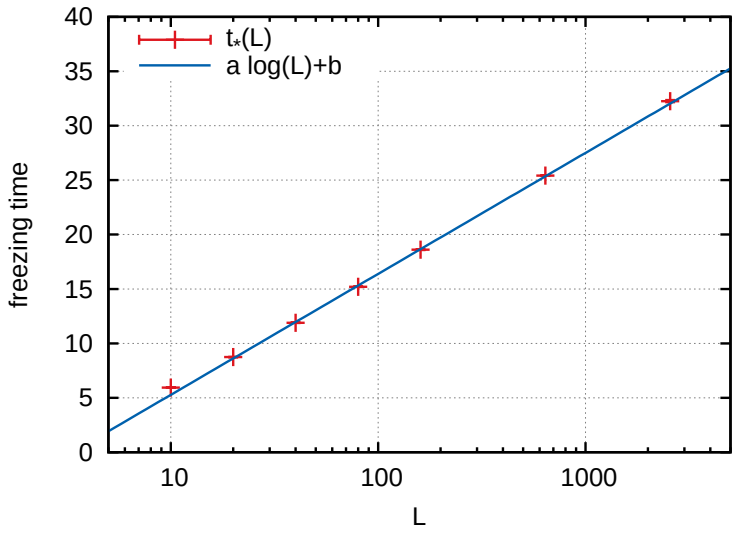

Figure 2.15 – Mean freezing time vs. system linear size L a hexagonal lattice with FBC with the abscissa in logarithmic scale.

appears in observables related to frozen sites as for example a correlation function.

Now let us come back to the question of the relative speed of the onset of percolation vs. the freezing process. We have already shown the probability distribution of spin cluster areas, $n_d(A,t)$, as a function of the number of spins in a cluster, A, and time, t. It acquires a power-law behaviour very quickly with the precise form of a critical percolation distribution as we have seen in figure 2.14. This description is nonetheless incomplete as the distribution is not solely a power-law and for the biggest clusters one can observe a bump. This bump corresponds to clusters with a linear size of the size of the system, that is percolating clusters. A more complete form for the distribution is therefore:

$$n_d(A,t) \simeq 2cA^{-\tau} + N_p(A/L^D, t) \tag{2.9}$$

with $D = d/(\tau - 1) = 91/48 \simeq 1.896$ is the fractal dimension of the percolating clusters. The bump N_p is written as function of A/L^D because the size of the percolating clusters grows with the system size according to their fractal dimension. Numerically this distribution is built by recording the areas of the biggest cluster of each sample separately. One can then plot the bump for different sizes and times (not shown). Qualitatively this distribution evolves at first very quickly from its initial subcritical Gumbel form towards bigger sizes. After some time the distributions for different system sizes converge to a distribution roughly independent of time. We can then estimate the time needed to reach this distribution which grows with the system size. This time is in fact the time to reach the percolative state. From the plots at different times, we remark that this time grows slower than a power law contrarily to the case of even-coordinated lattices which we will discuss

in more detail in the next subsection. It looks like the freezing process accelerates the onset of percolation. This is a bit surprising at first but in fact rather natural. What happens on the hexagonal lattice is that even very early after the quench clusters are already mostly frozen and thus constitute fixed building blocks for the forming percolating cluster. On even coordinated lattices the initial subcritical clusters are subject to much more change before the percolating cluster is formed. This argument is very qualitative but we think that the main difference between those two situations is here. We have studied the freezing process on the Shastry-Sutherland lattice which only possess a fraction of odd coordinated vertices and everything is very similar to what happens on the hexagonal lattice.

2.3.3 Definitive percolation state

In the previous subsection we have studied the approach to critical percolation. We have shown that a characteristic size dependent time exists to reach percolation. But when considering the final states only the last percolative state matters as it is its spanning cluster(s) that coarsens to give either stripe or ground states. We will now concentrate on the question of when this definitive state is reached. The work that we will now describe has been the subject of [50].

As before we study the transient between a fully disordered initial condition and a percolating structure in the low-temperature non-conserved order parameter dynamics of the two-dimensional Ising model. The stochastic evolution of the ferromagnetic Ising model (IM) quenched below T_c is a textbook example of coarsening phenomenology. However, the role played by the initial conditions and the pre-asymptotic dynamics leading to the scaling regime, and *atypical* ordered spatial regions, in this and other models have not been studied in detail yet.

Here we analyze the transient regime between the initial condition and the state that will actually control the large scale properties in the scaling regime and the eventually frozen asymptotic configurations. We study the $2d$IM on different lattices. We determine the dependence of the time-scale needed to reach this state, that we call t_p, on the lattice coordination and the system size by analyzing how t_p manifests itself in a number of non-trivial observables. We conjecture its dependence on the microscopic dynamics. Importantly enough, we generalize the dynamic scaling framework to include the influence of this time-scale, so-far ignored, on the dynamic correlations. Finally, we discuss the possible implications of our results on systems with more complex out of equilibrium dynamics.

We consider square, triangular, kagome and bowtie-a lattices with linear size L and either free (FBC) or periodic (PBC) boundary conditions. FBC are better suited to our study as it is slightly easier to consider spanning clusters for FBC than wrapping clusters for PBC. Still, we checked that there are no significant changes when taking one boundary condition or the other. The coordination numbers are $n_c^{\square} = 4$, $n_c^{\triangle} = 6$, $n_c^{K} = 4$, and $n_c^{\bowtie} = 5$ and the site percolation thresholds are $p_c^{\square} \simeq 0.59$, $p_c^{\triangle} = 0.5$, $p_c^{K} \simeq 0.65$ and $p_c^{\bowtie} \simeq 0.55$. $n_c^{\bowtie}$ is a mean coordination number since the sites have either 4 or 6 neighbors

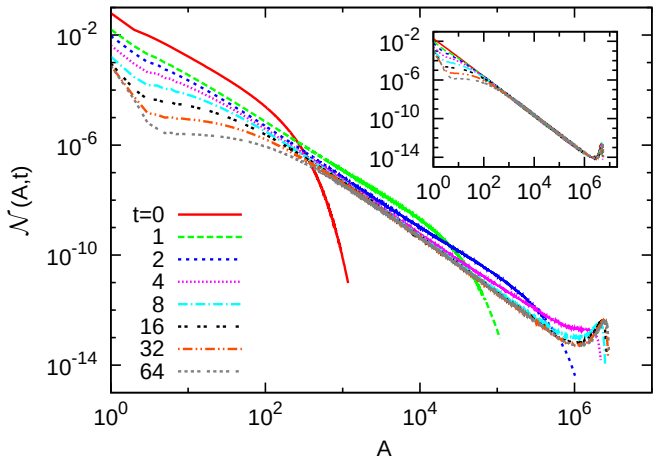

Figure 2.16 – $\mathcal{N}(A,t)$ vs. A at different times t given in the key after a quench from $T_i \to \infty$ to $T_c/2$ for a system with $L = 2560$. In the inset data obtained after a quench from T_c to $T_c/2$.

on this lattice.

Distributions of clusters areas

A first quantitative indication of critical percolation playing a role is given by the probability distribution of spin cluster areas, $\mathcal{N}(A,t)$, as a function of the number of spins in a cluster, A, and time, t [5, 6]. At $t = 0$ the system is not critical and $\mathcal{N}(A,0)$ decays exponentially with A, as shown by the solid (red) curve in the main panel in Fig. 2.16. After a very short time, $t \simeq 10$, the tail tends to an algebraic decay $\mathcal{N}(A,t) \simeq 2cA^{-\tau}$. For finite L and sufficiently long times the power-law is cut-off by a bump around areas that scale with L. For $t \gtrsim 16$ the power-law holds in the range $10^3 \leq A \leq 10^6$ and the bump is around $A \simeq 2\ 10^6$. The functional form

$$\mathcal{N}(A,t) \simeq 2cA^{-\tau} + N_p(A/L^D, t) \tag{2.10}$$

takes into account all these features as we have seen before. $D = d/(\tau - 1)$ is the fractal dimension of the percolating clusters.

A direct fit of the power-law yields $\tau = 2.020 - 2.040$ depending on the fitting range. While these values are close to the percolation one, $\tau = 187/91 \simeq 2.05495$, they are also close to the critical $2d$IM one, $\tau = 2.02674$, and it is difficult to distinguish between these two cases with this measurement (having said this, the numerical value of c is very close to the analytic one for percolation, $c = 1/(8\sqrt{3}\pi)$ [51] and distinctively different from the one for the critical IM [5, 6]).

The study of the bump, scaled as in the second term in (2.10), lifts all ambiguities on the value of τ. In Fig. 2.17 we plot $A^\tau \mathcal{N}(A,t)$ vs. A/L^D with the percolation τ for $t \in [2,16]$ and different L. For small t the height of the distribution depends on L while for $t \gtrsim 16$

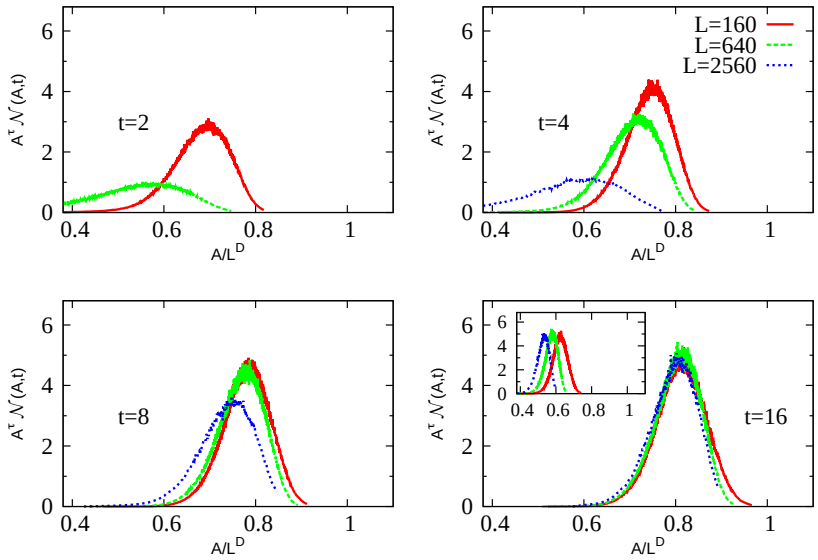

Figure 2.17 – $A^\tau \mathcal{N}(A,t)$ vs. A/L^D at different times t after a quench from $T_i \to \infty$ to $T_c/2$. We employ the parameters τ and D of critical percolation except in the inset of the lower right panel where we use the ones of the critical Ising model. The number of samples used to build the pdf is 10^6 for $L = 160$ and $L = 640$ and $2\ 10^5$ for $L = 2560$.

they all collapse. The inset in the lower right panel displays the same data scaled with the critical IM value of τ. Clearly, there is no scaling with this choice.

We note that the time required for the distribution to become percolation-like increases weakly with L. The curves for $L = 160$ and $L = 640$ at $t = 2$ are replaced by the curves for $L = 640$ and $L = 2560$ at $t = 4$. The same holds true between $t = 4$ and $t = 8$. At $t = 8$, the curves for $L = 160$ and $L = 640$ do collapse, as for data at $t = 16$ for $L = 640$ and $L = 2560$. This suggests that there is a time scale $t_p \sim L^{\alpha_p}$, with $\alpha_p \sim 0.5$, after which the bump remains stable in the scaling plot. It is still not clear whether this bump is made of everlasting percolating structures or whether these still appear and disappear as illustrated in Fig. 2.9.

Correlation with the final state

The time-scale t_p after which the actual percolating structure stabilizes can be estimated from the analysis of the correlation of the number of crossing clusters present at time t and those surviving in the blocked configuration at zero temperature. We introduce a particular case of the two-time autocorrelation function introduced previously:

$$\mathcal{A}_c(t) = \langle \delta_{n_v(t) n_v^\infty} \delta_{n_h(t) n_h^\infty} \rangle \ . \tag{2.11}$$

The correlation $\mathcal{A}_c(t)$ interpolates between 0 and 1. For sufficiently large system sizes, $n_h(0) = n_v(0) = 0$. In the blocked configuration there should be at least one crossing

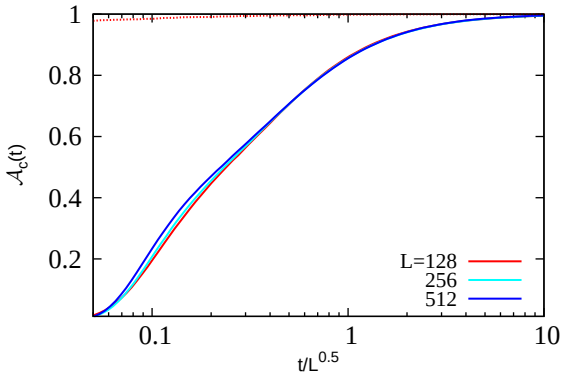

Figure 2.18 – Number of crossings autocorrelation, $\mathcal{A}_c(t)$ defined in Eq. (2.11), after a quench of the FBC square lattice form $T_i \to \infty$ to $T = 0$. Data are displayed as a function of $t/L^{0.5}$ in linear-log scale for the values of L given in the key. The dashed red line very close to 1 is the behavior of $\mathcal{A}_c(t)$ for a quench from T_c to $T = 0$ for $L = 128$.

cluster, leading to $n_h^\infty \neq 0$ and/or $n_v^\infty \neq 0$. In Fig. 2.18 we show $\mathcal{A}_c(t)$ on a square lattice with FBC. A very accurate data collapse for different sizes is found for $t/L^{0.5} \gtrsim 0.1$. At shorter times the scaling is not as good due to the large number of states with only one cluster percolating in one direction (see Fig. 2.9) present on the square lattice because of interface corners as we have already discussed with the crossing probabilities. As soon as interfaces become flat these configurations no longer exist. The convergence to 1 is fast since $\mathcal{A}_c(t) \sim 1$ for $t/L^{0.5} > 10$. This indicates that t_p scales as $t_p \sim L^{0.5}$ on the square lattice.

Overlap between twin systems

The overlap between two copies of the system similar up to some point but with different thermal histories afterwards also informs us about the time t_p. We have introduced this quantity when considering the critical initial condition case. We recall its definition here for simplicity. At $t = t_w$ one makes two copies of the configuration, say $s_i(t_w) = \sigma_i(t_w)$, and lets them evolve with different noises. The overlap between the clones at time t is

$$q_{t_w}(t, L) = \frac{1}{N} \sum_i \langle s_i(t)\sigma_i(t) \rangle \ , \tag{2.12}$$

where the angular brackets indicate an average over different realizations of this procedure. It was recently shown that $q_{t_w=0}(t, L)$ and $q_{t_w=0}(\infty, L)$ decrease algebraically with t and L, respectively [31]. The fact that $q_{t_w=0}(t, L)$ decreases with t is clear. Even though we know that there are a finite amount of stripes in the final state [7, 8], these are not encoded in the initial condition and there is no reason why the different thermal histories will take the two clones to the same percolating state. Instead, by letting t_w go beyond t_p, the two clones should be strongly correlated for all subsequent times since they are in the same percolating

state. We set this argument in practice by computing $\lim_{t\to\infty} q_{t_w}(t, L)$ for various $t_w(L)$. The outcome is shown in Fig. 2.19 for the square (a), kagome (b), and triangular (c) lattices. For the square and kagome lattices, we observe that if $t_w(L)$ increases as $L^{0.5}$, the overlap remains constant with a finite value, thus confirming that $t_p \sim L^{0.5}$ in these cases.

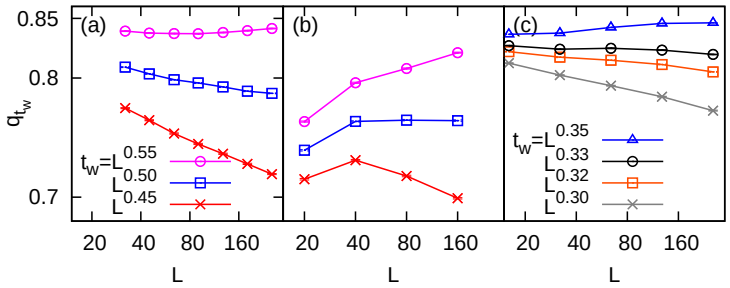

Figure 2.19 – The L-dependence of the asymptotic overlap $\lim_{t\to\infty} q_{t_w}(t, L)$ in the $2d$IM quenched from a PM state to $T = 0$ at $t = 0$. (a) Square lattice with FBC. (b) kagome lattice with FBC. (c) Triangular lattice with PBC. The values of $t_w(L)$ are given in the keys. Data have been averaged over $10^6 - 10^7$ samples.

On the triangular lattice $p_c^{\triangle} = 1/2$ and there is a percolating cluster in the initial condition with non-zero probability. A naive guess would be that this percolating state survives after the quench, and $t_p \equiv 0$. This, however, is not true as we have checked that $q_0(t, L)$ also decays to zero in the large size and time limits on this lattice. As shown in panel (c) in Fig. 2.19, only for $t_w > t_p \simeq L^{0.33}$, $\lim_{t\to\infty} q_{t_w}(t, L)$ saturates. The initial state, although percolating, is not stable under the dynamics and a transient scaling with L is still needed to reach the truly stable one. We have also simulated the bowtie-a lattice (not shown) and found $t_p \sim L^{0.38(5)}$. We have checked that in all the lattices studied the constant prefactor in t_p is of order 1.

These results suggest that, after a sub-critical quench from $T_i \to \infty$, the time t_p is compatible with

$$t_p \simeq L^{\alpha_p} , \qquad \alpha_p = z/n_c , \tag{2.13}$$

with z the dynamic exponent and n_c the regular or averaged lattice coordination. We have to say that we have no clear understanding of why this should stand but the agreement is very good for the four types of lattices considered.

Correction to dynamical scaling

For the system sizes commonly used in the literature $L \simeq 100 - 1000$, $t_p \simeq 10 - 30$, and percolation is very quickly attained. It is important to notice that, since the equilibration time remains at least $t_{eq} \sim L^2 \gg t_p$ [46], or even longer due to blocked states [2, 4, 3], after stable percolation of an ordered cluster is established at t_p the systems are still far from equilibrium, as shown by the correlation and response functions that continue to relax well beyond this time-scale [52, 53]. The new feature provided by our study is that the scaling properties are modified by the *extra* time-scale t_p. Indeed, according to the usual formulation of the dynamical scaling hypothesis, in the regime $\xi_{micro} \ll \xi(t) \ll L$, when

ξ is grown much larger than a microscopic length ξ_{micro} associated to the lattice spacing but is still much smaller than the system size when equilibration or blocked states start to occur, the statistical properties do not depend on time provided that distances are measured in units of the dominant length $\xi(t)$. Due to this fact, correlators such as $G(r,t) = \langle S_i(t)S_j(t)\rangle$, where $r = |i-j|$, take the scaling form

$$G(r,t,L) = f\left[\frac{r}{\xi(t)}\right], \tag{2.14}$$

where $f(x)$ is a scaling function, expressing the fact that there is a unique relevant length in the system. However, the presence of t_p introduces another characteristic length $\mathcal{L}(L) = \xi(t_p) \simeq L^{\alpha_p/z}$ separating an early stage in which there are no stable percolating structures from a late stage in which they exist. In the presence of two characteristic lengths, since $\mathcal{L}$ plays a companion role to that of ξ, the proper scaling form for $G(r,t,L)$ should read

$$G(r,t,L) = g\left[\frac{r}{\xi(t)}, \frac{\mathcal{L}(L)}{\xi(t)}\right] \tag{2.15}$$

with a new, two-variable, scaling function $g(x,y)$. The difference between Eqs. (2.14) and (2.15) is manifest when trying to collapse data for $G(r,t,L)$ at different times t. Indeed, according to Eq. (2.15) curves for a system of a given size L (and hence a given $\mathcal{L}$) cannot be superimposed on a master-curve by simply plotting them against $r/\xi(t)$, as Eq. (2.14) would suggest, because in so doing the second argument entering the scaling function g changes. Instead, Eq. (2.15) states that it is possible to collapse curves at different times $t = t_0, t_1, \ldots, t_i, \ldots$ if they are relative to systems of different sizes $L = L_0, L_1, \ldots, L_i, \ldots$ chosen in such a way that $\mathcal{L}(L_i)/\xi(t_i) = const.$, by still plotting them against $r/\xi(t)$.

In order to check this we have computed $G(r,t,L)$ on square lattices of sizes $L_i = 2^i \cdot L_0$, with $L_0 = 50$ and $i = 0{-}4$. Using Eq. (2.13) and $\xi(t) \sim t^{1/z}$ leads to $\mathcal{L}(L_i) \simeq L_i^{1/n_c}$. We have considered times t_i such that $t_0 = 15$ and $\mathcal{L}(L_i)/\xi(t_i) \simeq 16.86$. Having verified that, for these times, the scaling condition $\xi_{micro} \ll \xi(t) \ll L$ is met for any L_i, we try to collapse the data for the smaller system according to Eq. (2.14), namely by simply plotting the data against $r/\xi(t)$ (where ξ is obtained as the half-height width of G, namely from the condition $G(\xi,t) \equiv 1/2$). The result is shown in Fig. 2.20 (a), where one observes a systematic downward spreading of the curves from $r/\xi(t) \simeq 1.5$ onwards (the collapse of the curves at $r/\xi = 1$ is exact due to the operative definition of $\xi(t)$). In Fig. 2.20 (b), instead, we plot the data at the same times t_i but for systems with different sizes L_i. As expected, the quality of the collapse is, in this case, much better. Besides shedding some light on the scaling properties of coarsening systems, this results confirm the validity of Eq. (2.13) in an independent way.

We repeated the analysis for various choices of the constant $\mathcal{L}(L_i)/\xi(t_i)$ finding that, in all cases, Eq. (2.15) provides a better description of data than Eq. (2.14), although it is clear that for times $t \gg t_p$ (so that $\xi(t) \gg \mathcal{L}(L)$) the validity of Eq. (2.14) gets progressively restored since one expects $\lim_{y\to 0} g(x,y) \simeq g(x,0) = f(x)$. We have also checked that,

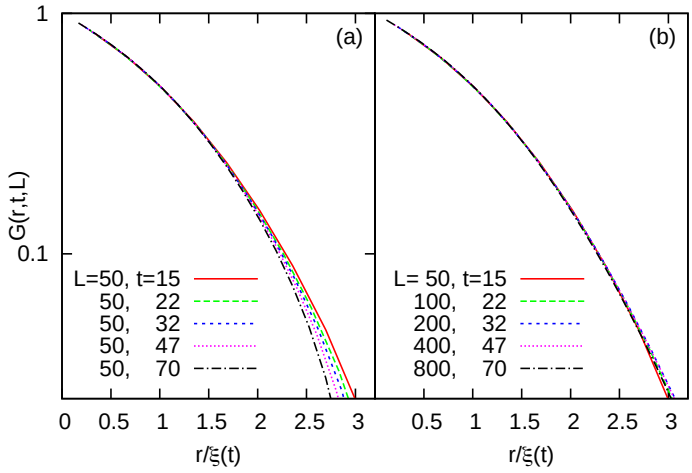

Figure 2.20 – $G(r,t,L)$ against $r/\xi(t)$ in the $2d$IM quenched from a PM state to $T=0$ at $t=0$. The system size and measuring times are given in the keys. Data have been averaged over $2\cdot 10^4$ samples.

similarly to what happens for G, a better scaling description of other correlators, such as, for instance, the autocorrelation function $C(t,t_w,L)=\langle S_i(t)S_i(t_w)\rangle$, can be obtained by taking into account the presence of t_p. Indeed, also for this quantity we have found that a two-variable scaling form $C(t,t_w,L)=h\left[\frac{\xi(t_w)}{\xi(t)},\frac{\mathcal{L}(L)}{\xi(t)}\right]$ improves the collapse with respect to the usually conjectured form where the role of the second argument in h is neglected.

As we have already discussed in the previous section the situation is different if we start from a configuration equilibrated at T_c. We higlight here some of the differences. The inset in Fig. 2.16 shows $\mathcal{N}(A,t)$ after a quench from T_c to $T_c/2$. In this case, the initial state is critical and the curve at $t=0$ is a power law [5, 6]. Again, extracting τ from it is hard. Instead, the bump described by the second term in (2.10) can only be scaled by using the critical IM τ (not shown). Moreover, the crossing properties of the final state are already contained in the initial configuration [1]. $\mathcal{A}_c(t)$ is immediately close to one, see the red dashed line in Fig. 2.18, as well as the clone overlap $q_{t_w}(t,L)$ previously shown in Fig. 2.7 and 2.8 for $t_w=0$. So for the critical initial condition the twins are strongly correlated even for $t_w=0$. All these results strongly suggest that $t_p=0$ in this case. We should stress that the initial presence of percolating clusters does not necessarily imply $t_p=0$ as, for example, $t_p>0$ on the triangular lattice when $T_i=\infty$. The difference between the two situations resides in the finer cluster structure; mainly the fact that red bonds are essentially inexistent at the critical temperature as opposed to what happens at critical percolation. We will come back to this point in the conclusion of this chapter.

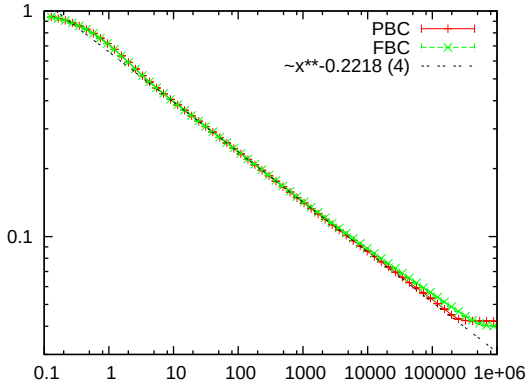

Figure 2.21 – The persistence $\mathcal{P}(t, L = 1024)$ vs. t for the ferromagnetic $2d$IM on the square lattice with PBC and FBC (red and green data, respectively, see the key) quenched at $t = 0$ from a $1/T \to 0$ initial state to $T = 0$. The dotted (grey) line corresponds to the best fit found over the interval $t \in [100 : 10000]$ with a power law for the PBC case.

2.3.4 Persistence

Previous works

We will focus on persistence as we did for critical initial condition. The case of persistence starting from an infinite temperature initial condition is the most studied case. After the initial study of Derrida, Bray and Godreche, Stauffer considered the Ising model from dimension one to five in [35], . He determined numerically that the persistence follows a power law scaling with time, $\mathcal{P}(t, L) \sim t^{-\theta}$ with a persistence exponent $\theta = 0.22$ in two dimensions. There have been many other estimates of the persistence exponent θ. The first numerical estimate by Stauffer was followed by an analytic value $\theta = 0.19$ by Majumdar and Sire using a perturbation scheme [38]. In [40] Yurke *et al.* measured experimentally $\theta = 0.19(3)$ using a system of liquid crystals in the same universality class, and other numerical estimates are 0.21 [44] and $0.209(4)$ [54]. Those various estimates are roughly compatible with each other but we wanted to see if a more accurate estimate was accessible.

In Fig. 2.21, we show numerical results for the persistence probability in the ferromagnetic $2d$IM as a function of the time. This figure contains data for the square lattice with $L = 1024$ and both FBC and PBC. At first sight, it seems that both cases have the same behaviour for $t > 10$ with an algebraic decay. The best fit of the data for PBC on the interval $t \in [100 : 10000]$ gives $\theta = 0.2218(4)$ in excellent agreement with Stauffer's result [35]. This fit is shown in Fig. 2.21 as a dotted grey line. For large $t \gtrsim 10^6$, there is saturation of data, *i.e.* $\mathcal{P}(t, L = 1024) \simeq \ cst$ for $t \gtrsim 10^6 \simeq L^2$. This is expected since for $t \simeq L^2$, the system gets close to equilibrium and the persistence reaches a finite L-dependent value due to finite size effects. We obtain that $\lim_{t\to\infty} \mathcal{P}(t, L) = P_\infty(L) \sim L^{-2\theta}$ with $2\theta = 0.45(1)$. This is consistent with previous results but we would like to describe more precisely the dependence of persistence with time.

New estimation

In this section, we want to reinvestigate the estimation of the persistence exponent. One reason to do so is that although the fit in Fig. 2.21 looks good, in fact it is not. The reduced chi-squared for the power law fit is $\simeq 6000$ which means that it is actually a terribly bad fit. (The data used for the plot in Fig. 2.21 contains one million samples.) By changing the fitting region, we observed that the value of the exponent is changing slightly, always in the range $\theta = 0.20 - 0.225$ though always with a very large reduced chi-squared. In the first panel of Fig. 2.22, we show again the persistence $\mathcal{P}(t, L)$ against time for the system with PBC, after a rescaling by the power t^θ with $\theta = 0.2218$, the value previously obtained. This quantity should be constant if the scaling were well-described by this power θ. This is clearly not the case. We observe different regimes as a function of time. A first regime for small times, $10 < t < 100$, with $\theta \simeq 0.2214$. In Stauffer's work [35], measurements were done on very small time scales, up to $t = 200$, thus in this first regime of our analysis. Next, for $100 < t < 1000$ the exponent increases up to $\theta \simeq 0.2241$. For longer times, it decreases again up to $\theta \simeq 0.207$ for $t > 100000$. We also note that the persistence does not depend on the size of the system up to $t \simeq L^2/10$. For each size, we observe a drop of the persistence beyond this time (this drop is followed by a rapid increase that, for clarity, we removed from the presentation since it corresponds to the final constant persistence) which signals the approach to equilibrium. The existence of finite size effects at $t = L^2/10$ was already observed in [35].

Systems with PBC In the second panel of Fig. 2.22, we plot the effective exponent, $\theta_{\text{eff}}(t, L)$, obtained from a fit of the persistence probability $\mathcal{P}(t, L)$ to a power law in the range $[t/3, 3t]$. For times $t \gtrsim 1000$, the effective exponent slowly decreases with time and it is well described by a fit to the form

$$\theta(t) = \theta_0 + \theta_1 t^{-\overline{\beta}} \tag{2.16}$$

with $\theta_0 = 0.198(3)$, $\theta_1 \simeq 0.07$, and $\overline{\beta} \simeq 0.15$. In conclusion, we obtain the following numerical estimate of the persistence exponent in the ferromagnetic $2d$IM on the square lattice with PBC: $\theta = 0.198(3)$ in the large size and large time limit.

In Fig. 2.23, we show the same quantities for the triangular lattice with PBC. We computed the effective exponent θ_{eff} and plotted as a function of time for different sizes L in the first panel of Fig. 2.23. The situation is similar to the square lattice. For the largest times, the effective exponent is $\theta \simeq 0.2065$. In the second panel we rescale the persistence with this value of θ. Again, the curves for different sizes coincide for a given time but this rescaling is not very convincing. To obtain a better estimate we also use a good quality fit to the form (2.16) with $\theta_0 = 0.200(3)$, $\theta_1 \simeq 0.04$, and $\overline{\beta} \simeq 0.15$. This value of $0.200(3)$ is compatible with the value obtained on the square lattice $0.198(3)$. We think those estimates are more reliable and accurate than those obtained with a direct fit of the persistence.

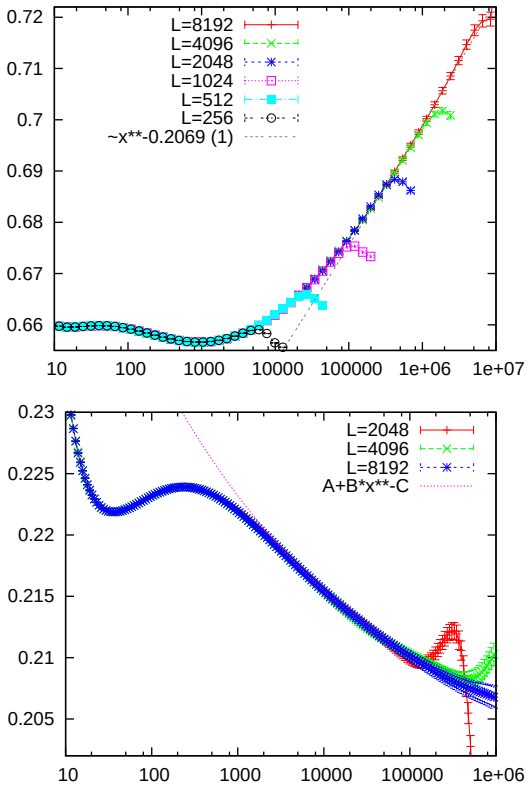

Figure 2.22 – First panel: $t^\theta \mathcal{P}(t, L)$ vs. t for the ferromagnetic $2d$ Ising model on the square lattice with PBC, $\theta = 0.2218$. Second panel: effective exponent θ vs. t for the model with PBC. The system sizes are given in the key.

Systems with FBC Next we turn to the case of FBC. Going back to Fig. 2.21, we can observe that in this case, there is a deviation from scaling behaviour for $t > 10000$. A fit to a power law also gives a very large reduced chi-squared, but the fit improves as we approach longer times. This can be better explained in Fig. 2.24.

In the left panel, we plot $t^\theta \mathcal{P}(t, L)$ as a function of t with $\theta = 0.2205$ which corresponds to the best fit for short times and $L = 1024$. We also observe that $t^\theta \mathcal{P}(t, L)$ still depends on the size, contrary to what was observed for PBC. This can also be seen in the right panel of Fig. 2.24 where we plot the effective exponent θ_{eff} as a function of time. For each size, we observe a plateau at long times $t \simeq L^2/10$. Thus, for FBC, finite size effects are much stronger. We also observe that $t^\theta \mathcal{P}(t, L)$ goes to a power law with $\theta = 0.1954(1)$ for long times and $L = 1024$, just before reaching equilibration. We found that the value of θ for long times has a weak size dependency. We measured $0.1950(1)$ for $L = 256$, $0.1953(1)$ for $L = 512$ and $0.1954(1)$ for $L = 1024$. Thus, it seems that a large size extrapolation will be compatible with the value obtained for PBC, $\theta_0 = 0.198(3)$. Let us come back to the behaviour of the persistence with the system size for PBC and FBC. When rescaling

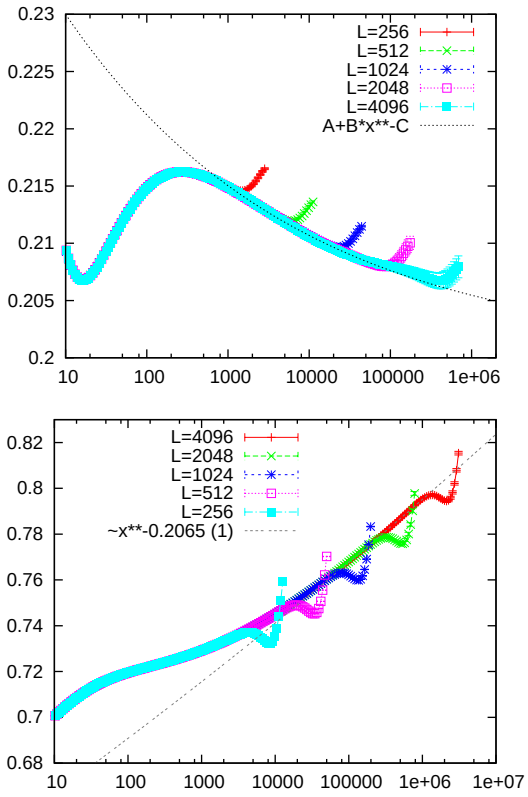

Figure 2.23 – First panel: Effective exponent θ vs. t for the PBC. Second panel: $t^{\theta}\mathcal{P}(t, L)$ vs. t for the PBC on the triangular lattice with $\theta = 0.2068$.

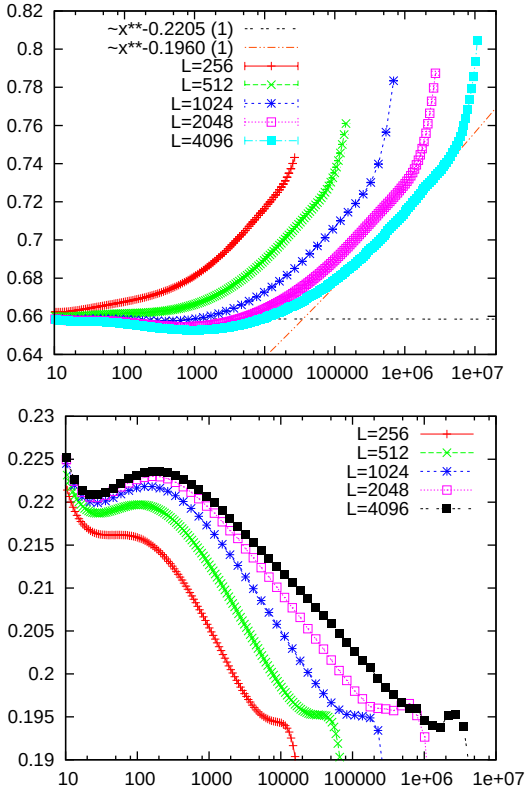

Figure 2.24 – First panel: $t^\theta \mathcal{P}(t,L)$ vs. t for the FBC with $\theta = 0.2205$. Second panel: Effective exponent θ vs. t for the FBC

by a power of time the PBC persistence all the curves fall on a same master curve. Thus for PBC $\mathcal{P}(t,L) \simeq f(t)$ with no apparent dependence on the system size. On the contrary for FBC this is not the case and it can be checked that $\mathcal{P}(t,L) \simeq f(t/L^2)$ which is a more usual form of scaling. We have no explanations for the intriguing difference between those two cases.

Final values We now turn to the determination of the exponent θ using the final value of the persistence for which $P_\infty(L) \simeq L^{-2\theta}$ once the system is equilibrated. This exponent is obtained by doing a two points fit of two successive increasing sizes L. The measurement of $P_\infty(L)$ is in fact very time consuming since we need to let the systems equilibrate. As a consequence, for this measurement, the largest systems that we considered are much smaller than for the finite time persistence. The results for 2θ are shown in Fig. 2.25.

It is computed as an effective exponent between two systems with sizes L and L' as

$$2\theta_{eft}((L+L')/2) = -\frac{\log\left(\frac{P(L)}{P(L')}\right)}{\log\left(\frac{L}{L'}\right)} \ . \tag{2.17}$$

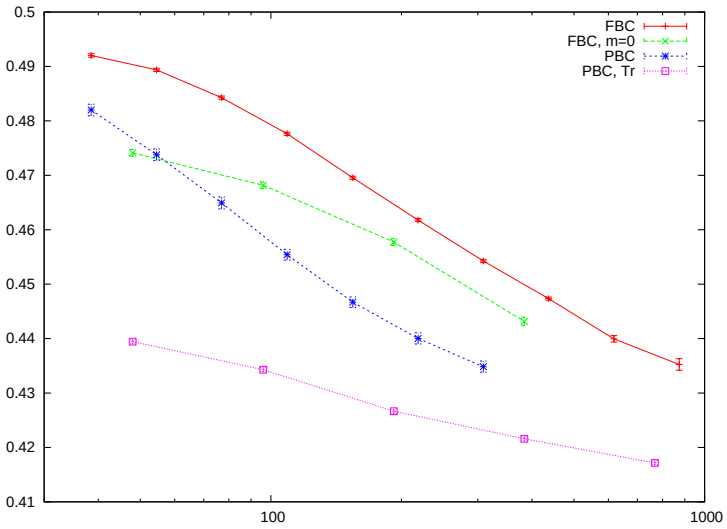

Figure 2.25 – The Effective exponent θ vs. L in the ferromagnetic $2d$IM with different boundary conditions and on different lattices (see the key for the line code).

In both cases, we observe that there are strong finite size corrections. The value of 2θ decreases with size but it is difficult to extrapolate an asymptotic value. We also show in Fig. 2.25 data obtained on a triangular lattice with PBC. There are two advantages with this lattice: first, the diagonal crossing states are absent and we can therefore simulate equilibrate configurations for large sizes, up to size $L = 1024$. Second, the results for PBC have smaller finite size corrections than the ones for FBC. Moreover, we observe that the finite size corrections on the PBC triangular lattice are much smaller than on the PBC square lattice without any obvious reason. Thus, the results on former case are much more accurate. A fit of these curves, skipping the data for the small sizes, will give a prediction in the range $2\theta = 0.40 - 0.41$ in the large size limit which is compatible with our previous estimates obtained from the time evolution. But since the sizes are more limited and since is more difficult to extrapolate a value of 2θ in this case we can say that this is not the optimal way to obtain an accurate estimate of θ. In Fig. 2.25, we also show the values obtained for 2θ starting from configurations with a strictly zero magnetisation. Those tend to be a bit lower but are also subject to strong finite size corrections.

Conclusion

We have showed that behind an apparently quiet power law behaviour the persistence exhibits a complex evolution with time. This makes the estimation of the exponent θ tricky and in particular one has to consider large systems to be able to reach the universal decay. The persistence also presents an intriguing difference of dynamic scaling depending on the type of boundary conditions used. We obtain the estimate $\theta = 0.198(3)$ which is somewhat

lower than previous numerical estimate but closer to the analytical estimate of [38, 39].

2.4 Conclusion

2.4.1 Initial condition and red bonds

We have studied subcritical quenches with two different initial conditions and have seen that they differ qualitatively even though the systems possess clusters with a fractal structure. Indeed the initial spanning clusters are very resilient during the evolution when starting from critical temperature as they see virtually no change in their topology. On the contrary the spanning clusters that one observes after an infinite initial temperature quench typically see many changes in their topology before they become thick enough to resist. The key feature that seems to control this difference of behaviour is whether a spanning cluster can be easily cut into several not percolating clusters. The finer structure of clusters has been studied and is quite well known. In bond percolation, one can categorize the bonds into the backbone, red bonds and dangling ends (first introduced by Pike and Stanley [55, 56]). This terminology is quite natural if one thinks to the spanning cluster as a network of wires that carries electrical current from one side of the system to the other. Then quite naturally there is a conducting backbone of bonds and dangling ends that do not contribute to the electric conductivity of the cluster. Within the backbone there are some special bonds such that all the current transmitted by the cluster has to pass through them so that they become red. If one cuts a red bond the spanning cluster will stop conducting the current hence the cluster will stop being percolating. So by studying the set of red bonds one can learn how a spanning cluster resist to some random bond cuts. The red bonds can be considered quite generally when one has clusters and not only for percolation. It was shown that the set of red bonds has a non-trivial fractal structure and that their fractal dimension is given by:

$$D_r = 1 - \frac{3}{8}g + \frac{2}{g} \tag{2.18}$$

with g the Coulomb gas parameter [57, 58, 59]. For the Ising spin cluster at the critical temperature ($g = 16/3$) it gives $D_r = -0.625$. The negative fractal dimension means that the number of red sites (and not even the fraction) goes to zero in the thermodynamic limit. In [59], the authors note that even for a system of moderate size there are often no red sites for a given system. On the contrary for percolation ($g = 8/3$) the fractal dimension of red sites is positive and equals $3/4$. Thus for a finite size system there is a non zero probability to cut a spanning cluster by updating a red site. However the fraction of red sites goes to zero in the infinite system size limit so it is not clear to us how a percolation cluster behaves upon updates in this limit. Nevertheless for finite size systems the difference of red bond structure between Ising spin clusters and percolation clusters qualitatively explains the difference of behaviour during a subcritical quench. This may of course be made more precise, for example by testing numerically the structure of red

bonds with time. We expect that the time t_p corresponds to the moment when the spanning clusters are thick enough to be free of red bonds.

2.4.2 Perspectives

A lot of quantities have not been studied starting from a correlated initial condition: persistence, percolative autocorrelation exponent, twin overlap. One may wonder about what can be done analytically? We have seen that for the autocorrelation exponent λ the value of the exponent is known exactly when initial long-range correlations are relevant as opposed to the case with only short-range initial correlations where only an estimate is known. Maybe similar results could be obtained for other quantities.

We think that we have shed some light upon the appearance of critical percolation. Nonetheless, some question still remains. For example we have no quantitative explanation of the mechanism behind the fast growth of the spanning clusters. It is certainly through an aggregation of smaller clusters but how exactly does it happen? An explanation of the exponent appearing in the time to reach a definitive percolative state is also very desirable goal. We expect the effect of the working temperature to be weak and alter only the prefactor in (2.13). The effect that the microscopic dynamics (conserved quantities) may have on t_p remains to be clarified. Weak quenched disorder slows down the curvature driven growth. Does it also affect the transient regime? It would also be interesting to pinpoint the implications of these results in higher dimensions.

It should be possible to search for percolation effects experimentally in systems undergoing phase ordering kinetics for which visualization techniques have proven to be successful. Two examples are liquid crystals [60] and phase separating glasses [61].

Bibliography

[1] T. Blanchard and M. Picco. Frozen into stripes: Fate of the critical Ising model after a quench. *Phys. Rev. E*, 88(3):032131, September 2013.

[2] Adam Lipowski. Anomalous phase-ordering kinetics in the Ising model. *Physica A*, 268(1–2):6–13, June 1999.

[3] V. Spirin, P. L. Krapivsky, and S. Redner. Freezing in Ising ferromagnets. *Phys. Rev. E*, 65(1):016119, December 2001.

[4] V. Spirin, P. L. Krapivsky, and S. Redner. Fate of zero-temperature Ising ferromagnets. *Phys. Rev. E*, 63(3):036118, February 2001.

[5] Jeferson J. Arenzon, Alan J. Bray, Leticia F. Cugliandolo, and Alberto Sicilia. Exact results for curvature-driven coarsening in two dimensions. *Phy. Rev. Lett.*, 98(14):145701, April 2007.

[6] Alberto Sicilia, Jeferson J Arenzon, Alan J Bray, and Leticia F Cugliandolo. Domain growth morphology in curvature driven two dimensional coarsening. *0706.4314*, June 2007. Phys. Rev. E 76, 061116 (2007).

[7] Kipton Barros, P. L. Krapivsky, and S. Redner. Freezing into stripe states in two-dimensional ferromagnets and crossing probabilities in critical percolation. *Phys. Rev. E*, 80(4):040101, October 2009.

[8] J. Olejarz, P. L. Krapivsky, and S. Redner. Fate of 2D kinetic ferromagnets and critical percolation crossing probabilities. *Phys. Rev. Lett.*, 109(19):195702, November 2012.

[9] J. L. Cardy. Critical percolation in finite geometries. *J. Phys. A: Math. Gen.*, 25(4):L201–L206, February 1992.

[10] Haru T. Pinson. Critical percolation on the torus. *J. Stat. Phys.*, 75(5-6):1167–1177, June 1994.

[11] G. M. T. Watts. A crossing probability for critical percolation in two dimensions. *J. Phys. A: Math. Gen.*, 29(14):L363, July 1996.

[12] John Cardy. Crossing formulae for critical percolation in an annulus. *J. Phys. A: Math. Gen.*, 35(41):L565–L572, October 2002.

[13] Ervig Lapalme and Yvan Saint-Aubin. Crossing probabilities on same-spin clusters in the two-dimensional Ising model. *J. Phys. A: Math. Gen.*, 34(9):1825–1835, March 2001.

[14] Louis-Pierre Arguin and Yvan Saint-Aubin. Non-unitary observables in the 2d critical Ising model. *Phys. Lett. B*, 541(3-4):384–389, August 2002.

[15] Michel Bauer, Denis Bernard, and Kalle Kytölä. Multiple Schramm–Loewner evolutions and statistical mechanics martingales. *J. Stat. Phys.*, 120(5-6):1125–1163, September 2005.

[16] Michael J Kozdron. Using the Schramm–Loewner evolution to explain certain non-local observables in the 2D critical Ising model. *J. Phys. A: Math. Theo.*, 42(26):265003, July 2009.

[17] J. Dubail, J. L. Jacobsen, and H. Saleur. Conformal boundary conditions in the critical $O(n)$ model and dilute loop models. *Nuclear Physics B*, 827(3):457–502, March 2010.

[18] Oded Schramm. Scaling limits of loop-erased random walks and uniform spanning trees. *Israel J. Math.*, 118(1):221–288, December 2000.

[19] G. F. Lawler, O. Schramm, and W. Werner. On the scaling limit of planar self-avoiding walk. *Proc. Sympos. Pure Math.*, 72:339–364, 2004.

[20] S. Smirnov. Critical percolation in the plane: conformal invariance, Cardy's formula, scaling limits. *C.R.A.S. - Series I - Mathematics*, 333(3):239, August 2001.

[21] Ervig Lapalme and Yvan Saint-Aubin. Crossing probabilities on same-spin clusters in the two-dimensional Ising model. *J. Phys. A: Math. Gen.*, 34(9):1825–1835, March 2001.

[22] Ulli Wolff. Collective monte Carlo updating for spin systems. *Phys. Rev. Lett.*, 62(4):361, January 1989.

[23] A.B. Bortz, M.H. Kalos, and J.L. Lebowitz. A new algorithm for monte Carlo simulation of Ising spin systems. *J. Comput. Phys.*, 17(1):10–18, January 1975.

[24] Louis-Pierre Arguin. Homology of Fortuin-Kasteleyn clusters of Potts models on the torus. *J. Stat. Phys.*, 109(1):301–310, 2002.

[25] A. L. Stella and C. Vanderzande. Scaling and fractal dimension of Ising clusters at the d=2 critical point. *Phys. Rev. Lett.*, 62(10):1067, March 1989.

[26] T. Blanchard. Wrapping probabilities for ising spin clusters on a torus. *J. Phys. A: Math. Theor.*, 47(34):342002, August 2014.

[27] A. J. Bray, K. Humayun, and T. J. Newman. Kinetics of ordering for correlated initial conditions. *Phys. Rev. B*, 43(4):3699–3702, February 1991.

[28] B. Derrida. Dynamical phase transition in nonsymmetric spin glasses. *J. Phys. A: Math. Gen.*, 20(11):L721, August 1987.

[29] L. F. Cugliandolo and D. S. Dean. Full dynamical solution for a spherical spin-glass model. *J. Phys. A: Math. Gen.*, 28(15):4213, August 1995.

[30] A. Barrat, R. Burioni, and M. Mézard. Ageing classification in glassy dynamics. *J. Phys. A: Math. Gen.*, 29(7):1311, April 1996.

[31] J. Ye, J. Machta, C. M. Newman, and D. L. Stein. Nature versus nurture: Predictability in low-temperature Ising dynamics. *Phys. Rev. E*, 88(4):040101, October 2013.

[32] Alan J. Bray, Satya N. Majumdar, and Grégory Schehr. Persistence and first-passage properties in nonequilibrium systems. *Advances in Physics*, 62(3):225–361, 2013.

[33] A. J. Bray, B. Derrida, and C. Godréche. Non-trivial algebraic decay in a soluble model of coarsening. *EPL*, 27(3):175, July 1994.

[34] B. Derrida, A. J. Bray, and C. Godreche. Non-trivial exponents in the zero temperature dynamics of the 1D Ising and Potts models. *J. Phys. A: Math. Gen.*, 27(11):L357, June 1994.

[35] D. Stauffer. Ising spinodal decomposition at T=0 in one to five dimensions. *J. Phys. A: Math. Gen.*, 27(14):5029, July 1994.

[36] Bernard Derrida, Vincent Hakim, and Vincent Pasquier. Exact first-passage exponents of 1D domain growth: Relation to a reaction-diffusion model. *Phys. Rev. Lett.*, 75(4):751–754, July 1995.

[37] Bernard Derrida, Vincent Hakim, and Vincent Pasquier. Exact exponent for the number of persistent spins in the zero-temperature dynamics of the one-dimensional Potts model. *J. Stat. Phys.*, 85(5-6):763–797, December 1996.

[38] Satya N. Majumdar and Clément Sire. Survival probability of a gaussian nonmarkovian process: Application to the T=0 dynamics of the Ising model. *Phys. Rev. Lett.*, 77(8):1420–1423, August 1996.

[39] Clément Sire, Satya N. Majumdar, and Andreas Rüdinger. Analytical results for random walk persistence. *Phys. Rev. E*, 61(2):1258–1269, February 2000.

[40] B. Yurke, A. N. Pargellis, S. N. Majumdar, and C. Sire. Experimental measurement of the persistence exponent of the planar Ising model. *Phys. Rev. E*, 56(1):R40–R42, July 1997.

[41] G. Manoj and P. Ray. Scaling and fractal formation in persistence. *J. Phys. A: Math. Gen.*, 33(12):L109, March 2000.

[42] G. Manoj and P. Ray. Spatial distribution of persistent sites. *J. Phys. A: Math. Gen.*, 33(31):5489, August 2000.

[43] S. Jain and H. Flynn. Scaling and persistence in the two-dimensional Ising model. *J. Phys. A: Math. Gen.*, 33(47):8383, December 2000.

[44] G. Manoj and P. Ray. Persistence in higher dimensions: A finite size scaling study. *Phys. Rev. E*, 62(6):7755–7758, December 2000.

[45] Purusattam Ray. Persistence in extended dynamical systems. *Phase Transitions*, 77(5-7):563–579, 2004.

[46] A.J. Bray. Theory of phase-ordering kinetics. *Advances in Physics*, 43(3):357–459, 1994.

[47] J. Olejarz, P. L. Krapivsky, and S. Redner. Zero-temperature freezing in the three-dimensional kinetic Ising model. *Phys. Rev. E*, 83(3):030104, March 2011.

[48] J. Olejarz, P. L. Krapivsky, and S. Redner. Zero-temperature relaxation of three-dimensional Ising ferromagnets. *Phys. Rev. E*, 83(5):051104, May 2011.

[49] Hiroshi Takano and Seiji Miyashita. Ordering process in the kinetic Ising model on the honeycomb lattice. *Phys. Rev. B*, 48(10):7221, 1993.

[50] T. Blanchard, F. Corberi, L. F. Cugliandolo, and M. Picco. How soon after a zero-temperature quench is the fate of the Ising model sealed? *EPL*, 106(6):66001, June 2014.

[51] John Cardy and Robert Ziff. Exact results for the universal area distribution of clusters in percolation, Ising, and Potts models. *J. Stat. Phys.*, 110:1, 2003.

[52] A. Barrat. Monte Carlo simulations of the violation of the fluctuation-dissipation theorem in domain growth processes. *Phys. Rev. E*, 57(3):3629–3632, March 1998.

[53] F. Corberi, E. Lippiello, A. Sarracino, and M. Zannetti. Fluctuations of two-time quantities and non-linear response functions. *J. Stat. Mech.*, 2010(04):P04003, April 2010.

[54] S. Jain. Zero-temperature dynamics of the weakly disordered Ising model. *Phys. Rev. E*, 59(3):R2493–R2496, March 1999.

[55] H. E. Stanley. Cluster shapes at the percolation threshold: and effective cluster dimensionality and its connection with critical-point exponents. *J. Phys. A: Math. Gen.*, 10(11):L211, November 1977.

[56] R. Pike and H. E. Stanley. Order propagation near the percolation threshold. *J. Phys. A: Math. Gen.*, 14(5):L169, May 1981.

[57] Antonio Coniglio. Thermal phase transition of the dilute s-state Potts and n-vector models at the percolation threshold. *Phys. Rev. Lett.*, 46(4):250–253, January 1981.

[58] Antonio Coniglio. Fractal structure of Ising and Potts clusters: Exact results. *Phys. Rev. Lett.*, 62(26):3054–3057, June 1989.

[59] Guillaume Provencher, Yvan Saint-Aubin, Paul A. Pearce, and Jørgen Rasmussen. Geometric exponents of dilute loop models. *J. Stat. Phys.*, 147(2):315–350, April 2012.

[60] Alberto Sicilia, Jeferson J. Arenzon, Ingo Dierking, Alan J. Bray, Leticia F. Cugliandolo, Josu Martínez-Perdiguero, Ibon Alonso, and Inmaculada C. Pintre. Experimental test of curvature-driven dynamics in the phase ordering of a two dimensional liquid crystal. *Phys. Rev. Lett.*, 101(19):197801, November 2008.

[61] David Bouttes, Emmanuelle Gouillart, Elodie Boller, Davy Dalmas, and Damien Vandembroucq. Fragmentation and limits to dynamical scaling in viscous coarsening: An interrupted in situ X-ray tomographic study. *Phys. Rev. Lett.*, 112(24):245701, June 2014.

CHAPTER 3

Wrapping probabilities for Ising spin clusters on a torus

Contents

Introduction

This chapter describes the work I have done on wrapping probabilities. It is independent of the work described in the chapters 1 and 2 even though the wrapping formula obtained here has been used in relation with stripe states after a quench from the critical temperature. The content of this chapter is very similar to the article published in Journal of Physics A [1]. There are some repetitions about spin and FK clusters with what we have said before but it makes this chapter almost self-contained.

In the study of the critical properties of the Potts model, it was soon remarked that rewriting the model in terms of clusters was very enlightening [2, 3]. Indeed, the Fortuin-Kasteleyn (FK) clusters or droplets, obtained by casting the Potts partition function into a random cluster partition function, contain all the critical properties of the model and in particular are ruled by the same critical exponents. However, these are not the clusters one would observe in general in an experimental realisation of the Potts model, in this case one can only see the clusters formed by connected spins sharing the same value (spin clusters). It is only for bond percolation that the percolation clusters coincides with the FK clusters

of the 1-state Potts model. In two dimensions both types of clusters undergo a continuous percolation transition at the critical temperature but a measure of the fractal dimensions of FK and spin clusters quickly convinces that the two types of clusters possess different critical exponents [4, 5]. From a theoretical point of view there is then the question of the origin of this set of exponents ruling the properties of spin clusters. A clear answer can be given for the $Q = 2$ state Potts model, *i. e.* the Ising model. In [3] it was shown that the Ising Hamiltonian can be rewritten as a diluted Potts model with $Q' = 1$ state. This enabled the computation of the Ising spin clusters exponents [6]. Unfortunately no such mapping exists for other Potts models. It was nonetheless conjectured in [7, 8] that the exponents for spin clusters can be obtained by a similar mapping to a diluted Potts model with a different number of states at its tricritical point. This conjecture gives exponents compatible with numerical estimates [9, 4, 10] and there is little doubt that those are exact even though a rigorous proof is still lacking. An infinite set of critical exponents related to the geometrical structure of spin clusters was also obtained [11, 12, 13]. We will talk about those exponents in more details in the end of Sec. 3.3. The situation was thought to be more or less under control until recent works showed that a naive analytic continuation from the critical branch sometimes fails to give the correct results for some spin clusters properties. Even though no problem is encountered at the level of dimensions, a naive continuation is not able to explain the connectivity constants appearing in bulk three-point connectivity [14] and the corner contribution to cluster number [15]. It is thus very interesting to further study the properties of spin clusters to understand what can and cannot be obtained from an analytic continuation.

In percolation theory, the percolation threshold is defined as the point below which no infinite cluster exists and above which there exists one with probability one [16]. At the percolation threshold, an important question for finite-size systems is whether a cluster spanning the whole system is present or in other words: what is the crossing probability of a percolation cluster for a given system? The study of crossing probabilities has a long history and a landmark in this topic is due to Cardy and his eponymous formula [17]. This formula gives the probability of left-right crossing of an incipient spanning cluster at the critical percolation threshold on a rectangle. This probability depends only upon the aspect ratio r of the rectangle and can be expressed in terms of hypergeometric functions. This work of Cardy followed a numerical study by Langlands *et al.* [18] of the universality of crossing probabilities in different setups. This study prompted Michael Aizenman to suggest to Langlands and Cardy that conformal field theory (CFT) may lead to expressions for crossing probabilities. Using this suggestion and the data from Langlands *et al.* Cardy was able to obtain the first crossing probability formulae. Since then a number of percolation probabilities have been studied either for percolation [19, 20, 21] or other models [22, 23, 24, 25, 26]. One aspect that is particularly interesting is that although Cardy and others found those formulas using CFT, *i. e.* in a non rigorous way mathematically speaking, rigorous tools have been developed which can be used to tackle those systems. Schramm introduced the stochastic Loewner evolution (SLE) [27] which describes numerous physically occurring curves (see [28] with Lawler and Werner *e.g.*) and showed that

SLE proves Cardy's formula if the continuum limit of percolation is conformally invariant. In a slightly different line of research Smirnov proved the existence of a conformal scaling limit of the percolation critical point for site percolation on the triangular lattice and thus gave the missing piece to the proof of Cardy's formula [29].

As a generalisation of the case of simply connected surfaces, Langlands *et al.* introduced the notion of crossing probabilities on compact Riemann surfaces after a suggestion of Israel Gelfand [30]. For percolation on a compact Riemann surface S, one has to consider the clusters with boundaries forming non-contractible loops, *i.e.* non homotopic to a point, winding around S. We will call such clusters non-trivial clusters. Then counting the numbers of winding of non-trivial clusters, one can relate the configuration to which they belong to a subgroup of the first homology group $H_1(S)$ of S. The probability that a configuration contains clusters related to the subgroup $G \subset H_1(S)$ is:

$$\pi_G = \frac{Z_G}{Z} \tag{3.1}$$

where Z is the total partition function of the model considered and Z_G the partition function restricted to the configurations generating G. Among other cases Langlands *et al.* studied numerically those probabilities for percolation on a torus. Shortly after they were derived analytically for percolation by Pinson [19] building on the works of Nienhuis [31, 32] and Di Francesco *et al.* [33]. Arguin [34] then extended the work of Pinson to the case of FK clusters of the Q state Potts model for $Q \in [1, 4]$. He was also able to derive closed forms in terms of Jacobi θ functions in the case of percolation ($Q = 1$) and Ising FK clusters ($Q = 2$) and supported his formula for integer values of Q with simulations. In [35] it was checked numerically that the formula obtained by Arguin is also valid for real values of Q.

In this chapter we further generalise the derivation of wrapping probabilities of FK clusters by Arguin to the case of Ising spin clusters. In this case a closed form in terms of Jacobi θ function is obtained and checked numerically. Even though other cases (mainly the 3-Potts model) are not treated explicity in this work it is expected that the arguments developped for the Ising spin clusters can be generalized to other cases. This work was motivated by the study of the appearance of long-lived stripe states in the Ising model after a quench from $T = T_c$ to $T = 0$ with various boundary conditions as we have discusssed in chapter 2. When periodic boundary condition are applied, the system has the topology of a torus and wrapping probabilities of spin clusters are relevant to explain the appearance of long-lived stripe states [36, 37]. We also present expressions for the probabilities of cross-shaped FK and spin clusters for the Ising model on untwisted tori. This chapter is divided as follows: we further discuss FK and spin clusters, present how wrapping probabilities can be computed, show the derivation for Ising spin clusters and check it numerically and finally we provide expressions for cross-shaped clusters.

3.1 Potts model and spin clusters

In the following we study the ferromagnetic Potts model whose Hamiltonian is written as:

$$\mathcal{H} = -J \sum_{\langle ij \rangle} \delta_{S_i S_j} \ , \tag{3.2}$$

where the sum is over all the pairs of nearest neighbor spins of a d-dimensional system, $J > 0$ and δ the Kronecker delta and S_i the spin at site i taking integer values in $[1, Q]$.

This model undergoes a magnetic phase transition at the inverse temperature $\beta_c = 1/T_c$ and this transition is continuous for $Q \leq Q_c(d)$. For $d = 2$, $Q_c(2) = 4$ and $\beta_c = \ln(1 + \sqrt{Q})$ for the square lattice [9].

In the study of the Potts model two types of clusters emerge: the FK clusters and the same-spin clusters. The FK clusters appear naturally when the Potts partition function is rewritten in the form of the random cluster model [2]. The construction of FK clusters is simple, edges between spins with the same value are open with probability $p = 1 - e^{-\beta J}$ and edges between spins with different values are always closed. A FK cluster is a connected component of *open* edges. Defined this way the Potts model is really a correlated site-bond percolation model. The FK clusters undergo a continuous percolation transition at T_c in $d = 2$ for $Q \leq 4$ which coincides with the magnetic transition and their exponents are the usual Potts model ones.

We can also define another type of clusters by the same construction as before with $p = 1$, *i. e.* all bonds connecting spins with equal value are open. We will call the connected components of such a construction same-spin clusters or simply spin clusters. Those clusters are the ones occurring naturally in experimental realisations of the Potts model and are most frequently studied in coarsening and more generally out of equilibrium situations [38, 39, 40]. The spin clusters also undergo a continuous percolation transition but at a temperature T_s in general different from T_c. It is only in $d = 2$ that $T_s = T_c$, hence both types of clusters are self-similar at the critical temperature. Moreover, in this case, they are both described by a conformal field theory (CFT) with the same central charge c . However they correspond to different realisations of the CFT since their critical exponents differ, hence the conformal dimensions of the operators of the two models are different as well. As mentioned in the introduction, it has been shown that the Ising spin clusters arise naturally if one considers the $Q = 1$ Potts model with dilution at its tricritical point [3]. This correspondence has been used extensively, for example to derive the fractal dimension of the Ising spin clusters [6].

Even though in the initial formulation of Eq. (3.2) the number of states Q has to be an integer, it can readily be extended to real values for the FK clusters in the random cluster formulation. For example the $Q \to 1$ limit of this model is known to correspond to percolation. One can also make sense of the spin clusters for real values of Q, see for example [11, 12, 13]

Two dimensional critical systems can be conveniently described using the Coulomb gas formalism [33, 32]. In the case of the Potts model, the Coulomb gas parameter g can be

parametrized in the following way:

$$Q \;=\; 2+2\cos\left(\frac{\pi g}{2}\right). \tag{3.3}$$

For the critical branch we have $g \in [2,4]$ and $g \in [4,8]$ for the tricritical branch following the conjectured duality. In particular we have $g = 8/3$ for percolation, $g = 3$ for Ising FK clusters and $g = 16/3$ for Ising spin clusters.

3.2 Wrapping probabilities on a torus

In this section we recall shortly the derivation of FK clusters wrapping probabilities on a torus. For more details, we refer the reader to the works [33, 19, 34]. We will consider a torus $\mathbb{T} = \mathbb{C}/(\mathbb{Z}+\tau\mathbb{Z})$ with parameter $\tau \in \mathbb{C}$ such that $\tau = \tau_R + i\tau_I$. In other words, we build a torus in the complex plane by identifying the opposite sides of the parallelogram with vertices 0, 1, $1+\tau$, τ. The first homology group of a torus is $H_1(\mathbb{T}) = \mathbb{Z}\times\mathbb{Z}$. We will be interested in the probabilities $\pi^{a,b}(\tau)$ of subgroups $\{a,b\}$ of $\mathbb{Z}\times\mathbb{Z}$ with $(a,b)\in\mathbb{Z}^2$, $\pi^0(\tau)$ for the trivial subgroup $\{0\}$ and $\pi^+(\tau)$ for $\mathbb{Z}\times\mathbb{Z}$. The configurations corresponding to $\{a,b\}$ contain at least one non-trivial cluster winding a times horizontally from the left to the right and b times vertically from top to bottom. It can be easily shown that if a configuration contains a non trivial $\{a,b\}$ cluster then all other non trivial clusters that might be present are of the same topology [33]. Since the cluster boundaries cannot intersect themselves a and b must be coprime [33]. The clusters $\{-a,-b\}$ are identified with $\{a,b\}$ so we assume $a>0$. The trivial subgroup $\{0\}$ corresponds to configurations containing only clusters homotopic to a point. $\mathbb{Z}\times\mathbb{Z}$ is generated by clusters containing at least two sub-components with different non-trivial winding numbers, that is generators from two different subgroups. The simplest of those clusters contain sub-components $(1,0)$ and $(0,1)$ and have a cross shape so in the following we will simply call them cross-shaped clusters. It is easy to check that a given configuration can only contain one such cluster.

From Eq. (3.1) we see that the derivation reduces to the computation of restricted partition functions. In particular, the partition function Z_Q of the Q state Potts model can be decomposed on the different cluster homology classes such that $Z_Q = Z_Q^0 + Z_Q^+ + \sum_{a\wedge b=1} Z_Q^{a,b}$ where $a\wedge b$ stands for the greatest common divisor of a and b. The sum is taken with a and b coprime for the reason mentioned previously. Z_Q^0, Z_Q^+ and $Z_Q^{a,b}$ are the partition functions restricted to the configurations containing respectively only trivial clusters, one cross cluster and a least one non trivial cluster of type $\{a,b\}$.

The derivation of the crossing probabilities uses extensively a chain of equivalences between the Q state Potts model, the six vertex model and solid on solid (SOS) models which are known to renormalise into a bosonic free field with parameter g. We will not describe those equivalences which have been extensively discussed in the literature, *e.g.* see [32, 41]. We just need to know that clusters are represented by oriented loops formed by their interfaces and that height variables are introduced such that the height varies of $\pm\pi/2$ when crossing a line depending on its orientation. It is this height which becomes the

bosonic free field in the continuum limit. One can easily see that a configuration containing only trivial clusters or a cross-shaped cluster yields a periodic field in both periods of the torus. On the contrary, a configuration with non trivial $\{a, b\}$ clusters may induce discontinuities in the field, for example in this case $\{a, b\}$ cluster induces a discontinuity of $bk\pi$ horizontally and $ak\pi$ vertically with $k \in \mathbb{Z}$. The discontinuities are multiple of π because for a single non trivial cluster there is a pair of interfaces.

Di Francesco *et al.* [33] showed that the partition function Z_Q can be expressed with bosonic partition functions $Z_{m,m'}(g)$ corresponding to a bosonic free field with discontinuities $m\pi$ horizontally and $m'\pi$ vertically. $Z_{m,m'}(g)$ has the following expression:

$$Z_{m,m'}(g) = \sqrt{\frac{g}{\tau_I}} \frac{1}{|\eta(q)|^2} \exp\left[-\pi g \frac{m^2\tau_I^2 + (m' - m\tau_R)^2}{\tau_I}\right] \tag{3.4}$$

with $q = e^{2i\pi\tau}$ and $\eta(q) = q^{1/24}\prod_{n=1}^{\infty}(1 - q^n)$ is the Dedekind η function. One has to be careful so as to give the correct weight $\sqrt{Q}$ to non trivial interfaces. To achieve this we have to add an electric charge e_0 such that:

$$\sqrt{Q} = 2\cos\left(\frac{\pi e_0}{2}\right). \tag{3.5}$$

With this we can give the proper weight to all interfaces in the partition function by multiplying $Z_{m,m'}(g)$ to a cosine factor $\cos[\pi e_0(m \wedge m')]$. One can see that choosing $e_0 = 1$ kills the contribution of non trivial loops. This allows the determination of Z_Q^0:

$$Z_Q^0 = \frac{1}{2}\sum_{m,m'\in\mathbb{Z}} Z_{m,m'}(g/4)\cos[\pi(m \wedge m')] = \frac{1}{2}Z_c(g, 1) \tag{3.6}$$

where $Z_c(g, e_0)$ is the Coulombic partition function defined by Di Francesco *et al.* whose expression is:

$$Z_c(g, e_0) = \sum_{m,m'\in\mathbb{Z}} Z_{m,m'}(g/4)\cos[\pi e_0(m \wedge m')]. \tag{3.7}$$

Then using the duality relation $Z_Q^+ = QZ_Q^0$ coming from Euler's relation, one obtains the partition function restricted to cross-shaped clusters. Now to obtain $Z_Q^{a,b}$ one has to consider the sum over all configurations with the desired discontinuities:

$$Z_Q^{a,b} = \sum_{\substack{m=bk\\ m'=ak\\ k\in\mathbb{Z}\setminus\{0\}}} \left(Z_{m,m'}(g/4)\cos[e_0\pi(m \wedge m')] - Z_{m,m'}(g/4)\cos[\pi(m \wedge m')]\right). \tag{3.8}$$

The second term in the sum accounts for the contribution of configurations with non trivial $\{a, b\}$ clusters inducing a periodic field [34].

The complete partition function Z_Q can be obtained by summing over all topology classes:

$$Z_Q = \frac{(Q+1)}{2}Z_c(g, 1) + \sum_{a\wedge b=1} Z_Q^{a,b} = \frac{(Q-1)}{2}Z_c(g, 1) + Z_c(g, e_0). \tag{3.9}$$

3.3 Closed forms for Ising spin clusters probabilities

We now turn to the determination of the closed form for the probability $\pi^{a,b}_{2,\mathrm{spin}}(\tau)$ for Ising spin clusters to wind around the torus. To compute this probability, we use the equivalence to the $Q'=1$ Potts model with dilution at its tricritical point, so that $\pi_2^{\mathrm{spin}}(\{a,b\}) = \pi_1^{\mathrm{tri}}(\{a,b\})$. We know from Eq. (3.3) that the tricritical Potts model with $Q'=1$ renormalises to a Coulomb gas with parameter $g=16/3$. The value $e_0=2/3$ comes from Eq. (3.5) taking $Q'=1$. We can now compute $Z^{a,b}_{2,\mathrm{spin}}$:

$$\begin{aligned} Z^{a,b}_{2,\mathrm{spin}} &= \sum_{\substack{m=bk\\ m'=ak\\ k\in\mathbb{Z}\setminus\{0\}}} \left[Z_{m,m'}(4/3)\cos\left[2\pi/3(m\wedge m')\right] - Z_{m,m'}(4/3)\cos\left[\pi(m\wedge m')\right]\right] \\ &= \sum_{k\in\mathbb{Z}\setminus\{0\}} \left[\cos\left(\frac{2\pi}{3}k\right) - (-1)^k\right] Z_{bk,ak}(4/3) \\ &= \frac{2/\sqrt{3}}{{\tau_I}^{1/2}|\eta(q)|^2}\left[\sum_{k\in\mathbb{Z}\setminus\{0\}} \cos\left(\frac{2\pi}{3}k\right) e^{-\pi\frac{4}{3}\frac{|\tau_{a,b}|^2}{\tau_I}k^2} - \sum_{k\in\mathbb{Z}\setminus\{0\}} (-1)^k e^{-\pi\frac{4}{3}\frac{|\tau_{a,b}|^2}{\tau_I}k^2}\right] \end{aligned} \tag{3.10}$$

where $\tau_{a,b} = a - b\tau$. The second sum can be expressed with a Jacobi θ function as $\theta_4\left(i\frac{4}{3}\frac{|\tau_{a,b}|^2}{\tau_I}\right)$ with $\theta_4(\tau) = \sum_{n\in\mathbb{Z}}(-1)^n q^{n^2/2}$ with $q = e^{2i\pi\tau}$. The first sum has to be decomposed so that the cosine has a constant value, *i. e.* $k \equiv 0,1,2 \bmod 3$. Then the sums obtained are all expressed with Jacobi θ functions:

$$\begin{aligned} Z^{a,b}_{2,\mathrm{spin}}(\tau) &= \frac{2/\sqrt{3}}{{\tau_I}^{1/2}|\eta(q)|^2}\left[\left(\sum_{k\equiv 0 \bmod 3} - \frac{1}{2}\sum_{k\equiv 1,2 \bmod 3}\right) e^{-\pi\frac{4}{3}\frac{|\tau_{a,b}|^2}{\tau_I}k^2} - \theta_4\left(i\frac{4}{3}\frac{|\tau_{a,b}|^2}{\tau_I}\right)\right] \\ &= \frac{2/\sqrt{3}}{{\tau_I}^{1/2}|\eta(q)|^2}\left[\frac{3}{2}\theta_3\left(12i\frac{|\tau_{a,b}|^2}{\tau_I}\right) - \frac{1}{2}\theta_3\left(i\frac{4}{3}\frac{|\tau_{a,b}|^2}{\tau_I}\right) - \theta_4\left(i\frac{4}{3}\frac{|\tau_{a,b}|^2}{\tau_I}\right)\right] \end{aligned} \tag{3.11}$$

where $\theta_2(\tau) = \sum_{n\in\mathbb{Z}} q^{(n+1/2)^2/2}$ and $\theta_3(\tau) = \sum_{n\in\mathbb{Z}} q^{n^2/2}$. We now use identities on the θ functions to invert their arguments to obtain this compact expression:

$$Z^{a,b}_{2,\mathrm{spin}}(\tau) = \frac{1}{2|\tau_{a,b}||\eta(q)|^2}\left[\theta_3\left(i\frac{\tau_I}{12|\tau_{a,b}|^2}\right) - \theta_3\left(i\frac{3}{4}\frac{\tau_I}{|\tau_{a,b}|^2}\right) - 2\theta_2\left(i\frac{3}{4}\frac{\tau_I}{|\tau_{a,b}|^2}\right)\right]. \tag{3.12}$$

With the expression of the Ising model partition function on a torus [42] one obtains the probability $\pi^{a,b}_{2,\mathrm{spin}}(\tau)$:

$$\pi^{a,b}_{2,\mathrm{spin}}(\tau) = \frac{1}{|\tau_{a,b}||\eta(q)|}\frac{\theta_3\left(i\frac{\tau_I}{12|\tau_{a,b}|^2}\right) - \theta_3\left(i\frac{3}{4}\frac{\tau_I}{|\tau_{a,b}|^2}\right) - 2\theta_2\left(i\frac{3}{4}\frac{\tau_I}{|\tau_{a,b}|^2}\right)}{|\theta_2(\tau)| + |\theta_3(\tau)| + |\theta_4(\tau)|} \tag{3.13}$$

It is interesting to see if this formula can be related to other known results. For example one can recover the long cylinder limit by taking $\tau = ir$ and the limit $r \to \infty$. The question is now the probability that a spin cluster spans the cylinder from top to bottom. The answer depends on whether one also allows the cluster to wrap or not around the cylinder as was also discussed by Cardy for percolation [43]. If no wrapping is allowed the relevant probability is $\pi^{0,1}_{2,\mathrm{spin}}(ir)$. In this case $\frac{|\tau_{0,1}|^2}{\tau_I} = r$ and one can see that the dominant term in the sum of exponential of $Z^{a,b}_{2,\mathrm{spin}}(\tau)$ behaves as $e^{-4\pi r/3}$. For the probability one has to take into account the contribution coming from the Dedekind function $|\eta(e^{-2\pi r})|^{-1} \sim e^{\pi r/12}$ which gives that $\pi^{0,1}_{2,\mathrm{spin}}(ir) \sim e^{-5\pi r/4}$ when $r \to \infty$. In [11, 12], the authors considered exponents related to thick and thin domain walls (DW) of spin clusters. For a cylinder of size $l \times L$, they claim that the probability that the two ends of the cylinder are connected by $_1$ thin DW and l_2 thick DW decays as $e^{-4\pi(l/L)h(Q,l_1,l_2)}$ where $h(Q, l_1, l_2) = h_{l_1-l_2,2l_1}$ with the $h_{r,s}$ from the Kac table. They remark that in the case of a single thick DW the exponent $h(Q, 0, 1) = h_{-1,0}$ is related to the probability that the DW spans the cylinder without wrapping. As $h(2, 0, 1) = 5/16$ this probability behaves as $\sim e^{-5\pi r/4}$ which is exactly what we found using $\pi^{0,1}_{2,\mathrm{spin}}(ir)$. When wrapping is allowed the exponent is no longer $h_{-1,0}$ but $h_{0,1/2}$ which equals one half of the magnetic exponent that is $5/192$ in the case of the Ising spin clusters. This gives a probability which decays slower than when wrapping is forbidden as it behaves as $e^{-5\pi r/48} = e^{-2\pi xr}$ for $r \to \infty$ with $x = 5/96$ the magnetic scaling dimension . If one wants to recover this result from wrapping formulae, one has to determine which type of clusters gives the dominant contribution and as we will see in the last section this contribution comes from cross-shaped clusters. In [13] an infinite set of exponents related to joint spin and FK observables was obtained. One can also imagine obtaining wrapping formulae generalising Eq. (3.13) by considering situations where spin and FK clusters wraps around the torus.

3.4 Numerical check

We have checked numerically by means of Monte Carlo simulations the formula (3.13) obtained for spin clusters. The systems were equilibrated at T_c using a Wolff cluster algorithm [44]. 10^6 independent configurations were simulated for each value of the torus parameter τ considered. In all the simulations we used the triangular lattice where the interfaces are defined with no ambiguity as opposed to the square lattice where there exists intersecting interfaces. We have simulated the common case of untwisted tori such that $\tau = ir$ for different aspect ratio r. To implement those tori one has to, starting from a square lattice, add bonds on alternate diagonals on even or odd row. Adding periodic boundary conditions one obtains the desired tori with $\tau = ir$.

We present the results for this case ($\tau = ir$) with $r \in [0.1, 1]$. For a system composed of L_x sites horizontally and L_y sites vertically $r = (\sqrt{3}L_y/2)/L_x$. The factor $\sqrt{3}/2$ accounts for the fact that the system is composed of hexagons instead of squares. In the simulations we took $L_x = 128$ and $L_y \in \{148, 164, 180, 200, 224, 254, 296, 352,$

$434, 568, 822, 1478\}$. This gives aspect ratios $r \in [1, 10]$. We then use the trivial symmetry $\pi^{0,1}_{2,\mathrm{spin}}(i/r) = \pi^{1,0}_{2,\mathrm{spin}}(ir)$ to be able to plot graphs with $r \in [0, 1]$. In Fig. 3.1, $\pi^{0,1}_{2,\mathrm{spin}}(ir)$ and $\pi^{1,0}_{2,\mathrm{spin}}(ir)$ obtained from Eq. (3.13) are represented as function of r (lines) and compared with the probabilities measured from Monte Carlo simulations (symbols). The agreement

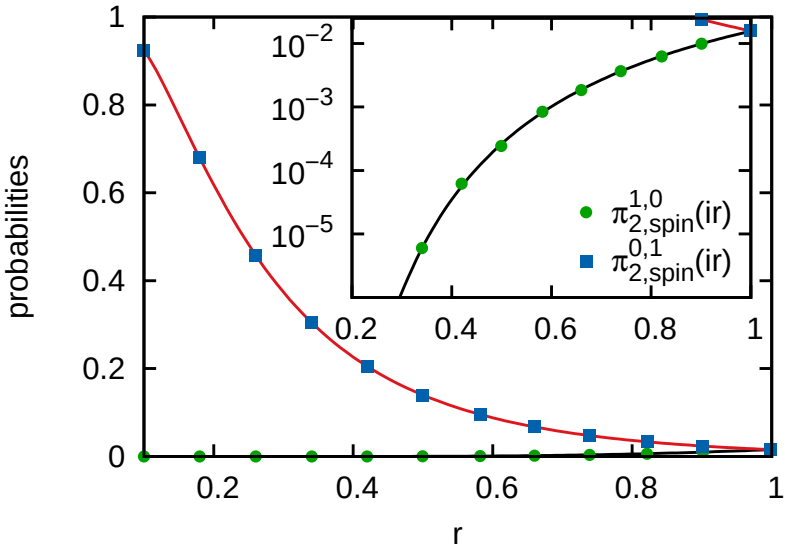

Figure 3.1 – (color online) Ising spin clusters wrapping probability $\pi^{0,1}_{2,\mathrm{spin}}(ir)$ (blue squares and red line) and $\pi^{1,0}_{2,\mathrm{spin}}(ir)$ (green circles and black line) at T_c vs. the aspect ratio r. The lines correspond to the expression of Eq. (3.13) and the symbols correspond to the results of simulations. The error bars are smaller than the symbols. In the inset the same probabilities are represented with the ordinate in logarithmic scale.

is excellent. Since in this range of aspect ratios $\pi^{1,0}_{2,\mathrm{spin}}(ir)$ is at most of order 10^{-2}, hence barely visible, we add an inset with the ordinate in logarithmic scale. In Fig. 3.2, the probabilities for clusters winding once vertically and horizontally are presented. The sum $\pi^{1,1}_{2,\mathrm{spin}}(ir) + \pi^{1,-1}_{2,\mathrm{spin}}(ir)$ is shown instead of each one individually because of the symmetry relation $\pi^{1,1}_{2,\mathrm{spin}}(ir) = \pi^{1,-1}_{2,\mathrm{spin}}(ir)$. Even at its maximum at $r = 1$ the sum is of the order of 5.10^{-5} which makes its numerical estimation less accurate than before but the agreement with the formula is still good. The probabilities for other homotopy groups are too small to allow a numerical estimation.

3.5 Wrapping probabilities for cross clusters on untwisted tori

In this section we are interested in clusters contributing to the subgroup $\mathbb{Z} \times \mathbb{Z}$, *i.e.* cross-shaped clusters. In [45] Ziff *et. al.* obtained a closed form for cross clusters on untwisted tori ($\tau = ir$). They give a closed form only for percolation but it is possible to do the same for the FK and spin clusters as well. As seen in section 3.2, the partition function of

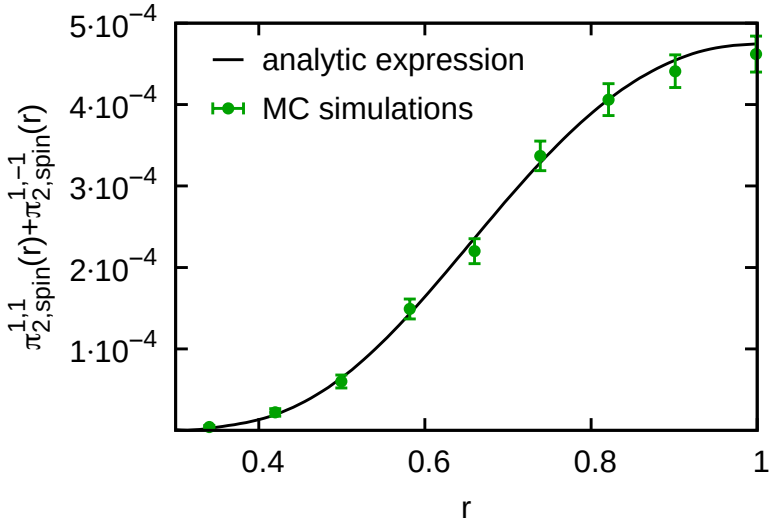

Figure 3.2 – (color online) Ising spin clusters wrapping probability $\pi^{1,1}_{2,\mathrm{spin}}(ir) + \pi^{1,-1}_{2,\mathrm{spin}}(ir)$ (green circles and black line) at T_c vs. the aspect ratio r. The line corresponds to the expression of Eq. (3.13) and the symbols correspond to the results of simulations.

interest Z^+_Q is:

$$\begin{aligned} Z^+_Q &= \frac{Q}{2} Z_c(g,1) = \frac{Q}{2} \sum_{m,m' \in \mathbb{Z}} \left[Z_{m,m'}(g) - Z_{m,m'}(g/4) \right] \\ &= \frac{Q}{2} \left[Z_c(4g,0) - Z_c(g,0) \right]. \end{aligned} \tag{3.14}$$

For untwisted tori ($\tau = ir$) $Z_c(g,0)$ becomes:

$$\begin{aligned} Z_c(g,0) &= \sqrt{\frac{g}{r}} \frac{1}{|\eta(q)|^2} \sum_{m,m' \in \mathbb{Z}} \exp\left[-\pi g \left(m^2 r + \frac{m'^2}{r} \right) \right] \\ &= \sqrt{\frac{g}{r}} \frac{\theta_3\left(igr\right) \theta_3\left(\frac{ig}{r}\right)}{|\eta(q)|^2} \end{aligned} \tag{3.15}$$

because in this case the sum over two integers reduces to a product of θ functions. Finally:

$$Z^+_Q = \frac{Q}{4} \sqrt{\frac{g}{r}} \frac{2\theta_3\left(igr\right) \theta_3\left(\frac{ig}{r}\right) - \theta_3\left(\frac{igr}{4}\right) \theta_3\left(\frac{ig}{4r}\right)}{|\eta(q)|^2} \tag{3.16}$$

This formula is valid for all g but the probability is in general more complicated because of the total partition function. For the Ising model the probability is simply:

$$\pi_Q^+(r) = \frac{Q}{2|\eta(q)|}\sqrt{\frac{g}{r}}\frac{2\theta_3\left(igr\right)\theta_3\left(\frac{ig}{r}\right) - \theta_3\left(\frac{igr}{4}\right)\theta_3\left(\frac{ig}{4r}\right)}{|\theta_2\left(ir\right)| + |\theta_3\left(ir\right)| + |\theta_4\left(ir\right)|}. \tag{3.17}$$

Taking $g = 3$ and $Q = 2$ yields the result for the Ising FK clusters in agreement with the values obtained by Arguin in [34]. For spin clusters the probability is expected to be given by taking $g = 16/3$ and $Q = 1$. The situation is however slightly more subtle as a direct measurement from MC simulations shows that $\pi^0_{2,\text{spin}} = 0$ and that $\pi^+_{2,\text{spin}}$ is twice the quantity given by Eq. (3.17). This can be explained by the fact that when spin clusters of a given color are all trivial then there exists a cluster of the other color wrapping in both direction and thus contributing to the subgroup $\mathbb{Z} \times \mathbb{Z}$. This means that no configuration can contribute to $\{0\}$ while considering simultaneously both colors. Furthermore one has to remember that we are extrapolating those results from the critical line using the mapping to a tricritical model with only one state. By doing so, one of the two spin values of the Ising spin is absorbed to generate the vacancies of the tricritical model. Hence considering one color at a time is natural when considering the properties of spin clusters. It makes no difference to the discussion for the configurations contributing to the subgroups $\{a, b\}$ since in this case at least one cluster of each color is present. However, for the cross-shaped clusters, it is necessary to consider only one color as those clusters come alone. This enables us to recover the relation $\pi^0_{2,\text{spin}} = \pi^+_{2,\text{spin}}$ expected with $Q' = 1$. Indeed, because of the symmetry between the two colors, considering only one color reduces the value $\pi^+_{2,\text{spin}}$ measured in MC simulation by a factor two which is in agreement with Eq. (3.17) with $g = 16/3$ and $Q = 1$.

We can also study the asymptotes for this probability. We find that $\pi_Q^+(r) \sim e^{-\pi(1/g-1/12)r}$ for $r \to \infty$. For the Ising spin clusters ($g = 16/3$) this gives $e^{-5\pi r/48}$ as for the unrestricted probability that the two ends of the cylinder are linked by a spin cluster. For the FK clusters it gives $e^{-\pi r/4}$ which is also of the form $e^{-2\pi x r}$ with $x = 1/8$ the magnetic scaling dimension of the Ising model. The fact that the unrestricted probability is dominated by cross-shaped clusters was also pointed out for percolation [46].

Conclusion

In this chapter, we checked that the natural analytic continuation from the critical branch yields the correct results for the wrapping probabilities of Ising spin clusters. We also obtained an elegant expression for those wrapping probabilities. As a generalisation the study of the 3-Potts spin clusters is definitely interesting but might be more subtle as the mapping corresponds to a tricritical Potts model with a non integer number of states. This case is also interesting since the conjectured continuation to the tricritical branch is known to fail in some cases as already mentioned.

Bibliography

[1] T. Blanchard. Wrapping probabilities for ising spin clusters on a torus. *J. Phys. A: Math. Theor.*, 47(34):342002, August 2014.

[2] C. M. Fortuin and P. W. Kasteleyn. On the random-cluster model : I. introduction and relation to other models. *Physica*, 57(4):536, February 1972.

[3] A Coniglio and W Klein. Clusters and Ising critical droplets: a renormalisation group approach. *J. Phys. A: Math. Gen.*, 13(8):2775, August 1980.

[4] Wolfhard Janke and Adriaan M.J. Schakel. Geometrical vs. Fortuin-Kasteleyn clusters in the two-dimensional q-state Potts model. *Nucl. Phys. B*, 700(1-3):385, November 2004.

[5] W. Janke and A. M. J. Schakel. Fractal structure of spin clusters and domain walls in the two-dimensional Ising model. *Phys. Rev. E*, 71(3):036703, March 2005.

[6] A. L. Stella and C. Vanderzande. Scaling and fractal dimension of Ising clusters at the d=2 critical point. *Phys. Rev. Lett.*, 62(10):1067, March 1989.

[7] A Coniglio and F Peruggi. Clusters and droplets in the q-state Potts model. *J. Phys. A: Math. Gen.*, 15(6):1873, 1982.

[8] C. Vanderzande. Fractal dimensions of Potts clusters. *J. Phys. A: Math. Gen.*, 25(2):L75, January 1992.

[9] F. Y. Wu. The Potts model. *Reviews of Modern Physics*, 54(1):235, January 1982.

[10] Youjin Deng, Henk W. J. Blöte, and Benard Nienhuis. Geometric properties of two-dimensional critical and tricritical Potts models. *Phys. Rev. E*, 69(2):026123, February 2004.

[11] J. Dubail, J. L. Jacobsen, and H. Saleur. Bulk and boundary critical behaviour of thin and thick domain walls in the two-dimensional Potts model. *arXiv:1010.1700 [cond-mat]*, October 2010. arXiv: 1010.1700.

[12] J. Dubail, J. L. Jacobsen, and H. Saleur. Critical exponents of domain walls in the two-dimensional Potts model. *J. Phys. A: Math. Theor.*, 43(48):482002, December 2010.

[13] R. Vasseur and J. L. Jacobsen. Critical properties of joint spin and Fortuin–Kasteleyn observables in the two-dimensional Potts model. *J. Phys. A: Math. Theor.*, 45(16):165001, April 2012.

[14] G. Delfino, M. Picco, R. Santachiara, and J. Viti. Spin clusters and conformal field theory. *J. Stat. Mech.: Theo. Exp.*, 2013(11):P11011, November 2013.

[15] István A. Kovács, Eren Metin Elçi, Martin Weigel, and Ferenc Iglói. Corner contribution to cluster numbers in the Potts model. *arXiv:1311.4186 [cond-mat]*, November 2013.

[16] Dietrich Stauffer and Amnon Aharony. *Introduction to percolation theory*. Taylor & Francis, 1994.

[17] J. L. Cardy. Critical percolation in finite geometries. *J. Phys. A: Math. Gen.*, 25(4):L201–L206, February 1992.

[18] R. P. Langlands, C. Pichet, Ph. Pouliot, and Y. Saint-Aubin. On the universality of crossing probabilities in two-dimensional percolation. *J. Stat. Phys.*, 67(3):553–574, 1992.

[19] Haru T. Pinson. Critical percolation on the torus. *J. Stat. Phys.*, 75(5-6):1167–1177, June 1994.

[20] G. M. T. Watts. A crossing probability for critical percolation in two dimensions. *J. Phys. A: Math. Gen.*, 29(14):L363, July 1996.

[21] John Cardy. Crossing formulae for critical percolation in an annulus. *J. Phys. A: Math. Gen.*, 35(41):L565–L572, October 2002.

[22] Ervig Lapalme and Yvan Saint-Aubin. Crossing probabilities on same-spin clusters in the two-dimensional Ising model. *J. Phys. A: Math. Gen.*, 34(9):1825–1835, March 2001.

[23] Louis-Pierre Arguin and Yvan Saint-Aubin. Non-unitary observables in the 2d critical Ising model. *Phys. Lett. B*, 541(3-4):384–389, August 2002.

[24] Michel Bauer, Denis Bernard, and Kalle Kytölä. Multiple Schramm–Loewner evolutions and statistical mechanics martingales. *J. Stat. Phys.*, 120(5-6):1125–1163, September 2005.

[25] Michael J Kozdron. Using the Schramm–Loewner evolution to explain certain non-local observables in the 2D critical Ising model. *J. Phys. A: Math. Theo.*, 42(26):265003, July 2009.

[26] J. Dubail, J. L. Jacobsen, and H. Saleur. Conformal boundary conditions in the critical $O(n)$ model and dilute loop models. *Nuclear Physics B*, 827(3):457–502, March 2010.

[27] Oded Schramm. Scaling limits of loop-erased random walks and uniform spanning trees. *Israel J. Math.*, 118(1):221–288, December 2000.

[28] G. F. Lawler, O. Schramm, and W. Werner. On the scaling limit of planar self-avoiding walk. *Proc. Sympos. Pure Math.*, 72:339–364, 2004.

[29] S. Smirnov. Critical percolation in the plane: conformal invariance, Cardy's formula, scaling limits. *C.R.A.S. - Series I - Mathematics*, 333(3):239, August 2001.

[30] Robert Langlands, Philippe Pouliot, and Yvan Saint-Aubin. Conformal invariance in two-dimensional percolation. *Bulletin of the American Mathematical Society*, 30(1):1–61, 1994.

[31] B. Nienhuis. Critical behavior of two-dimensional spin models and charge asymmetry in the Coulomb gas. *J. Stat. Phys.*, 34(5-6):731–761, March 1984.

[32] B. Nienhuis. *Coulomb gas formulation of two dimensional phase transitions*, volume 11 of *Phase Transitions and Critical Phenomena*, chapter 1, page 1. Academic Press London, 1987.

[33] P. di Francesco, H. Saleur, and J. B. Zuber. Relations between the Coulomb gas picture and conformal invariance of two-dimensional critical models. *J. Stat. Phys.*, 49(1-2):57–79, October 1987.

[34] Louis-Pierre Arguin. Homology of Fortuin-Kasteleyn clusters of Potts models on the torus. *J. Stat. Phys.*, 109(1):301–310, 2002.

[35] Alexi Morin-Duchesne and Yvan Saint-Aubin. Critical exponents for the homology of fortuin-kasteleyn clusters on a torus. *Phys. Rev. E*, 80(2):021130, 2009.

[36] Kipton Barros, P. L. Krapivsky, and S. Redner. Freezing into stripe states in two-dimensional ferromagnets and crossing probabilities in critical percolation. *Phys. Rev. E*, 80(4):040101, October 2009.

[37] J. Olejarz, P. L. Krapivsky, and S. Redner. Fate of 2D kinetic ferromagnets and critical percolation crossing probabilities. *Phys. Rev. Lett.*, 109(19):195702, November 2012.

[38] T. Blanchard and M. Picco. Frozen into stripes: Fate of the critical Ising model after a quench. *Phys. Rev. E*, 88(3):032131, September 2013.

[39] Thibault Blanchard, Leticia F. Cugliandolo, and Marco Picco. A morphological study of cluster dynamics between critical points. *J. Stat. Mech.: Theo. Exp.*, 2012(05):P05026, May 2012.

[40] T. Blanchard, F. Corberi, L. F. Cugliandolo, and M. Picco. How soon after a zero-temperature quench is the fate of the Ising model sealed? *EPL*, 106(6):66001, June 2014.

[41] Rodney J. Baxter. *Exactly Solved Models in Statistical Mechanics*. Dover Publications, January 2008.

[42] P. Di Francesco, Pierre Mathieu, and David Sénéchal. *Conformal Field Theory*. Springer, 1997.

[43] J. Cardy. The number of incipient spanning clusters in two-dimensional percolation. *J. Phys. A: Math. Gen.*, 31(5):L105–L110, February 1998.

[44] Ulli Wolff. Collective monte Carlo updating for spin systems. *Phys. Rev. Lett.*, 62(4):361, January 1989.

[45] Robert M Ziff, Christian D Lorenz, and Peter Kleban. Shape-dependent universality in percolation. *Physica A: Statistical Mechanics and its Applications*, 266(1–4):17–26, April 1999.

[46] Gunnar Pruessner and Nicholas R. Moloney. Winding clusters in percolation on the torus and the möbius strip. *J. Stat. Phys.*, 115(3-4):839–853, May 2004.

CHAPTER 4

Ising model with long-range interactions

Contents

4.1 Introduction and history

4.1.1 Systems with long-range interactions

Systems with long-range interactions (LRI) form a huge class of systems in physics. One might even say that most physical systems are under the influence of LRI. Gravity and electromagnetic forces just to name the two most famous are omnipresent. In traditional thermodynamics and statistical phyics, the usual assumption is that the system components

interact with each other only through interactions that are short-range enough so that extensivity of thermodynamical quantities is preserved. If this is not the case, the study is completely different and much more involved but nonetheless very interesting.

In recent years there has been a lot of interest in the statistical physics of classical and quantum systems with long-range interactions, for a review see [1]. The role of quasistationary states and ergodicity breaking in long-range interacting systems was investigated in [2] and [3]. In [4] the approaching to equilibrium for long-range quantum systems was examined and there has been a lot of enthusiasm in investigating the entanglement entropy in long-range spin chains [5, 6, 7]. Very recently an experiment was conducted on a quantum system with tunable long-range interactions [8].

4.1.2 Ising model with long-range interactions

In the present manuscript we focus on the Ising model which is probably the most studied model in statistical mechanics, especially in the context of critical phenomena. Most of the studies about the Ising model are concentrated around the short-range case which is exactly solvable in one and two dimensions [9]. In three dimensions the problem was perturbatively studied using the ϵ-expansion technique [10] of the renormalization group (RG) combined with the Borel resummation of the perturbation series, see [11] and references therein. Most recently the problem was revisited by using conformal bootstrap technique [12].

Although now there are few unknown facts about the short-range Ising model the long-range Ising model is still the subject of many contradicting theoretical and numerical studies. The long-range Ising model was introduced by Dyson [13] in 1969 as an example of a one dimensional system exhibiting a phase transition at a positive temperature, which is not possible for system with short-range interactions. Its generalisation to arbitrary dimensions has the following hamiltonian

$$\mathcal{H} = -\sum_{\langle ij \rangle} \frac{J}{r_{ij}^{d+\sigma}} S_i S_j \ , \tag{4.1}$$

where the sum is over all pairs of spins of a d dimensional system, r_{ij} the distance between sites i and j and $J > 0$ the ferromagnetic interaction strength. The exponent is written as $d + \sigma$ with $\sigma > 0$ to emphasize the fact that we study the regime where interactions decay faster than $1/r^d$. Ths condition is required to maintain the extensivity property. It comes from the fact that the sum over all interactions must be finite in order to define properly thermodynamics averages [14]. We will restrict ourselves to systems where this condition is verified.

After Dyson's result on the existence of a phase transition, a natural question concerns the universality class to which the system belongs. This universality class depends a priori upon the value of the exponent σ. We will now review some of the existing analyses of the critical properties of the Ising model with LRI relevant to our work.

4.1.3 Fisher, Ma and Nickel analysis

Shortly after the introduction of the ϵ-expansion technique [10], Fisher, Ma and Nickel (FMN) applied this method to compute the critical exponents of a d-dimensional system with an isotropic n-component order parameter and LRI decaying as $1/r^{d+\sigma}$ [15]. Their study is quite general as it concerns the Ising ($n = 1$), XY ($n = 2$) and Heisenberg models ($n = 3$). In momentum space the action for the Ising model with LRI has the following expression:

$$S = \frac{1}{2}\int_q \phi(q)(r + j_\sigma q^\sigma + j_2 q^2)\phi(-q) + \lambda \int_{q_1,q_2,q_3} \phi(q_1)\phi(q_2)\phi(q_3)\phi(-q_1 - q_2 - q_3). \quad (4.2)$$

We write it for the Ising model for simplicity but the $O(n)$ action is quite straightforward to write. The action (4.2) differs from the canonical $\lambda\phi^4$ action only through the term $j_\sigma q^\sigma$ which is due to the presence of LRI. This action can also be written is real space using a fractional Laplacian defined as $|\nabla^2|^\alpha = \int_q |q|^\alpha \phi(q) e^{iqx}$ with α a real number:

$$S = \int_x \mathrm{d}^d x \frac{1}{2}\phi(x)(r + j_\sigma |\nabla^2|^{\sigma/2} + j_2\nabla^2)\phi(x) + \frac{\lambda}{4!}\phi^4(x). \quad (4.3)$$

FMN did a naive analysis of the action (4.2) simply comparing the relative power of the terms q^2 and q^σ. We can easily see that for $\sigma > 2$ the term q^σ is negligible at low momenta compared to q^2. More precisely three regimes were discovered for all values of n: (a) the classical regime $0 < \sigma < d/2$ with mean field critical exponents; (b) the intermediate regime $d/2 < \sigma < 2$, where the exponents are functions of σ and (c) the short-range regime $\sigma > 2$ where the exponents are the same as for the short-range models for all d.

In the classical regime and for all n the anomalous dimension $\eta = 2 - \sigma$, $\nu = 1/\sigma$ and the susceptibility exponent $\gamma = 1$. The conjectures around the first regime were proved in [16] and the results of the third regime are widely accepted. It is the intermediate regime that has been the subject of many controversies in the last forty years. In [15] FMN obtained the expression for η and γ the susceptibility exponent up to ϵ'^2 for $\sigma < 2$ with $\epsilon' = 2\sigma - d$. It corresponds to an ϵ expansion from the upper critical dimension $d_c = 2\sigma$. For $\sigma = 2$ one recovers $d_c = 4$ as for the Ising model with SRI. They observed a discrepancy for both exponents at this order at $\sigma = 2$ between their expression for $\sigma < 2$ and their short-range value for $\sigma > 2$. The case of the exponent η is special because it gets no corrections at this order so that it sticks to its classical regime's value; *i.e.* $\eta = 2 - \sigma$. So for η the situation is the following: for $0 < \sigma < 2$, $\eta = 2 - \sigma$ and then for $\sigma > 2$ η takes the value η_{SR} of the corresponding model with SRI. This means that η goes from 0 to $\eta_{\text{SR}} \neq 0$ as σ passes 2. This is not prohibited by thermodynamics arguments which only requires $\eta \leq 2 + \sigma$ but it is nonetheless puzzling enough so that soon after that Sak disscussed this point in more details [17].

4.1.4 Sak's scenario

A few month after FMN's article, Sak [17] argued that there is no such discontinuity for η, γ and φ the crossover exponent because if one looks at the long-range interaction as a perturbation of the short-range Ising, $\sigma = 2$, one can discover that the short-range Ising exponents should be extended to $\sigma = 2 - \eta_{\text{SR}}$. It gives that for $0 < \sigma \leq 2 - \eta_{\text{SR}}$, $\eta = 2 - \sigma$ and then for $\sigma \geq 2 - \eta_{\text{SR}}$ $\eta = \eta_{\text{SR}}$ and so there is no discontinuity for the anomalous dimension as a function of σ.

His analysis relies on a careful study of the renormalisation group recursion relations and of the fixed points' stability. He showed that, when terms of order ϵ'^2 are taken into account in the recursion relation for the coefficient in front of the short-range term, the long-range fixed point is unstable when $2 - \sigma < \eta_{\text{SR}}$. After reorganising the ϵ expansion, one can show that in this case the stable fixed is the usual fixed point of short-range $O(n)$ model. Furthermore, when evaluating the RG expressions for the LR exponents at $\sigma = 2 - \eta_{\text{SR}}$, one recovers the corresponding RG short-range expressions. This is a strong indication that the discontinuity was an artefact of the series truncated at the first order in ϵ'.

Many authors have considered this model, some confirming Sak's analysis or infirming it while others provided alternative scenarii. We can cite the works of Yamazaki [18, 19, 20] who obtained other expressions for the critical exponents.

4.2 New simulations for an old model

4.2.1 Luijten and Blöte

What was lacking for a long time was a numerical estimation of the LR exponents to give support to one RG scenario or another. One of the difficulties with LRI models is that it is very consuming in CPU time to generate independent configurations compared with model with SRI. Indeed for a single spin flip one has to sum over all the lattice spins just to compute the energy change whereas for SRI it only concerns a few neighbouring sites. It is only in 2002 that Luijten and Blöte conducted a numerical study of the 2d Ising model with LRI in the controversial σ range [21]. Their results clearly exclude a discontinuity à la FMN and are compatible with the situation depicted by Sak. They use an efficient cluster Monte Carlo algorithm that makes a number of operations per spin flip that does not depend on the system size which is the case for naive Monte Carlo implementations [22]. Furthermore, the interest of using a cluster algorithm is that it greatly suppresses the critical slow-down that burdens single spin flip schemes as for example does the cluster based Wolff algorithm for SRI Ising model [23]. They used systems with periodic boundary condition with linear sizes L ranging from 4 to 1000. They carried simulations in the range $\sigma \in [1.2, 3.0]$ and evaluated the amplitude ratio $B = \langle m^2 \rangle^2 / \langle m^4 \rangle$ with m the magnetization[1] (related to the Binder cumulant) and the anomalous dimension η by monitoring the divergence of

[1] The amplitude ratio B is noted Q in [21]

the magnetic susceptibility. Indeed the susceptibility diverges as $L^{\gamma/\nu}$ so η can be obtained through the scaling relation $\gamma = (2-\eta)\nu$. In the table 4.1 are shown the values, taken from [21], measured for η for different values of σ. The values of η for $\sigma = 1.85$ and 1.95 exclude clearly a discontinuity with σ, and even if the error bars are quite big, the authors argued that this gives supports to Sak's scenario. Together with the theoretical analysis done by Sak, those simulations seem to settle the discussion between the contradicting RG scenarios.

4.2.2 Picco's analysis

As we have seen the numerical simulation done by Blöte and Luijten [21] completely ruled out any possible jump in the value of η. Again their algorithm uses the fact that for a ferromagnetic model, one can use clusters of spins to improve the speed of the simulations as is done in the Wolff cluster algorithm for short-range ferromagnetic models [23]. Even if their work argues convincingly for Sak's scenario the accuracy on η in the crossover region was not completely satisfactory. This left room for improvement, which was achieved in Picco's work [24]. The improvement in [24] concerns the construction of the clusters by optimizing the search of connected spins over large regions. With this new algorithm, one can simulate systems up to size 5120×5120 with a typical update time of order one second on an ordinary workstation. To update N spins Picco's algorithm requires $\mathcal{O}(N)$ operations compared to $\mathcal{O}(N \log N)$ for Luijten and Blöte's algorithm. By analyzing much bigger sizes than in previous studies, Picco concluded that η displays an intriguing behaviour in particular in the intermediate regime and close to the boundary with the short-range regime that neither Fisher et al. procedure nor Sak's analysis are able to account for.

The estimation of η goes as follows. First one needs to determine the critical coupling K_c defined as J/kT_c with T_c the critical temperature for each value of σ. To do so, one can compute the cumulant $B(L,K) = \langle m^2 \rangle^2 / \langle m^4 \rangle$ for different temperatures K and system sizes L. When considerng one correction to scaling the cumulant B is expected to behave as:

$$B(L,K) \simeq f((K-K_c)L^{1/\nu}) + A_1 L^{-y_1} \tag{4.4}$$

close to the critical point. The addition of subleading term is guided by the analysis of the numerical data. Without the correction the curves of $B(L,K)$ as a function of K for different sizes are expected to cross at the same critical temperature K_c. But with the correction term $A_1 L^{-y_1}$ the curves for two system sizes L and L' cross at a temperature depending of both L and L'. For simplicity one can choose $L' = 2L$ so that only L appears. This leads to a finite size correction for the critical temperature:

$$K_c(L) \simeq K_c + \alpha_1 L^{-w_1} \tag{4.5}$$

with $w_1 = y_1 + 1/\nu$ and α_1 a constant. Now by monitoring the temperatures at which the successive curves cross, one obtains several values of $K_c(L)$ from which the infinite system value $K_c = \lim_{L\to\infty} K_c(L)$ can be extrapolated. Once the critical temperature is obtained one can obtain the exponent η by observing the behaviour of the magnetisation m

σ	LB	Picco	$\max(2-\sigma, \frac{1}{4})$
1.20	0.798 (18)	-	0.80
1.40	0.616 (10)	0.619 (12)	0.60
1.60	0.410 (24)	0.420 (8)	0.40
1.7	-	0.357 (7)	0.30
1.75	0.286 (24)	0.332 (8)	0.25
1.8	-	0.307 (5)	0.25
1.85	0.30 (6)	-	0.25
1.9	-	0.279 (5)	0.25
1.95	0.24 (4)	-	0.25
2.00	0.266 (16)	0.262 (4)	0.25
2.05	0.260 (14)	-	0.25
2.2	-	0.251 (7)	0.25
2.25	0.248 (12)	-	0.25
2.50	0.246 (8)	-	0.25
2.75	0.250 (10)	-	0.25
3.00	0.248 (8)	-	0.25

Table 4.1 – Exponent η from Luijten-Blöte and Picco for different values of σ. The last column contains the prediction from the RG analysis of Sak, $\eta = \max(2-\sigma, 1/4)$.

which behaves as $L^{-\beta/\nu}$ with the system size at the critical point and then using the relation $\eta = 2\beta/\nu$. Is has been checked that the value obtained for η depends only very weakly on the maximum system size used to compute the critical coupling K_c. The values obtained are shown in the table 4.1.

The values of η computed agree with the values predicted by Sak's RG analysis only for $\sigma \leq 1.5$ and $\sigma \geq 2$. In the intermediate region $1.5 \leq \sigma \leq 2$, the data interpolates smoothly between the LR classical regime and the SR regime. At $\sigma = 2 - \eta_{\text{SR}} = 1.75$ where the discrepancy is at its maximum the deviation approximately equals 10 times the uncertainty on η. Due to greater error bars Luijten and Blöte's estimations are compatible with both Sak's scenario and Picco's simulation. This results are quite puzzling at it suggests that an important ingredient has been forgotten in previous analyses. It clearly invites for further study which were undertaken soon after and are presented in the next section.

4.2.3 Stability of the fixed points

In the present section, we will compare the long-range behavior with the short-range one in two dimensions. We provide numerical evidences that the long-range interactions dominate for $\sigma \leq 2$. As we have seen, it was observed in [24] that the behavior of the model with long-range interactions and for $\sigma < 2$ is different from what is expected for the short-range model. Then we must worry about the relevance of the long-range interactions compared to the short-range ones. If we start from a short-range model and consider the addition of long-range term $g \sum_{ij} S_i S_j / r_{ij}^{d+\sigma}$ as a small perturbation, then a simple dimensional argument predicts the relevance of the perturbation as a function of the dimension of g [25].

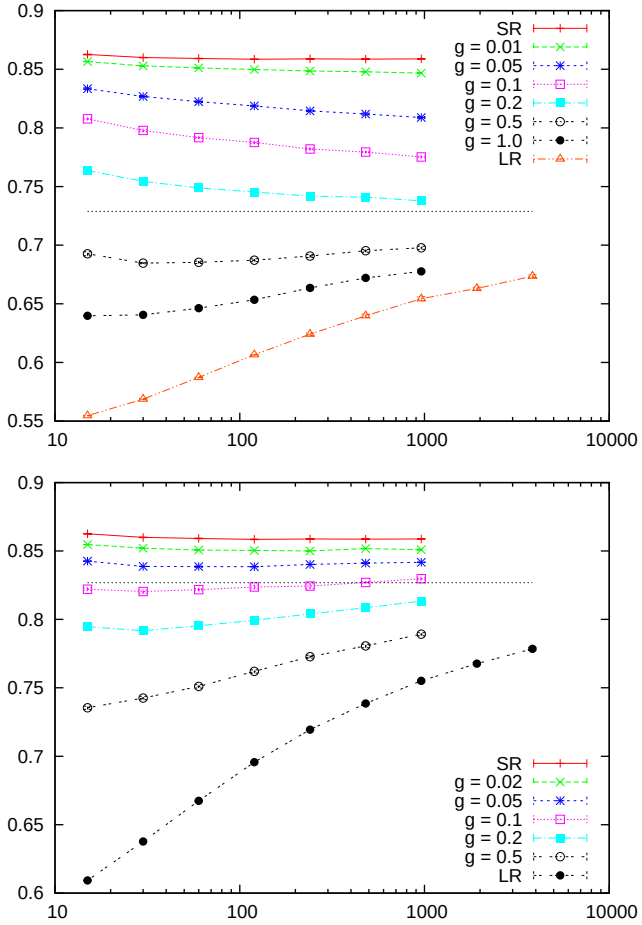

Figure 4.1 – (Color online) $B(g, L)$ vs. L for $\sigma = 1.6$ (top panel) and $\sigma = 1.8$ (bottom panel). The SR results are depicted in red and have the largest $B(g, L)$. The dotted line corresponds to the extrapolated value for the LR model (see [24]).

Since for large distances we have $\langle S_i S_j \rangle \simeq r_{ij}^{2-d-\eta_{\rm SR}}$, with $\eta_{\rm SR} = \frac{1}{4}$ in two dimensions, we expect that the dimension of g is $2 - \eta_{\rm SR} - \sigma$. Then the result is that the perturbation is relevant for $\sigma < 2 - \eta_{\rm SR}$ and irrelevant otherwise. We will now test this argument. We consider the case of the perturbation as a function of σ and g. We will use the magnetic cumulant $B(g, L, K)$ defined previously. For each value of g, we consider the quantity $B_c(g, L, L')$ which corresponds to the crossing of $B(g, L, K)$ and $B(g, L', K)$ as a function of K. By choosing a set of increasing values L and L' not too far apart, we can determine for each pair the value of K which corresponds to the crossing and $B_c(g, L, L')$ is expected to converge towards a finite limit for $L \to +\infty$. In the following, we will always consider $L' = 2L$ and then we will just denote the crossing value by $B(g, L)$. In [24], it was determined that the corresponding quantity for the long-range interaction model, which

can be considered as the limit $g \to \infty$, converges to a value smaller than the one of the short-range model for $\sigma \leq 2$. In Fig. 4.1, we present the measured values of $B(g, L)$ for $\sigma = 1.6$ and $\sigma = 1.8$. For the first case, we observe a clear tendency for $B(g, L)$ to converge towards the same limit as the LR model (which is shown as a dotted line) and this for all the values of g in the range $g = 0.01$ up to $g = 1$. For the second case, the situation is less clear. For the small values of $g \leq 0.1$, it seems first that $B(g, L)$ converges towards the model with short-range interactions. For larger values of the perturbation, we just observe that $B(g, L)$ increases with the size. While it can be assumed that this just corresponds to the flow towards the value for the SR model, one can also invoke the effect of strong finite size corrections.

In fact, since we are considering a case in which there is both a flow towards either the LR model or the SR model and very strong finite size effects, it is difficult to know which one is the dominant effect. We then adopt another strategy. We will look in the following to the quantity defined as

$$X(g, L) = \frac{B(g, L) - B_{\text{LR}}(L)}{B_{\text{SR}}(L) - B_{\text{LR}}(L)} \, . \tag{4.6}$$

This quantity is defined such that it takes a value between 0 and 1. If $B(g, L)$ flows towards the SR point, then $X(g, L)$ goes to 1. On the contrary, if it flows towards the LR point, then it goes to 0. We then expect the crossover to be controlled by a crossover parameter $g/|t|^{\phi}$ with t the reduced temperature and $\phi = \nu\Delta_\sigma$ which defines Δ_σ. On a finite lattice of linear size L and at the critical point, this becomes gL^{Δ_σ} with the correspondence $t^{-\nu} \sim \xi \sim L$. According to the naive dimensional analysis made above, $\Delta_\sigma = 2 - \sigma - \eta_{\text{SR}}$. In Fig. 4.2, we show a plot of $X(g, L)$ vs. the crossover parameter for various values of g in $[0.01, 1]$ and σ. For each value of σ, we determined a single parameter Δ_σ which allows to make a scaling for all the values of g on a single curve. The values that we obtained are reported in the caption of the figure. It is quite remarkable that the curves for all values of σ collapse on a single curve. We obtain that for $gL^{\Delta_\sigma} \ll 1$, the curves follow an exponential, *i.e.* $X(g, L) \simeq \exp(-gL^{\Delta_\sigma})$. For $gL^{\Delta_\sigma} \gg 1$, the curves behave as a power law *i.e.* $X(g, L) \simeq (gL^{\Delta_\sigma})^{-\alpha}$ with $\alpha \simeq 0.75$.

A second fact is that the value of Δ_σ does not follow the prediction obtained from the naive dimensional analysis. While for small values of σ, the correspondence between the measured crossover exponent and the predicted one is acceptable, this is clearly not the case for larger values of σ. And in particular, this exponent does not cancel at $\sigma = 2 - \eta_{\text{SR}}$. Note also that the precision on this exponent is not very good for larger values of σ since in that case the denominator of $X(g, L)$ becomes small and will cancel in the large size limit for $\sigma = 2$.

The conclusion of this analysis is that we observe a clear signal for a crossover between the short-range interaction model and the long-range interaction model. This crossover seems to be present in all the range that we can consider $1.2 \leq \sigma \leq 1.9$. Of course, such a crossover is expected for small values of σ, *i.e.* $\sigma \leq 2 - \eta_{\text{SR}} = 1.75$. We observed that in fact this crossover between the SR model towards the LR model remains present even for

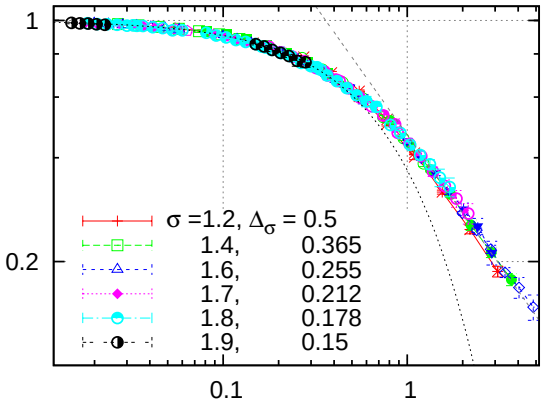

Figure 4.2 – (Color online) $X(g, L)$ vs. gL^{Δ_σ}. The straight dashed line corresponds to $(gL^{\Delta_\sigma})^{-0.75}$, while the other dashed curve is for $\exp(-gL^{\Delta_\sigma})$.

larger values of σ, presumably up to $\sigma = 2.0$.

4.3 Renormalisation group approach

4.3.1 Dimensional deformation

Now we propose another way to compute the η exponent guided by the simulations' results presented in the previous section. The main idea is to make a correspondence between

$$A_1 = \int \mathrm{d}^d x \left(\frac{1}{2} |\nabla^{\sigma/2} s_b(x)|^2 + \frac{\lambda_0}{4!} |s_b(x)|^4 \right), \tag{4.7}$$

with $\epsilon' = 2\sigma - d$ and

$$A_2 = \int \mathrm{d}^D x \left(\frac{1}{2} |\nabla s_b(x)|^2 + \frac{\lambda_0}{4!} |s_b(x)|^4 \right), \tag{4.8}$$

with $\epsilon = 4 - D$. The first expression A_1 is a formal way of writing in real space a model with long-range interactions. The second expression A_2 is the usual way of expressing a short-range ϕ^4 model for a D dimensional theory. For $\sigma \simeq 2$ and with the condition $\epsilon = \epsilon'$, the ϵ-expansion of both models, A_1 and A_2 will be the same apart from a term proportional to $\delta\sigma = 2 - \sigma$. Thus the computation will be done from the model A_2 with $D = 4 + d - 2\sigma$. The deviation of σ from 2 is replaced by a deformation of the dimension from d to D.

In this section we propose a new way of doing RG analysis for long-range Ising model. Although our analysis shares some similarities with the work of Yamazaki the final results are more general [18, 19, 20]. We implement our RG analysis around the critical point [26, 27], then we can avoid calculating more complicated integrals. Based on the arguments

of the last section one can write the Lagrangian of the long-range Ising model, forgetting about the irrelevant short-range part, with respect to the renormalized coupling and field as

$$\mathcal{L} = \frac{1}{2}|\nabla^{\sigma/2}s(x)|^2 + \frac{\lambda}{4!}\mu^{\epsilon'}|s(x)|^4 + (Z-1)\frac{1}{2}|\nabla^{\sigma/2}s(x)|^2 + \frac{\lambda}{4!}\mu^{\epsilon'}(Z^2Z_\lambda - 1)|s(x)|^4 + \cdots, \tag{4.9}$$

where $\epsilon' = 2\sigma - d$, $s = Z^{-1/2}s_b$ and $\lambda_0 = \lambda\mu^{\epsilon'}Z_\lambda$ with s_b and λ_0 as bare parameters. The scale μ is introduced because we want to do the expansion around the massless theory [26]. The third and fourth terms are designed to remove divergent contributions in vertex functions. The renormalization conditions are

$$\Gamma^{(2)}(0) = 0; \tag{4.10}$$

$$\frac{\partial}{\partial|p|^\sigma}\Gamma^{(2)}(p,-p)|_{|p|^\sigma=\mu^\sigma} = 1; \tag{4.11}$$

$$\Gamma^{(4)}(p_1,p_2,p_3,p_4)|_{S_\mu} = \lambda\mu^{\epsilon'}. \tag{4.12}$$

The symmetric point S_μ is chosen in such a way that $p_i^2 = \frac{3}{4}\mu^2$ and $p_i.p_j = -\mu^2/4$. Using the relevant graphs of the Fig. 4.3 one can write

$$\Gamma^{(2)}(p,-p) = Z|p|^\sigma - \frac{\lambda^2}{3!}\mu^{2\epsilon'}\int\frac{d^dq_1}{(2\pi)^d}\frac{d^dq_2}{(2\pi)^d}\frac{1}{|q_1|^\sigma|q_2|^\sigma|p-q_1-q_2|^\sigma}; \tag{4.13}$$

$$\Gamma^{(4)}(p_1,p_2,p_3,p_4)|_{S_\mu} = \lambda\mu^{\epsilon'}Z_\lambda Z^2 - \frac{\lambda^2}{2}\frac{4!}{(2!)^3}\mu^{2\epsilon'}\int\frac{d^dq}{(2\pi)^d}\frac{1}{|q|^\sigma|p_1+p_2-q|^\sigma}. \tag{4.14}$$

The integrals are infrared divergent for $\epsilon' > 0$ and need to be calculated by analytical continuation from the convergent region. This is the same situation as in the usual ϵ-expansion in the short-range Ising model. Although the integrals are complicated, they can be calculated using the formulas in [26], and after using the renormalization conditions we will have

$$Z = 1 - \frac{\lambda^2}{3\sigma(4\pi)^d}\frac{\Gamma^3[\frac{d-\sigma}{2}]}{\Gamma[\frac{3d-3\sigma}{2}]}\frac{\Gamma[\frac{3\sigma}{2}-d+1]}{\Gamma^3[\frac{\sigma}{2}]}, \tag{4.15}$$

$$Z_\lambda = 1 + \frac{3\lambda}{2(4\pi)^{d/2}}\frac{\Gamma^2[\frac{d-\sigma}{2}]}{\Gamma[d-\sigma]}\frac{\Gamma[\epsilon'/2]}{\Gamma^2[\sigma/2]}. \tag{4.16}$$

The very important point is that if we expand Z with respect to ϵ' there will not be any pole and one cannot get sensible contribution to the critical exponent of the field $s(x)$. However, since the integrals are infrared divergent, the right way to get a sensible perturbation theory is to expand Z first around $\sigma = 2$ and then around $\epsilon' = 0$. The situation is very similar

to the short-range case; we have an integral which is divergent and would like to control its divergency. If we expand the above equations first around ϵ' we actually get a finite term which is apparently wrong. Our choice of order of expansion is not arbitrary and it was actually forced by the divergent integrals. Since we have two parameters dimension d and σ; and they can be changed independently, one can first consider having $\delta\sigma = 2 - \sigma$ small and then do the perturbation theory with respect to ϵ'. After expanding Z and Z_g with respect to $\delta\sigma$ and then ϵ' we get

$$Z = 1 - \frac{\lambda^2}{12(4\pi)^d\epsilon'}\left[1 - \left(\frac{1}{2\epsilon'} + \frac{12\gamma - 13}{8}\right)\delta\sigma + \cdots\right] + \mathcal{O}(\lambda^3), \tag{4.17}$$

$$Z_\lambda = 1 + \frac{3\lambda}{(4\pi)^{d/2}\epsilon'}\left[1 + (1-\gamma)\delta\sigma + \cdots\right] + \mathcal{O}(\lambda^2). \tag{4.18}$$

with $\gamma = 0.5772...$ as the Euler-Mascheroni constant. Using the Callan-Symanzik equation which states that the derivative of the bare quantities with respect to μ is zero, one can get the beta functions as

$$\beta(\lambda) = \mu\frac{\partial}{\partial\mu}\lambda = -\epsilon'\lambda + \frac{3\lambda^2}{(4\pi)^{d/2}}\left[1 + (1-\gamma)\,\delta\sigma\right], \tag{4.19}$$

$$\gamma(\lambda) = \mu\frac{\partial}{\partial\mu}\ln Z = \frac{\lambda^2}{6(4\pi)^d}\left[1 - \left(\frac{1}{2\epsilon'} + \frac{12\gamma - 13}{8}\right)\delta\sigma\right]. \tag{4.20}$$

To derive the above formula we first use the equation (4.18) to get a relation between λ, λ_0 and μ. Using the above beta functions at the critical point where $\beta(\lambda^*) = 0$ one can easily get the correction to the mean field value of the critical exponent $\delta\eta = \eta - (2 - \sigma)$ as

$$\delta\eta = \gamma(\lambda^*) = \frac{1}{54}\epsilon'^2 - \frac{1}{108}\epsilon'\delta\sigma - \frac{1}{432}\epsilon'^2(3 - 4\gamma)\delta\sigma + \cdots \tag{4.21}$$

Based on our prescription it is obvious that in the ϵ'-expansion of the η exponent the zeroth order terms of $\delta\sigma$ expansion will be the same as the ϵ-expansion of the short-range Ising model but with $\epsilon' = 2\sigma - d$ instead of $\epsilon = 4 - D$. So in principle close to the $\sigma = 2$ we will have

$$\eta = 2 - \sigma + \frac{1}{54}\epsilon'^2 + \cdots + \mathcal{O}(\delta\sigma), \tag{4.22}$$

where dots represent the higher order terms of the ϵ'-expansion. Since in our proposal of doing the RG we first expand all the contributions around $\sigma = 2$ and then around $\epsilon' = 0$ we expect that the dots in the formula (4.22) are exactly the same as in the short-range Ising model with ϵ' instead of ϵ. The above expansion suggest that for $\delta\sigma$ small one can argue that the critical exponent of the long-range Ising model in d dimensions is approximately the same as the critical exponent of $D = 4 + d - 2\sigma$ short-range Ising model. For the short-range Ising model $\delta\eta$ is known up to ϵ^5 for various dimensions [28, 29]. The first correction to this value comes from the second and third terms of the equation (4.21) which are both negative. If the higher order terms, $(\delta\sigma)^n$ with $n \geq 2$, do not

change the sign of the contribution to η one can conclude that the critical exponent η of the short-range Ising model in $D = 4 + d - 2\sigma$ gives an upper bound for the $\delta\eta$ of the long-range Ising model in d dimension. Of course this conjecture needs to be checked by calculating higher loop corrections to the critical exponents. Based on the above arguments we compared in Fig. 4.4 the η coming from the numerical calculations for the long-range Ising model in two dimensions with the results coming from the five loop calculation of $D = 6 - 2\sigma$ dimensional short-range Ising model. The results are well comparable in the region $1.75 < \sigma < 2$ and as we argued for the smaller values of σ the actual values lie below our approximation.

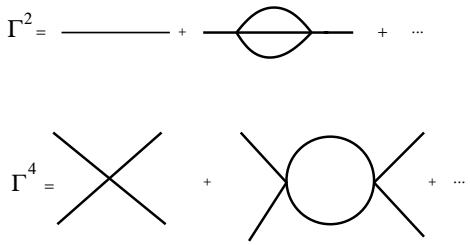

Figure 4.3 – The relevant Feynman diagrams in RG calculation of the beta function and wave function normalization.

4.3.2 Recent developments

Since the publication of our analysis of the Ising model with LRI [30], several authors have considered this model as well.

Baczyk and collaborators have considered several models using the non-pertubative renormalisation group (NPRG) [31, 32, 33, 34]. Their goal was to study the dimensional reduction and its breakdown in different disordered models with or without LRI. The pure Ising model with LRI was included in their study as a particular case and after a careful analysis of the model in all dimensions their analysis gives support to the scenario of Sak. They found no extra-contribution to the anomalous dimension η that could change it from its mean field value $2 - \sigma$.

Angelini *et al.* considered in [35, 36] various questions related to models with LRI. In particular they re-investigated the Ising model with LRI in $d = 2$ in the crossover region, and studied the behaviour of the spin-spin correlation function for $\sigma = 1.75$. They remarked that the correlation function displays a very peculiar behaviour with the presence of two distinct power-law decays for short or long distances and that it does not seem to be a finite-size correction. They propose that the usual expression for the correlation function $G(x) \sim x^{-\eta}$ should be changed to

$$G(x) = \frac{A + Bx^{\delta}}{x^{\eta}} \tag{4.23}$$

where the exponent δ accounts for the preasymptotic power law decay $x^{-\eta-\delta}$. They have

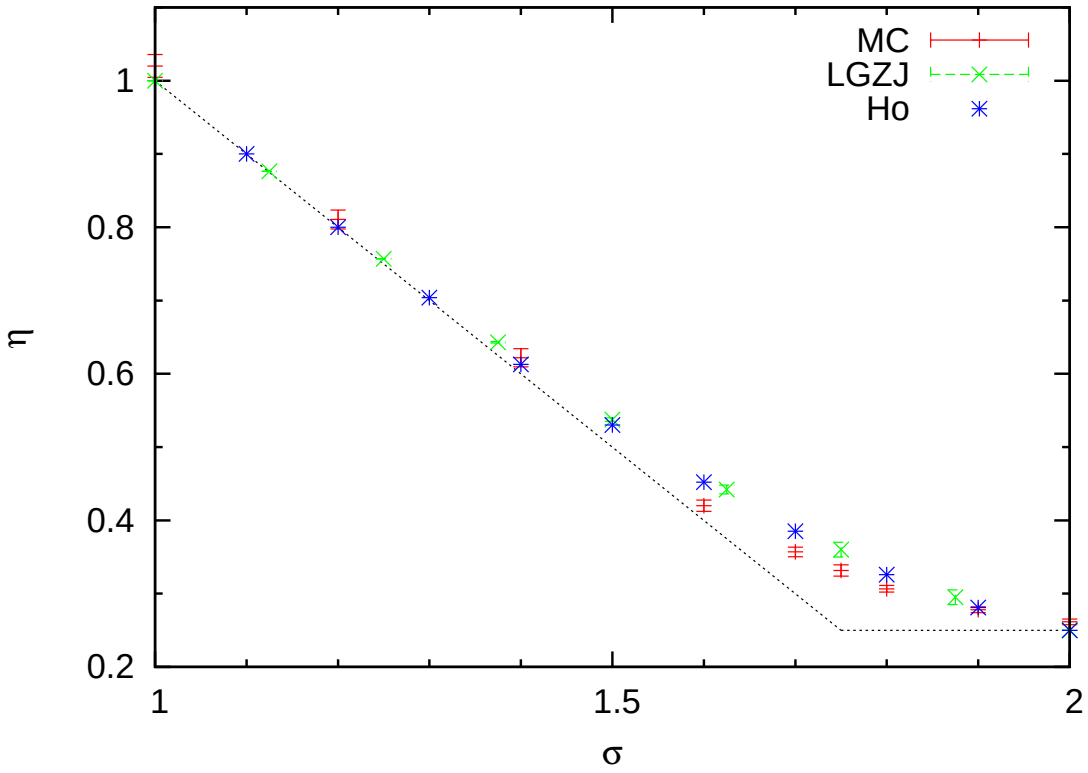

Figure 4.4 – Data depicted in red are the result of the simulation in [24]. Green and blue data are coming from our approximation using the results of [28] and [29] respectively. The dotted line is Sak's result [17].

no explanation for this additional preasymptotic regime which furthermore only seem to appear for σ close enough to the SR regime. They argue that if one overlooks this additional power law decay, the value of η obtained can be overestimated and they say that this might be the reason for the discrepancy between Picco's and Sak's values. However they note that both values are compatible with their more complete analysis, but for the sake of simplicity they claim that Sak's analysis should be kept owing to its simpler scenario. So we can say that their analysis brings a few answers but also rises some questions, most notably concerning the physical reasons for this additional preasymptotic decay.

Finally a very recent work by Brezin, Parisi and Ricci-Tersenghi has been posted on the arXiv [37]. It aims at providing a theoretical explanation for the puzzling crossover behaviour in simulations displayed by models with LRI.

4.4 Conclusion

The model considered in this chapter has seen several interesting developments in the last few years. Interestingly some new questions have been asked concerning this forty years

old debate. In particular the question of the value of the exponents in the crossover region is quite interesting and not completely settled. Even if one accepts the analysis from Angelini and collaborators with the two power laws, the physical origin of this peculiarity is quite mysterious. This definitely calls for further studies.

Another line of research which seems very interesting is the determination of spin clusters properties for the Ising model with LRI. As we have discussed extensively in previous chapters, a rich description of spin clusters in terms of percolation, fractal dimensions... is possible. What happens in the case of the model with LRI? For the critical exponents of the model, the short-range regime is recovered as soon as $\sigma \geq 2$. Is it also true for the spin cluster properties? Some questions that could be adressed are: do spin clusters undergo a percolation phase transition with temperature for all values of σ? If yes is their fractal dimension the same as in the SR case? And can the interfaces be described in terms of Schramm-Loewner evolutions? Basically all the studies of geometrical properties in the SR case are potentially interesting in the LR case. We plan to carry such a work in the near future.

Bibliography

[1] Alessandro Campa, Thierry Dauxois, and Stefano Ruffo. Statistical mechanics and dynamics of solvable models with long-range interactions. *Physics Reports*, 480(3–6):57–159, September 2009.

[2] A. Gabrielli, M. Joyce, and B. Marcos. Quasistationary states and the range of pair interactions. *Phys. Rev. Lett.*, 105(21):210602, November 2010.

[3] Fernanda P. da C. Benetti, Tarcísio N. Teles, Renato Pakter, and Yan Levin. Ergodicity breaking and parametric resonances in systems with long-range interactions. *Phys. Rev. Lett.*, 108(14):140601, April 2012.

[4] Michael Kastner. Diverging equilibration times in long-range quantum spin models. *Phys. Rev. Lett.*, 106(13):130601, March 2011.

[5] Thomas Barthel, Sébastien Dusuel, and Julien Vidal. Entanglement entropy beyond the free case. *Phys. Rev. Lett.*, 97(22):220402, November 2006.

[6] Thomas Koffel, M. Lewenstein, and Luca Tagliacozzo. Entanglement entropy for the long-range Ising chain in a transverse field. *Phys. Rev. Lett.*, 109(26):267203, December 2012.

[7] Andrea Cadarso, Mikel Sanz, Michael M. Wolf, J. Ignacio Cirac, and David Pérez-García. Entanglement, fractional magnetization, and long-range interactions. *Phys. Rev. B*, 87(3):035114, January 2013.

[8] Joseph W. Britton, Brian C. Sawyer, Adam C. Keith, C.-C. Joseph Wang, James K. Freericks, Hermann Uys, Michael J. Biercuk, and John J. Bollinger. Engineered two-dimensional Ising interactions in a trapped-ion quantum simulator with hundreds of spins. *Nature*, 484(7395):489–492, April 2012.

[9] Rodney J. Baxter. *Exactly Solved Models in Statistical Mechanics*. Dover Publications, January 2008.

[10] Kenneth G. Wilson and Michael E. Fisher. Critical exponents in 3.99 dimensions. *Phys. Rev. Lett.*, 28(4):240–243, January 1972.

[11] R. Guida and J. Zinn-Justin. Critical exponents of the n-vector model. *J. Phys. A: Math. Gen.*, 31(40):8103, October 1998.

[12] Sheer El-Showk, Miguel F. Paulos, David Poland, Slava Rychkov, David Simmons-Duffin, and Alessandro Vichi. Solving the 3D Ising model with the conformal bootstrap. *Phys. Rev. D*, 86(2):025022, July 2012.

[13] Freeman J. Dyson. Existence of a phase-transition in a one-dimensional Ising ferromagnet. *Commun. in Math. Phys.*, 12(2):91–107, June 1969.

[14] G. Gallavotti and S. Miracle-Sole. Statistical mechanics of lattice systems. *Commun.Math. Phys.*, 5(5):317–323, October 1967.

[15] Michael E. Fisher, Shang-keng Ma, and B. G. Nickel. Critical exponents for long-range interactions. *Phys. Rev. Lett.*, 29(14):917–920, October 1972.

[16] Michael Aizenman and Roberto Fernández. Critical exponents for long-range interactions. *Lett Math Phys*, 16(1):39–49, July 1988.

[17] J. Sak. Recursion relations and fixed points for ferromagnets with long-range interactions. *Phys. Rev. B*, 8(1):281–285, July 1973.

[18] Yoshitake Yamazaki. Critical exponent η of isotropic spin systems with long and short-range interactions. *Physics Letters A*, 61(4):207–210, May 1977.

[19] Y. Yamazaki. Comments on the critical behavior of isotropic spin systems with long- and short-range interactions. *Physica A: Statistical Mechanics and its Applications*, 92(3–4):446–458, July 1978.

[20] Y. Yamazaki. Critical behaviour of isotropic spin systems with long- and short-range interactions. *Nuov Cim A*, 55(1):59–77, January 1980.

[21] Erik Luijten and Henk W. J. Blöte. Boundary between long-range and short-range critical behavior in systems with algebraic interactions. *Phys. Rev. Lett.*, 89(2):025703, June 2002.

[22] Erik Luijten and Henk W.J. Blöte. MONTE CARLO METHOD FOR SPIN MODELS WITH LONG-RANGE INTERACTIONS. *International Journal of Modern Physics C*, 06(03):359–370, June 1995.

[23] Ulli Wolff. Collective monte Carlo updating for spin systems. *Phys. Rev. Lett.*, 62(4):361, January 1989.

[24] Marco Picco. Critical behavior of the Ising model with long range interactions. *arXiv:1207.1018*, July 2012.

[25] John L. Cardy. *Scaling and Renormalization in Statistical Physics*. Cambridge University Press, April 1996.

[26] Claude Itzykson and Jean-Michel Drouffe. *Statistical Field Theory: From Brownian Motion to Renormalization and Lattice Gauge Theory*. Cambridge University Press, March 1991.

[27] Hagen Kleinert and Verena Schulte-Frohlinde. *Critical Properties of ϕ^4-theories*. World Scientific, 2001.

[28] J. C. Le Guillou and J. Zinn-Justin. Critical exponents for the n-vector model in three dimensions from field theory. *Phys. Rev. Lett.*, 39(2):95–98, July 1977.

[29] Yu Holovatch. Critical exponents of Ising-like systems in general dimensions. *Theor Math Phys*, 96(3):1099–1109, September 1993.

[30] T. Blanchard, M. Picco, and M. A. Rajabpour. Influence of long-range interactions on the critical behavior of the Ising model. *EPL*, 101(5):56003, March 2013.

[31] Gilles Tarjus, Maxime Baczyk, and Matthieu Tissier. Avalanches and dimensional reduction breakdown in the critical behavior of disordered systems. *Phys. Rev. Lett.*, 110(13):135703, March 2013.

[32] Maxime Baczyk, Matthieu Tissier, Gilles Tarjus, and Yoshinori Sakamoto. Dimensional reduction and its breakdown in the three-dimensional long-range random-field Ising model. *Phys. Rev. B*, 88(1):014204, July 2013.

[33] Maxime Baczyk, Gilles Tarjus, Matthieu Tissier, and Ivan Balog. Fixed points and their stability in the functional renormalization group of random field models. *arXiv:1312.6375 [cond-mat]*, December 2013. arXiv: 1312.6375.

[34] Maxime Baczyk. *Influence du champ aléatoire et des interactions à longue portée sur le comportement critique du modèle d'Ising; une approche par le groupe de renormalisation non perturbatif*. Doctoral thesis, June 2014.

[35] Maria Chiara Angelini. *Renormalization group and critical properties of Long Range models*. Doctoral thesis, August 2013.

[36] Maria Chiara Angelini, Giorgio Parisi, and Federico Ricci-Tersenghi. Relations between short-range and long-range Ising models. *Phys. Rev. E*, 89(6):062120, June 2014.

[37] Edouard Brezin, Giorgio Parisi, and Federico Ricci-Tersenghi. The crossover region between long-range and short-range interactions for the critical exponents. *arXiv:1407.3358 [cond-mat]*, July 2014. arXiv: 1407.3358.